

MACROSCOPIC DIVERSITY APPLICATIONS OF
MULTI-INPUT MULTI-OUTPUT (MIMO) SYSTEMS
FOR BROADBAND MOBILE COMMUNICATION

By

DONGFANG LIU

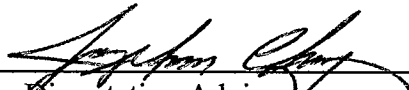
Bachelor of Science
University of Science and Technology Beijing
Beijing, China
1993

Master of Science
University of Science and Technology Beijing
Beijing, China
1996

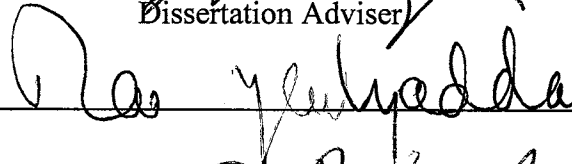
Submitted to the Faculty of the
Graduate College of the
Oklahoma State University
in partial fulfillment of
the requirements for
the Degree of
DOCTOR OF PHILOSOPHY
May, 2005

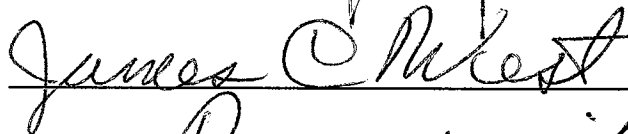
MACROSCOPIC DIVERSITY APPLICATIONS OF
MULTI-INPUT MULTI-OUTPUT (MIMO) SYSTEMS
FOR BROADBAND MOBILE COMMUNICATION

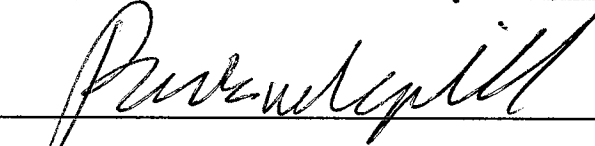
Dissertation Approved:



Dissertation Adviser









Dean of the Graduate College

PREFACE

This dissertation analyzes the evolution of mobile cellular communication technology and identifies the necessity of implementing the multi-input multi-output (MIMO) structure in future generation mobile systems. The properties and implementation issues of MIMO systems in wireless fading environments are studied. While the effects of large-scale shadowing components have been largely ignored in other MIMO technology literatures, it is intensively investigated in this dissertation. It is found that the shadowing components have a substantial influence on the capacity of MIMO systems and make other capacity improvement schemes much less effective.

Based on the investigation conducted on the shadowing effects in MIMO systems, a macroscopic selection diversity (MSD) MIMO scheme is proposed to overcome the deteriorative influences of shadowing and other effects, and to improve the MIMO system capacity. In the theoretical analysis of the proposed system, both large-scale shadowing and small-scale fading components are integrated in the exact capacity outage expression. This expression gives a general and accurate evaluation method to calculate the MIMO system capacity. Both optimal and simplified base station selection schemes are evaluated in the MSD-MIMO system. For both schemes, significant capacity improvements are obtained.

ACKNOWLEDGMENTS

I wish to express my sincere appreciation to my adviser, Dr. Jong-Moon Chung, for his guidance, encouragement, inspiration, and mentoring during this four-year and eight-month memorable period at the Oklahoma State University. He is far more than an academic adviser to me. I learned a lot from him in the aspects of life as well as academia. My sincere appreciation extends to my other committee members Dr. Rao Yarlagadda, Dr. James West, and Dr. Nohpill Park for their guidance and encouragement. I wish to express my sincere gratitude to Dr. Wun-Cheol Jeong, who helped by guiding me on the MIMO research and provided consistent care throughout the research process.

I would like to thank all my friends and colleagues in Stillwater. They made my life in Stillwater more worthwhile. I enjoyed working with all colleagues in the ACSEL & OCLNB laboratories. I appreciate their support and wish them all the best. I appreciate all the help I received from the professors and staff members in the School of Electrical and Computer Engineering.

I am indebt to my parents and younger brother for always encouraging me to do the things I like. Family traditions, such as dedication and appreciation of hard working, will definitely accompany me throughout my whole life.

Special honor and appreciation are given to my wife, Yue Wang. Her love and understanding not only gave me the strength to complete my studies and research, but also made my life enjoyable. We thank our little boy, Zachary Liu, for bringing lots of joys into our life. We wish him a bright future.

TABLE OF CONTENTS

Chapter	Page
I. INTRODUCTION	1
1.1 Background.....	1
1.2 Motivation.....	5
1.3 Dissertation Outline	9
1.4 Research Flowchart.....	11
II. EVOLUTION OF CELLULAR SYSTEMS.....	14
2.1 Evolutions of 1G and 2G Systems	14
2.1.1 The First Generation (1G) Systems	14
2.1.2 The Second Generation (2G) Systems.....	15
2.2 3G Systems	19
2.2.1 Review of 3G Standards	19
2.2.2 3G Standards Bodies.....	21
2.3 Evolution to WCDMA and CDMA2000	22
2.3.1 Current Status.....	22
2.3.2 Evolution to 3G.....	23
2.4 Case Study of Capacity and Data Rate	27
2.4.1 Evolution of System Capacity	27
2.4.2 High Data Rate in CDMA2000 1xEV-DO	28
2.4.3 Discussion.....	30
2.5 Summary.....	32
III. BACKGROUND RESEARCH IN MIMO SYSTEMS.....	33
3.1 MIMO System Introduction.....	33
3.2 MIMO System Capacity	35
3.2.1 Capacity Derivation	35
3.2.2 Comparison with Other Diversity Systems.....	37
3.2.3 Effects of the Number of Antennas	42
3.3 MIMO Systems in a Multi-cell Environment.....	44
3.3.1 Capacity Derivation	44
3.3.2 Simulation Results	46
3.4 Adaptive Modulation	47
3.4.1 MIMO System Adaptive Modulation – Scheme 1	48
3.4.2 MIMO System Adaptive Modulation – Scheme 2	51

IV. ANALYTICAL MODEL OF MIMO SYSTEMS	58
4.1 Correlation Effect in MIMO Systems	58
4.1.1 Continuous Scatter One-Ring Model	60
4.1.2 Discrete Scatter One-Ring Model	62
4.1.3 Exponential Correlation Model	63
4.1.4 Correlation Effect	64
4.2 Introduction to Random Matrix	66
4.2.1 Normally Distributed Random Matrix	66
4.2.2 Special Case Normally Distributed Matrix	67
4.2.3 Wishart Distribution	67
4.3 Eigenvalue Distribution	67
4.3.1 Eigenvalue Distribution of Positive Definite Random Matrix	67
4.3.2 Eigenvalue Distribution of Wishart Random Matrix	68
4.3.3 Hypergeometric Function Representation	68
4.4 Evaluation of Eigenvalue Distribution	71
4.4.1 Truncated Summation Approach	71
4.4.2 Closed-Form Expression	73
4.5 Characteristic Function (c.f.) Method for MIMO System Throughput	76
4.5.1 Characteristic Function Method	77
4.5.2 Results and Analysis	80
4.6 Summary	81
V. MACROSCOPIC DIVERSITY MIMO SYSTEM	83
5.1 Introduction to Shadowing Effect	83
5.2 System Model	84
5.2.1 Standard MIMO System	85
5.2.2 Macroscopic Diversity MIMO System	86
5.3 Capacity Upper Bound	86
5.3.1 Capacity Comparison	86
5.3.2 Simulation Results	93
5.4 Summary	97
VI. EXACT CAPACITY OF MSD-MIMO SYSTEM	99
6.1 Capacity of MSD-MIMO Systems	99
6.1.1 Shadowing Effects in Correlated MIMO Systems	99
6.1.2 Characteristics of MSD-MIMO Systems	102
6.2 Outage Probability of MSD-MIMO Systems	105
6.2.1 MSD-MIMO Systems with Optimum BS Selection Scheme	108
6.2.2 MSD-MIMO Systems with Suboptimum BS Selection Scheme	111
6.2.3 Numerical Results	112
6.3 Mean Capacity of MSD-MIMO Systems	120
6.3.1 Mean Capacity of MIMO Systems in Composite Fading	120

6.3.2 Mean Capacity of MSD-MIMO.....	124
6.4 Summary.....	125
VII. CONCLUSION AND FUTURE WORK.....	126
7.1 Conclusion	126
7.2 Future Work.....	128
BIBLIOGRAPHY.....	130

LIST OF TABLES

Table	Page
2.1 Comparison of 2G systems.....	18
2.2 Basic requirements for 3G systems.....	19
2.3 Comparison of WCDMA and CDMA2000 standards.....	23
2.4 Evolution of IS-95 systems.....	25
2.5 Evolution of GSM systems.....	26
3.1 Simulation parameters for capacity comparison.....	39
3.2 Simulation parameters for multi-cell environment.....	46
4.1 Simulation parameters for correlation effects.....	64
5.1 Simulation parameters for macroscopic MIMO systems.....	94

LIST OF FIGURES

Figure	Page
1.1 MIMO system diagram	4
1.2 MIMO mobile communication system experiencing shadowing effect.....	7
1.3 Macroscopic diversity MIMO systems.....	8
1.4 Research proposal flowchart.....	13
2.1 Evolution paths to 3G.....	24
2.2 Frame structure in CDMA2000 1xEV-DO.....	29
3.1 Capacity of receiver diversity systems.....	40
3.2 Capacity of transmitter diversity systems.....	41
3.3 Capacity of MIMO systems.....	42
3.4 Capacity of MIMO systems with different $\{n_r, n_t\}$ pairs.....	43
3.5 MIMO capacity in multi-cell environment.....	47
3.6 Channel capacity with/without power adaptation.....	55
3.7 Adaptive modulation data rate with/without power adaptation.....	56
$(BER = 10^{-3})$	
4.1 Outdoor cellular signal propagation environment.. ..	60
4.2 Continuous scatter one-ring model.	60
4.3 Discrete scatter one-ring model.	63
4.4 Correlation effect in MIMO systems.....	65
4.5 Eigenvalue distributions for 2×2 un-correlated MIMO systems.....	75

4.6	Eigenvalue distributions for 2×2 correlation MIMO systems.....	76
	(30° angle spread)	
4.7	Eigenvalue distributions for 2×2 correlation MIMO systems.....	76
	(10° angle spread)	
4.8	Outage capacity in different correlation situations.....	81
5.1	Capacity upper bound comparison.....	91
5.2	Monte-Carlo simulation verification	92
5.3	Capacity comparison of standard MIMO vs. macroscopic MIMO systems.....	94
5.4	Capacity Comparison of standard MIMO vs. macroscopic MIMO systems.....	96
	(10% outage and 50% outage)	
5.5	Capacity Comparison of standard MIMO vs. macroscopic MIMO systems.....	97
	(5% outage)	
6.1	Capacity outage probability of a MIMO system for a multipath fading channel.....	101
6.2	Capacity outage probability of a MIMO system for a composite fading channel ($\sigma_\omega = 8$ dB).....	102
6.3	Illustration of the (M, n_t, n_r) MSD-MIMO system with $M = 3, n_t = n_r = 3$	103
6.4	Outage Capacity of $(M, 3, 3)$ MSD-MIMO system for different number of BSs ($r = 0.5$).....	114
6.5	Outage Capacity of $(3, 3, 3)$ MSD-MIMO system for different multipath correlation values (the suboptimum BS scheme is applied).....	115
6.6	10%-Capacity outage of $(3, 3, 3)$ MSD-MIMO system for different multipath correlation values (the suboptimum BS scheme is applied).....	116

6.7	Capacity outage probability of $(M, 3, 3)$ MSD-MIMO system for a different number of BSs (Angle spread of 10 degree is used).....	118
6.8	Capacity outage probability of $(M, 3, 3)$ MSD-MIMO system for different number of BSs (Angle spread of 30 degree is used).....	119
6.9	Capacity outage probability of $(M, 3, 3)$ MSD-MIMO system for different number of BSs (Angle spread of 50 degree is used).....	120
6.10	Mean capacity of 2×2 standard MIMO systems.....	123
6.11	Mean capacity of $(M, 3, 3)$ MSD-MIMO systems.....	124

LIST OF SYMBOLS

C	Capacity
D	Data rate
n_t	Number of transmit antennas
n_r	Number of receive antennas
n_{\min}	$\min\{n_r, n_t\}$
n_{\max}	$\max\{n_r, n_t\}$
\mathbf{H}	Channel matrix, small-scale fading only
\mathbf{H}_w	Channel matrix, small-scale fading only, un-correlated
\mathbf{H}_c	Channel matrix, composite fading
Σ	Channel correlation matrix
\mathbf{I}	Identity matrix
\mathbf{x}	Transmitted signal, $n_t \times 1$ vector
\mathbf{y}	Received signal, $n_r \times 1$ vector
\mathbf{n}	Noise at receiver, $n_r \times 1$ vector
P_t	Total transmit power
σ_n^2	Noise power at receiver
ρ	Average SNR at receiver
γ	Instantaneous SNR at receiver
λ	Eigenvalue vector of channel matrix

ω	Shadowing component
Ω	Matrix of shadowing component
$\det(\mathbf{X})$	Determinant of matrix \mathbf{X}
$tr(\mathbf{X})$	Trace of a square matrix \mathbf{X} , $trace(\mathbf{X})$
$etr(\mathbf{X})$	$\exp[trace(\mathbf{X})]$
$vec(\mathbf{X})$	Column vector formed by stacking the columns of matrix \mathbf{X}
\mathbf{X}^T	Transpose of matrix \mathbf{X}
\mathbf{X}^H	Conjugate transpose (Hermitian transpose) of matrix \mathbf{X}
\otimes	Kronecker product

NOMENCLATURE

1G	First Generation Mobile Wireless System
2G	Second Generation Mobile Wireless System
3G	Third Generation Mobile Wireless System
3GPP	Third Generation Partnership Project
3GPP2	Third Generation Partnership Project 2
4G	Fourth Generation Mobile Wireless System
ARQ	Automatic Retransmission Request
AWGN	Additive White Gaussian Noise
BER	Bit Error Rate
BLAST	Bell Labs Layered Space-Time
BS	Base Station
CDF	Cumulative Distribution Function
CDMA	Code-Division Multiple Access
c.f.	Characteristic Function
CSI	Channel State Information
DOF	Degree of Freedom
EDGE	Enhanced Data Rates for GSM Evolution
FCC	Federal Communications Commission
FDD	Frequency-Division Duplex

FDM	Frequency-Division Multiplexing
FDMA	Frequency-Division Multiple Access
FEC	Forward Error Correction
FM	Frequency Modulation
FPLMITS	Future Public Land Mobile Telecommunications Systems
GPRS	General Packet Radio Services
GSM	Global System for Mobile Communications
HSPDA	High Speed Packet Downlink Access
i.i.d.	Independently and Identically Distributed
IMT-2000	International Mobile Telecommunications-2000
ITU	International Telecommunication Union
LPF	Low-Pass Filter
MDC	Macroscopic Diversity Combining
MSD	Macroscopic Selection Diversity
MIMO	Multi-Input Multi-Output
ML	Maximum Likelihood
MRC	Maximal Ratio Combining
MT	Mobile Terminal
OFDM	Orthogonal Frequency-Division Multiplexing
OQPSK	Offset QPSK
PCS	Personal Communications Systems
PDF	Probability Density Function
QAM	Quadrature Amplitude Modulation

QPSK	Quadrature Phase Shift Keying
RF	Radio Frequency
RV	Random Variable
RX	Receiver
SNR	Signal-to-Noise Ratio
SIR	Signal-to-Interference Ratio
SMS	Short Message Service
TDD	Time-Division Duplex
TDM	Time-Division Multiplexing
TDMA	Time-Division Multiple Access
TX	Transmitter
UMTS	Universal Mobile Telecommunications System
UWB	Ultra Wide Band
WCDMA	Wide-band CDMA
WLAN	Wireless Local Area Network

CHAPTER I

INTRODUCTION

1.1 Background

The wireless communications industry is growing rapidly in both fixed and mobile applications. During the 1990s, it has emerged as one of the largest sectors of the electronic industry, evolving from a niche business to one of the most promising areas for growth in the 21st century [54]. Now the wireless communications industry has evolved from providing voice-only services to being both data and voice oriented. Although improved compression technologies have decreased the bandwidth needed for voice communications, new data services like multi-media and Internet traffic are continuing to demand high-speed wireless data access ability [40]. Accordingly, new standards and technologies are continually proposed. In the third-generation (3G) mobile communication systems, data rates as high as 2.048 Mbps is required for indoor low-mobility users. For indoor wireless local area networks (WLANs), the IEEE 802.11a/g standards support a maximum data rate of 54 Mbps. The ultra wide band (UWB) specifications, which have been approved by the Federal Communications Commission (FCC) for a number of communication and sensing applications, are expected to provide reliable data rates exceeding 100 Mbps for short distance indoor applications [54]. However, these data rates of wireless networks are still low compared to that of the cable networks. Also in most of the practical environments, the actual data rates that can be realized in wireless connections are much lower than the theoretical maximum limits mentioned above. Wireless communication still has some limiting factors that hinder realizing any-where any-time high-speed network connections that consist of both

wireless and wired networks. As wireless systems continue striving for ever higher data rates, the goal becomes particularly challenging for systems that are power, bandwidth, and complexity limited. New wireless system structures supporting much higher data rates are therefore urgently needed.

The distinct characteristics of the wireless environment include fading effects and signal interference. Fading is caused by the changes in the channel environment. The fading phenomenon makes the strength of the received signal randomly change and causes burst symbol errors. Interference problems arise because the wireless channel is not guided. Thus signals from one wireless system may be picked up by the receiver of another wireless system if these two systems reside in the same frequency band. In some cases, the interference noise may exceed the thermal noise and become the most dominating factor limiting the performance of a wireless system. Traditionally, these two effects have been seen as deteriorative factors in wireless communication system design and thus need to be suppressed. For example, multiple antennas may be used at either the transmitter or the receiver end to increase the diversity in order to combat channel fading. In diversity systems, signals carrying the same information are transmitted through different paths. The receiver receives independently-faded replicas of the same symbol. Thus, more reliable receptions are realized [67]. Another method is to use smart antennas. Smart antennas are introduced based on the fact that the desired signal and the co-channel interference typically arrive at the receiver from different directions. By adapting antenna patterns in such a way that the main lobe is always pointing to the desired signal and the interference signals arrive at the nulls, the differences of arriving directions are exploited.

This method increases the signal-to-interference ratio (SIR), and thereby the system capacity is increased [50], [51].

The idea of the multi-input multi-output (MIMO) structure can be traced back to the 1980s [27]. But it was the pioneering work of Foschini [1], [26] and Telatar [15] in the late 1990s that proved the scattering effects in wireless channels can be incorporated in a single communication link and can contribute to an enormous capacity gain. They introduced a MIMO system where multiple antennas were mounted at both the transmitter and the receiver, and parallel data streams were transmitted and received at the same time. The system diagram is shown in Figure 1.1. This MIMO system structure was proven to have the potential to go far beyond any currently available wireless system. For example, given a MIMO system with n_t transmit antennas and n_r receive antennas, the system capacity can be increased up to $\min\{n_r, n_t\}$ times in a rich-scattering environment compared to a single transmit/receive antenna system. Data transmission and reception of the MIMO system occurs in the same way as solving n_t unknowns from a linear system of n_r equations. As long as $n_r > n_t$, the unknowns can be exactly recovered. The idea that the data is transmitted through a matrix channel rather than a vector channel creates enormous opportunities beyond just adding diversity or array gain. Because of this, MIMO systems are seen as one of the most significant technical breakthroughs in modern wireless communication. Now MIMO technology is being considered in wide-band CDMA (WCDMA) specification release 6 to further increase data rate in high speed packet downlink access (HSPDA), and it is widely believed that the MIMO structure will be used in the future fourth generation (4G) mobile communication systems.

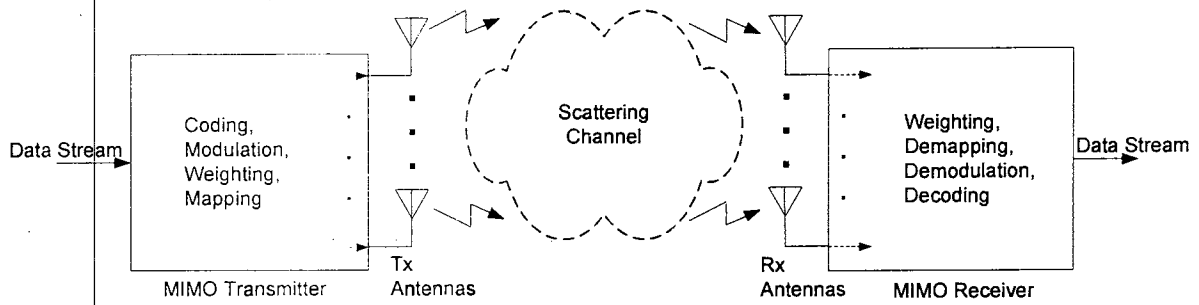


Figure 1.1 MIMO system diagram.

The key feature of a MIMO system is the ability to turn multi-path propagation, traditionally considered as a pitfall of wireless transmission, into a beneficial feature. Just as shown in the former works by Winters *et al.* [28], in independent flat Rayleigh fading wireless systems with N mutually interfering users, $N-1$ interferers can be nulled out and a $K+1$ path diversity improvement can be achieved for each of the N users by using $N+K$ antennas. Thus in independently distributed channels, rich multi-path fading provides multiple parallel channels between the transmitter and the receiver (both have multiple antennas). For fixed transmission power and bandwidth, simultaneously increasing the number of both transmit and receive antennas will open up multiple spatial sub-channels. Therefore, a multi-fold capacity increase can be achieved without increasing the transmission power and bandwidth. The MIMO system has been proven to be an effective way to improve system capacity in wireless data communications and it is seen as the 'final frontier' in wireless data communications [1]-[4]. MIMO systems have prompted progress in areas as diverse as channel modeling, information theory, coding, signal processing, antenna design. [25].

A strong analogous comparison of MIMO systems can be made with code-division multiple access (CDMA) systems where multiple users can transmit signals at the same time using the same frequency band. In CDMA systems, all transmitted signals mix up in the channel but they can be recovered at the receiver through their distinct spreading codes. However, the advantage of MIMO systems is that the unique signatures of input streams (“virtual users”) are provided naturally by the channel environment in a close-to-orthogonal manner without frequency spreading. Therefore, unlike CDMA systems, user signals in MIMO systems can be separated at no loss of spectral efficiency [25].

Orthogonal frequency-division multiplexing (OFDM) is another technology proposed to increase the data rates by efficiently opening up multiple frequency sub-channels [81]-[85]. OFDM has been successfully implemented in Hiperlan-2 and IEEE 802.11a/g to provide high-speed data communication [86]. However, in OFDM the whole frequency band is divided into multiple frequency sub-bands, each of them is used as a sub-channel to transmit parallel data. Therefore, each sub-channel in an OFDM system just uses a small portion of the whole bandwidth. Thus the system capacity is not comparable with the capacity of MIMO systems, where all sub-channels use the whole bandwidth to transmit data.

1.2 Motivation

Although linear capacity increase is predicted in MIMO systems when the number of transmit antennas and receive antennas increase, this capacity has been shown to be difficult to achieve in practical systems. One of the main reasons is that in real wireless propagation environments, the faded signals are correlated due to insufficient antenna

spacing or lack of local scatters [31]. The correlation effect among antennas can significantly reduce the channel capacity compared to the independently and identically distributed (i.i.d.) fading phenomena [30], [31], [37], [39].

Another important reason is the reduction of received signal-to-noise ratio (SNR). MIMO systems use multiple antennas in a different way from diversity systems. As explained earlier, in diversity systems, multiple antennas are used to obtain different faded versions of the same symbol and combine or select them to get the highest SNR. In MIMO systems, however, multiple antennas are used to generate multiple space sub-channels to transmit multiple parallel signals. Multiple information streams can be seen as being transmitted through different space sub-channels and received at the receiver separately. As more space sub-channels are generated, less signal power is allocated to each sub-channel under the constraint that the total transmission power remains the same. As shown in [43] and [44], multiple antennas at the transmitter side and the receiver side can be used either for signal diversity, or for space multiplexing. For a MIMO system with given number of transmit antennas and receive antennas, the implementation of the system requires a trade-off between diversity gain and multiplexing gain.

As shown in [44], for MIMO systems with n_t transmit antennas and n_r receive antennas, the maximum spatial multiplexing gain that can be achieved is $\min\{n_r, n_t\}$. In practical systems, the number of antennas at a mobile terminal (MT) is usually limited because of the space and power restrictions. In this case, although more antennas can be mounted at the base station (BS), all it does is provide an increase in the SNR instead of creating extra spatial sub-channels. Furthermore, since all these BS antennas are at the same location, they experience the same shadowing effect. The different signal replicas

received at the BSs still have the same local mean. Once the MT is obstructed by some big objects, all these replicas will experience the same deep shadowing effect. This scenario is shown in Figure 1.2 for a cellular system.

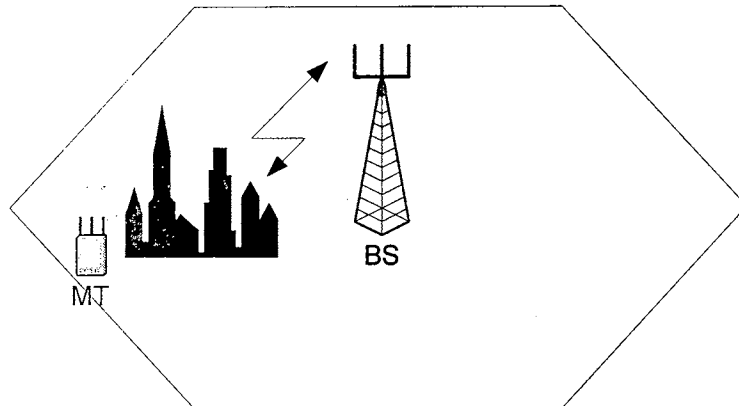


Figure 1.2 MIMO mobile communication systems experiencing shadowing effect.

Large-scale shadowing is a fading effect that represents the variation of the local mean power of the received signal. It is a random variable due to the shadow variations caused by large terrain features between the BS and MT, such as buildings and hills. In the situation shown in Figure 1.2, all BS antennas are at the same location. Thus all signals from BS to MT experience the same shadowing effect. Although diversity can average out the deep small-scale fading, the single BS topology can do nothing to mitigate the deep large-scale shadowing effect. Thus the received SNR will be very low and the data rate will be significantly reduced. This is a very serious practical problem but it has not drawn much attention from researchers so far.

In this dissertation, we propose to use macroscopic diversity in MIMO systems to take advantage of multiple shadowing components. By placing transmit antennas at different BSs as shown in Figure 1.3, it is very unlikely that their shadowing factors are

correlated to each other [119]. This system will greatly reduce the deep shadowing effect experienced by the one-BS system. This is why a large-scale shadowing diversity performance gain can be obtained.

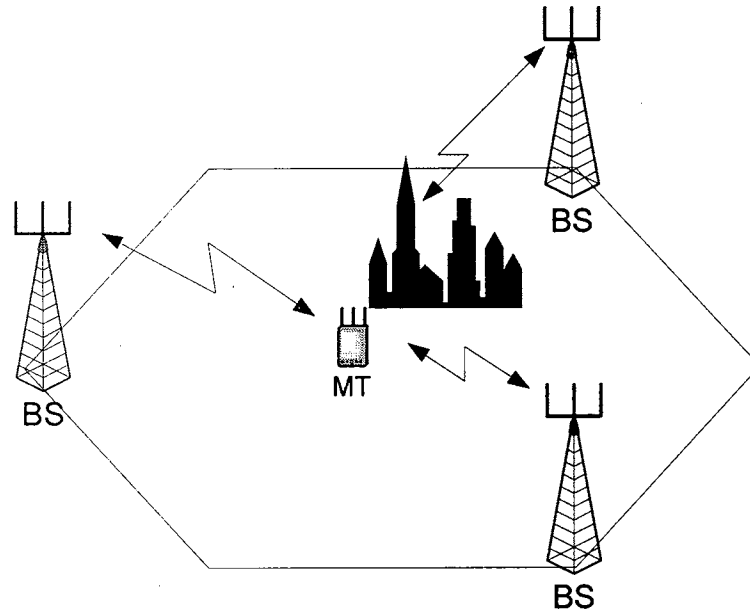


Figure 1.3 Macroscopic diversity MIMO systems.

The whole macroscopic diversity MIMO system in Figure 1.3 can be treated as several standard MIMO systems, with each system realizing multiplexing gain individually. Then macroscopic diversity gain is realized amongst all BSs after signal reception. In this way, the chance of deep small-scale fading and deep large-scale shadowing can be greatly reduced and the SNR value in each sub-channel becomes much higher and more stable. Thus the multi-fold data rate increase predicted for MIMO systems will be much easier to realize in a practical system. However, before being able to make investment to the macroscopic infrastructure, there must be solid evidence of the

obtainable performance gain. In addition, the performance gain must be quantifiable, which becomes one of the objectives of this dissertation.

1.3 Dissertation Outline

In this dissertation, the development of broadband mobile communication technology is analyzed and the future MIMO system structure is studied. The objective of this research is to advance the MIMO research in several areas, with the focus of how to more effectively implement MIMO systems in practical environments. The remainder of this dissertation is organized as follows.

Chapter II gives a historic overview of the cellular mobile communication systems. Starting from first generation (1G) mobile systems, the standards and their corresponding technologies are explained during this evolution process leading all the way to 2G and 2.5G technologies. The newly-implemented third generation (3G) mobile system is studied in detail. The technologies applied in 3G systems to provide high-speed data access is reviewed. It is shown that the performances provided by current 3G standards are still limited in terms of providing MT users the comparable experience as wired users. MIMO technology, with its ability to provide unprecedented spectral efficiency in wireless channels, is introduced and expected to be used in future mobile systems.

In chapter III the fundamentals of MIMO systems are studied. Capacity equations are derived to show the linear capacity increment in both single cell and multi-cell environments. The MIMO system capacity is compared with the capacities of the traditional diversity systems to show the extraordinary increase. Then, adaptive modulation is introduced in MIMO systems to maximize the practical data rate. Two different approaches for realizing adaptive modulation in MIMO systems are

investigated. It is shown that in MIMO systems, the adaptive data rate is in the same form as that of the capacity. Therefore, they can be analyzed in a similar way. The adaptive data rates of MIMO systems with transmission power and bit error rate (BER) constraints are evaluated.

Initial investigations on MIMO systems were conducted under the assumption that all pairs of transmit-receive antennas have independent fading. However, in real propagation systems, the fades are correlated to each other due to, for example, insufficient antenna spacing or the lack of local scatters. The spatial correlation model applied in this dissertation is introduced in chapter IV. The effects of correlation in MIMO systems are studied and its deteriorate effects are demonstrated. Because the MIMO capacity can be easily calculated by using eigenvalues of the channel matrix, an investigation is conducted focusing on deriving the eigenvalue distributions of MIMO systems in the correlated fading case. The general case eigenvalue distribution is derived and a numerical method is verified for future research.

Chapter V proposes the macroscopic diversity MIMO system and studies the performance of this system. The capacity upper bounds of MIMO systems with and without macroscopic diversity are derived. It is shown that this bound effectively reflects the effects of having multiple BSs in MIMO systems, which is the system configuration proposed. The capacity difference between standard MIMO systems and macroscopic diversity MIMO systems is compared by theoretical analysis as well as Monte-Carlo simulation. Significant throughput improvements are observed by using macroscopic diversity techniques for MIMO systems.

Former research has shown that correlation effects significantly reduce the MIMO system capacity and the effective way to combat correlation is to increase antenna spacing. However, in chapter VI we show that once large-scale shadowing is considered, the effect of small-scale correlation becomes less significant, and it also becomes difficult to increase system capacity just by increasing antenna spacing. The reason for these changes is that all sub-channels share the same shadowing component. Based on this observation, the macroscopic selection diversity (MSD) topology is enabled in MIMO systems to maximize the spatial multiplexing gain while combating the shadowing phenomena. Two BS selection algorithms are presented and their exact capacity representations are derived. The first algorithm is optimal but requires high-levels of computation. The second algorithm presented is suboptimal, but requires much less complexity. The proofs of optimality and suboptimality are also provided with a performance comparison of the two algorithms. Significant performance improvements are demonstrated by both algorithms.

Chapter VII gives the conclusion and future research topics. The research directions such as OFDM MIMO systems and cross-layer optimization in MIMO wireless networking systems are introduced.

1.4 Research Flowchart

The research flow is shown in Figure 1.4. The main steps are represented in grey blocks; the assisting steps are shown in white blocks on the right and explanations are included on the left. In the same order as mentioned above, the research begins at the research of the MIMO capacity, and then practical data rate. Correlation effects and other

problems in MIMO systems are investigated and the macroscopic diversity MIMO system is proposed as the effective way to mitigate these problems. In future research, to consider a more practical channel in high data-rate communication systems, frequency-selective channels will be studied where the OFDM modulation method will be combined with the MIMO structure to optimize the system performance.

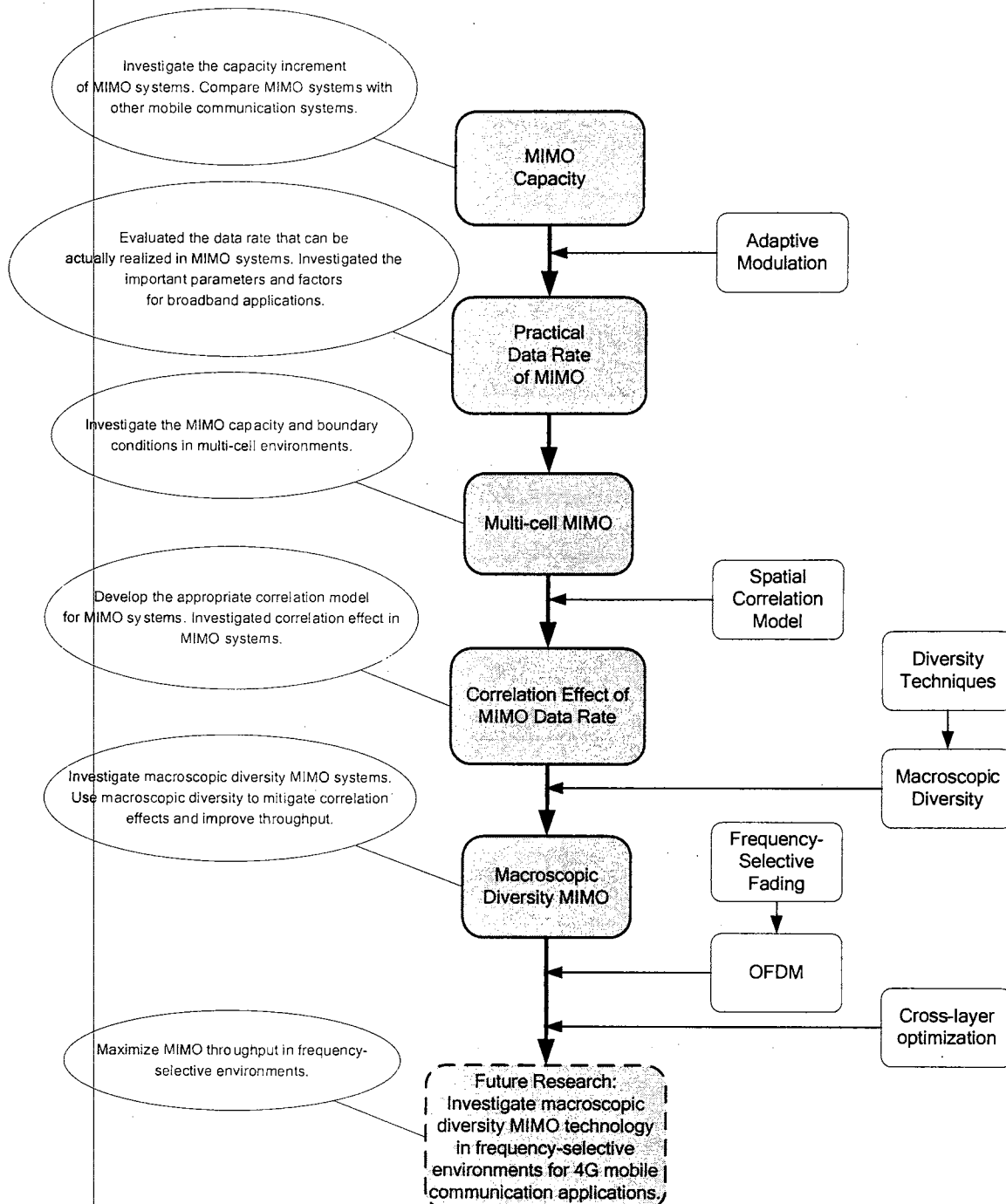


Figure 1.4 Research flowchart.

CHAPTER II

EVOLUTION OF CELLULAR SYSTEMS

Cellular mobile communication systems started in the early 1980s by using analog modulation. Over the past 25 years of development, cellular systems have gone through different generations. Technology advances in voice coding, error control coding, and modulation, have given new systems a much higher user data rate and level of security. In this chapter, we will go through the evolution path from the first generation (1G) mobile system to the 3G mobile system.

2.1 Evolutions of 1G and 2G Systems

2.1.1 The First Generation (1G) Systems

The basic concept of cellular phones came out in 1947 when researchers at AT&T Bell Labs realized that using small cells of service areas and frequency reuse across cells could substantially increase the traffic capacity of mobile phones. After that, it took more than 20 years to realize the technology and get the frequency bands allocated by FCC. In 1977, AT&T Bell Labs constructed and operated a prototype cellular phone system. The commercial deployments of the first generation (1G) of mobile cellular telecommunication systems started in early 1980s. These systems became popular very soon. Using frequency-division multiple access (FDMA) and analog FM modulation, 1G systems were almost entirely for voice traffic. The cellular concept used in these systems gave much higher capacities than former mobile systems, and for the first time in history, the concept of a telephone being at a fixed point in the network was no longer valid [100].

There was no dominant 1G standard. Several different systems existed around the world. In America, the Advanced Mobile Phone Service (AMPS) was used in the 850 MHz frequency band, with each channel occupying 30 KHz. In Europe, the Nordic Mobile Telephony (NMT) was originally used in the 450 MHz band. Later another version known as NMT900 was introduced in the 900 MHz band. The British proposed the Total Access Communications System (TACS) standard in the 800 MHz band based on AMPS.

The 1G systems experienced successes far greater than anyone had expected. But people also realized various inherent problems like limited capacity and security and quickly started to look for better system structures and designs, which lead to 2G models.

2.1.2 The Second Generation (2G) Systems

The second generation (2G) mobile cellular systems use digital radio transmission techniques. It brought great improvements in various aspects of 1G systems to 2G systems, such as:

- Improved capacity, coverage, performance/quality and reliability
- Authentication
- Improved security (encryption)
- Enhanced services, such as, packet-switched data service, short message service (SMS), and paging service.

As in 1G systems, different kinds of 2G systems have been proposed and implemented. The four main standards are: Global System for Mobile Communications (GSM), Digital AMPS (D-AMPS), CDMA IS-95, and Personal Digital Cellular (PDC).

A. GSM

GSM was launched in 1991 and was originally designed as a pan-Europe standard. But it was quickly adopted around the world and became the most widely used 2G system. The basic GSM uses the 900 MHz band. At the request of the United Kingdom, a derivative is included in the specification to use the 1800 MHz band [103]. It is called the Digital Cellular System at 1800 MHz (DCS-1800, also know as GSM-1800). In North America, GSM is used in the 1900 MHz band and is called PCS-1900 (also know as GSM-1900). GSM uses time-division multiple access (TDMA) technology with 8 users sharing one 200 kHz channel. GSM uses paired uplink and downlink frequency bands for full-duplex transmission.

B. D-AMPS

D-AMPS is also called TDMA in America. It was first defined in the interim standard IS-54 and introduced in 1990. It uses digital channels for voice but analog channels for control. It is backward compatible with the analog AMPS system and operates in the 850 MHz band. In 1994, an all-digital version was defined in IS-136. Besides the 850 MHz band, IS-136 systems can also operate in the 1900 MHz band.

C. IS-95

CDMA was never considered a viable technique for cellular systems until 1989 when Qualcomm Inc. conducted a demonstration at San Diego, California, and showed its great potential of higher capacity, better voice quality and simplified system planning. The CDMA system started late when other 2G systems were already in place, but developed very fast. It was standardized as IS-95 in the year 1993 and was implemented in the same frequency band as AMPS systems in an effort to enable the handsets to switch between IS-95 systems and AMPS systems. The first commercial IS-95A network was deployed in 1996 by Hutchison in Hong Kong. With the introduction of Personal Communications Systems (PCS) in the United States, CDMA technology was made to operate in the 1900 MHz PCS bands. This version is called CDMA-PCS.

After that, the ANSI-J-STD-008 specification was published in 1995 to define a compatibility standard for 1.9 GHz CDMA-PCS systems. TSB-74 describes interaction between IS-95A and CDMA-PCS systems that conform to ANSI-J-STD-008. IS-95B revision combines IS-95A, ANSI-J-STD-008, and TSB-74 into a single document. In the downlink, up to eight Walsh codes can be assigned to the high data rate users [103]. IS-95B was first deployed in 1999 in South Korea. Nowadays, many operators have commercialized IS-95B systems offering 64 K bits per second (bps) packet-switched data in addition to voice services. Due to the high data speeds of IS-95B, it is categorized as a 2.5G technology.

QPSK modulation is used for all the channels in both uplink and downlink in IS-95 systems. In both cases, the same information symbols are multiplied by different in-phase (I) PN codes and quadrature-phase (Q) PN codes [103]. This is different from the

conventional QPSK modulation. For downlink, a pilot channel from the BS enables coherent demodulation at the MT. For uplink however, coherent demodulation is impossible because no pilot channel is available, therefore, offset QPSK (OQPSK) is used in the uplink transmission.

D. PDC

PDC is the Japanese 2G standard. It operates in the 800 MHz and 1500 MHz frequency band and is used only in Japan.

E. Comparisons

The four main 2G standards are listed and compared in the following table.

	GSM	IS-54/136	IS-95A	PDC
Multiplexing Scheme	FDD TDMA/FDMA	FDD TDMA/FDMA	FDD CDMA/FDMA	FDD TDMA/FDMA
Carrier Spacing	200 KHz	30 KHz	1.25 MHz	25 KHz
Time Slots per Frame	8/16	6/3	1	6/3
Modulation Scheme	GMSK	$\pi/4$ -DQPSK, 8PSK	QPSK (DL) OQPSK (UL)	$\pi/4$ -DQPSK
Channel Coding	1/2 CC	1/2 CC	1/2 CC (DL) 1/3 CC (UL)	1/2 BCH
Data rate	9.6 Kbps 14.4 Kbps	9.6 Kbps	9.6 Kbps 14.4 Kbps 64 Kbps(95B)	9.6 Kbps CSD 28.8 Kbps PSD

Table 2.1 Comparison of 2G systems.

Although the 2G systems provided significant improvements over 1G systems, they were still designed primarily for voice traffic. With typical data rates from 9.6 Kbps to 14.4 Kbps, it is sufficient to send text messages with tens or hundreds of characters, but incapable to handle multimedia pictures or other big attachment files. As wireless

networks are to be integrated with the Internet, much higher data transmission capabilities are required.

2.2 3G Systems

The initial work towards 3G was originally known as Future Public Land Mobile Telecommunications Systems (FPLMTS) [101]. It was proposed by the International Telecommunication Union (ITU) to be a single, unified, worldwide standard. The name was later changed to International Mobile Telecommunications-2000 (IMT-2000). The technical motivations behind this proposal are:

- Provide high-speed packet/circuit-switched data access.
- Improve voice capacity.
- Provide global roaming capability.
- Provide position location services.

The minimum required specifications of 3G systems are listed in Table 2.2.

Basic Specifications	Indoor	Indoor to Outdoor Pedestrian	Outdoor Vehicular
Mobility	Low	Medium	High
Data rate	≥ 2048 Kbps	≥ 384 Kbps	≥ 144 Kbps

Table 2.2 Basic requirements for 3G systems.

2.2.1 Review of 3G Standards

Different 3G versions arose during the standardization process. In 1999 ITU approved five radio interfaces for IMT-2000 as a part of the ITU-R M.1457 Recommendation. Three of them are CDMA based and the other two are TDMA based. These five standards are described in the following [102].

A. IMT-2000 CDMA Direct Spread

This standard is also known as Wideband CDMA (WCDMA). It is the European version of the 3G standard. WCDMA shares the same core network with GSM, and provides smooth transition for the dominant GSM systems to 3G. WCDMA is also referred to as UMTS, which stands for Universal Mobile Telecommunications System.

B. IMT-2000 CDMA Multi-Carrier

This is the United States' version of the 3G system. The main force behind it is Qualcomm, Inc. This standard is also known as CDMA2000, it is a successor to IS-95. Sharing the same IS-41 core network structure and even some air interface specifications, CDMA2000 provides a natural 3G evolution for the IS-95 systems. CDMA2000 is also very attractive to the IS-136 operators because they have the same IS-41 core network. Although both CDMA2000 and WCDMA are based on CDMA technology, they are incompatible to each other.

C. IMT-2000 CDMA TDD

This standard mainly refers to the Time Division Synchronous CDMA (TD-SCDMA), which is a 3G standard being pursued in China. It is based on CDMA technology, and provides an economical way for current GSM operators to evolve to 3G. Different from the frequency-division duplex (FDD) scheme used in the former two 3G standards, TD-SCDMA uses the TDD scheme to separate uplink and downlink. This makes it very suitable for asymmetric traffic support.

D. IMT-2000 TDMA Single Carrier (SC)

This standard is also known as UWC-136 (Universal Wireless Communications) or EDGE (Enhanced Data Rates for GSM Evolution). It is proposed to provide extended data for GSM and TDMA-136 without changing channel structure, frequency, or bandwidth.

E. IMT-2000 Frequency Time (FT)

Also known as Digital Enhanced Cordless Telecommunications (DECT), it is an ETSI standard for digital portable phones, commonly for domestic or corporate use.

2.2.2 3G Standards Bodies

Many regional, national and international standardization organizations have been participating in the 3G standardization processes and technology promotions. A list of the main regional and national groups is as follows.

- United States:
Telecommunication Industry Association (TIA)
Alliance for Telecommunications Industry Solutions (ATIS)
- Europe:
European Telecommunications Standards Institute (ETSI)
- Japan:
Association of Radio Industries and Businesses (ARIB)
Telecommunication Technology Committee (TTC)
- Korea:

Telecommunication Technology Association (TTA)

- China:

China Wireless Telecommunication Standard (CWTS)

China Communications Standards Association (CCSA)

These national and regional standardization bodies are collaborating in two main 3G partnership projects:

- The 3rd Generation Partnership Project (3GPP)

It is a collaborative organization established in December 1998. It works on the WCDMA standard. European companies are the main forces behind 3GPP. The current organizational partners are ARIB, ATIS, CCSA, ETSI, TTA, and TTC.

- The 3rd Generation Partnership Project 2 (3GPP2)

It is a collaborative organization established in January 1999. It comprises North American and Asian interests for developing 3G specifications based on ANSI-41 core network and relevant radio access technologies. There are five officially recognized standards development organizations (SDO) in 3GPP2: ARIB, CCSA, TTA, TTA, and TTC.

2.3 Evolution to WCDMA and CDMA2000

2.3.1 Current Status

Since the acceptance of the five 3G proposals in the IMT-2000 standard, there has been dramatic progress in 3G implementations. WCDMA and CDMA2000, supported by the 3GPP and 3GPP2 respectively, are currently in the front positions. Their commercial networks have already been launched around the world.

TD-SCDMA currently lags behind the former two standards. Its commercial products are expected to be available in mid 2005. The IMT-SC proposal was supported by Universal Wireless Communications Consortium (UWCC), but this organization has changed to IMT-DS as its 3G standard. The remainder of this chapter will focus on WCDMA and CDMA2000 technologies. Key features of these two standards are listed below [9], [105], [106]–[113].

Specifications	WCDMA	CDMA2000
Channel Bandwidth	5 MHz	1.25 MHz
Frequency Band	1920-1980 MHz (UL) 2110-2170 MHz (DL) for Europe and Africa	Operates in all existing allocated spectrum such as 450 MHz, 700 MHz 800 MHz, 900 MHz
	1850-1910 MHz (UL) 1930-1990 MHz (DL) for America	1700 MHz, 1800 MHz 1900 MHz, 2100 MHz
Chip Rate	3.84 M chips/s	1.2288 M chips/s
Core Network	GSM MAP based network	IS-41 based network
Partnership group	3GPP	3GPP2
Modulation	QPSK	QPSK, 8 PSK, 16 QAM
Channel Coding	Convolutional coding Turbo coding	Convolutional coding Turbo coding
Power Control	1500 Hz	800 Hz
BS Synchronization	Synchronous/Asynchronous	Synchronous (GPS)

Table 2.3 Comparison of WCDMA and CDMA2000 standards.

2.3.2 Evolution to 3G

According to the standards of current 2G systems, different paths can be adopted for their evolution to 3G systems. An illustration of the evolution paths is shown in Figure 2.1.

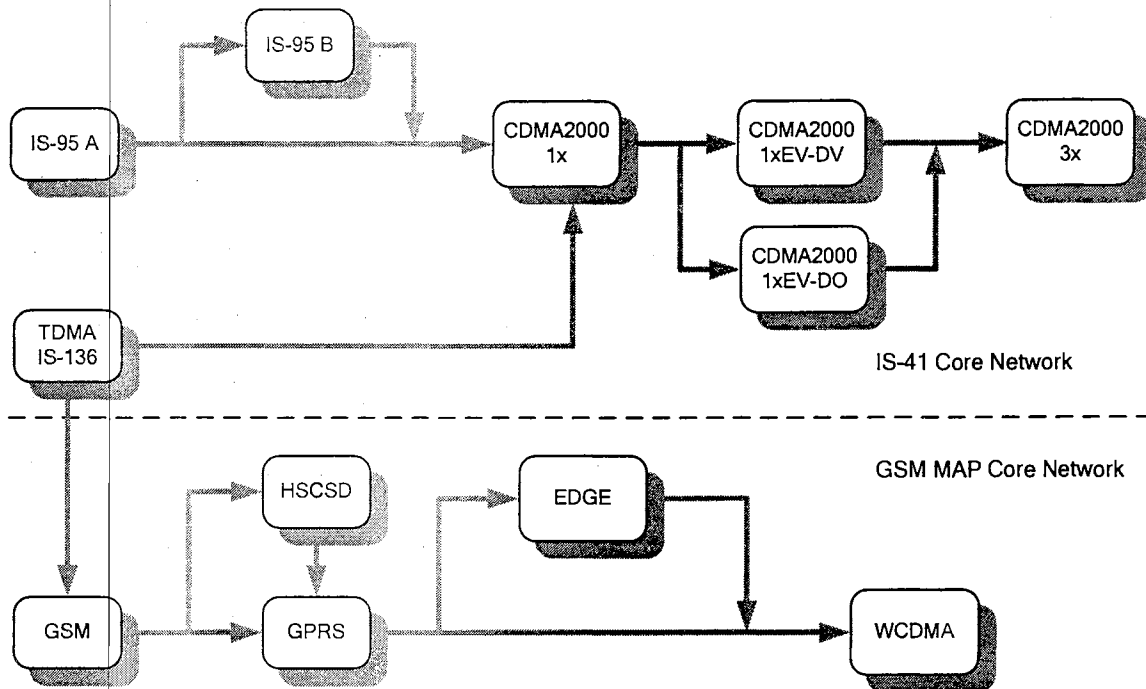


Figure 2.1 Evolution paths to 3G.

A. Evolution path for IS-95

For the current IS-95 systems, CDMA2000 is the natural choice of 3G evolution. There is a two-phase migration path: IS-95B and CDMA2000.

The key advantage of IS-95B and CDMA2000 for existing CDMA operators is the preservation of capital investments. Both IS-95B and CDMA2000 will maintain backward compatibility with existing IS-95 infrastructure. In order to maintain this backward compatibility, both IS-95B and CDMA2000 will be based on synchronous BS operations and will continue to support 20 ms frames and 800 times per second closed-loop power control on the uplink. At the same time, new CDMA2000 specifications with advanced features are continuously being published for better performance of the system.

1) CDMA2000 1xRTT (Radio Transmission Technology)

CDMA2000 1xRTT is the basic layer of CDMA2000. It nearly doubles the voice capacity over the 2G CDMA networks and offers a peak data rate of 307 Kbps in mobile environments. Although 1xRTT officially qualifies as 3G technology, it is still mostly considered to be 2.5G as it is not as fast as the newer 3G systems.

2) CDMA2000 1xEV (Evolution)

CDMA2000 1xEV is CDMA2000 1x with High Data Rate (HDR) capability added. 1xEV is commonly separated into two phases:

- Phase 1: 1xEV-DO (Data Optimized) supports downlink data rates up to 3.09 Mbps and uplink data rates of 154 Kbps. 1xEV-DO has been commercially deployed around the world beginning from 2004.
- Phase 2: 1xEV-DV (Data and Voice), supports downlink data rates up to 3.09 Mbps and uplink data rates of up to 451 Kbps. 1xEV-DV is backward compatible with 1x system and can also support 1x voice and data users.

3) CDMA2000 3x

CDMA2000 3x is planned to use a 3.75 MHz spectrum bandwidth (3×1.25 MHz) to provide even higher data rate support.

A comparison of the data rates and modulation schemes of the systems used along this evolution path is shown in Table 2.4.

Basic Specifications	IS-95A	IS-95B	CDMA2000 1x	CDMA2000 1xEV-DO	CDMA2000 1xEV-DV
Data Rate	14.4 Kbps	115 Kbps	307 Kbps	3.09 Mbps	3.09 Mbps
Modulation	QPSK	QPSK	QPSK	QPSK 8 PSK 16 QAM	QPSK 8 PSK 16 QAM

Table 2.4 Evolution of IS-95 systems.

B. Evolution path for GSM

WCDMA is the choice of 3G technology for GSM operators. GSM networks will enhance packet data services possibly in three phases. First, General Packet Radio Services (GPRS) can be used to connect MT users to IP or X.25 based networks. Then the Enhanced Data Rates for GSM Evolution (EDGE) provides high data rate of 384Kbps by aggregating all eight timeslots in a frame for one user. Finally, WCDMA provides a new air interface for GSM networks to meet or exceed the requirements of IMT-2000 specifications. High speed packet downlink access (HSPDA) will be used for high-speed data services. It is expected to offer data rate up to 8-10 Mbps using a 5 MHz bandwidth in WCDMA downlink. A comparison of data rates and modulation schemes of the systems used along this evolution path is shown in Table 2.5.

Basic Specifications	GSM	GPRS	EDGE	WCDMA	HSDPA
Data Rate	9.6 Kbps 14.4 Kbps	115.2 Kbps	384 Kbps	2.048 Mbps	10 Mbps
Modulation	GMSK	GMSK	8 PSK	QPSK	QPSK 16 QAM

Table 2.5 Evolution of GSM systems.

C. Evolution path for TDMA

The evolution path for the North American standard TDMA is not as clear as the former two 2G systems. It may go directly to CDMA20001x because they share the same core network architecture; or it may take the two phase migration path as defined by UWC-136. In the first phase, referred to as 136+, significant enhancement will be made to allow for improved voice and data over the existing 30 KHz carrier. The second phase,

referred to as 136 High Speed (136HS), will implement the EDGE standard to meet the 3G requirements.

2.4 Case Study of Capacity and Data Rate

2.4.1 Evolution of System Capacity

A. AMPS:

AMPS has 25 MHz bandwidth each for uplink and downlink. By using a 30 KHz channel spacing, the overall bandwidth will be divided into $25000/30 = 832$ channels + guard bands. If the frequency reuse factor $K = 7$, the maximum number of users is $832/7 = 118$ users/cell.

B. D-AMPS:

Although using the same bandwidths and channel spacing as AMPS, the D-AMPS divides one frame into 6 time slots. By multiplexing different MT users into these slots, the maximum number of users is automatically increase by 6 times (1 slot per user) or 3 times (2 slots per user) compared to AMPS.

C. IS-95:

For backward compatibility, IS-95 uses the same bandwidths as AMPS. However, IS-95 uses a much larger channels spacing of 1.25 MHz to spread the signal spectrum. So there are $25/1.25 = 20$ frequency channels. Each frequency channel has a chip rate of 1.2288 Mcps, which equals to a 128 code rate for a 9.6 Kbps data transmission. Theoretically, a 128 orthogonal Walsh code can be used to provide access to different MT users. Because CDMA systems use universal frequency allocation with $K = 1$, the

maximum number of users is $128 \times 20 = 2560$ users/cell, which is more than 20 times greater than the number of users in AMPS. However, in practical systems, the number of users supported in IS-95 is generally 6 to 10 times larger than AMPS.

C. CDMA2000:

New technologies are being developed and deployed to further boost the capacity of 3G networks. These include the new voice codec, antenna diversity at both BS and MT, and the smart antenna technologies. It is shown that in the practical systems, CDMA2000 1x doubles the capacity of the IS-95 networks in terms of the maximum number of voice calls supported.

2.4.2 High Data Rate in CDMA2000 1xEV-DO

CDMA2000 1xEV-DO focuses on providing high-speed data connections in downlink channels. In the system, time is measured in frames, with each frame having a time interval of 26.67 ms. This time period is divided into 16 slots with a slot duration of 1.67 ms. A data packet spans an integral number of slots by an interlacing technique, and may be early-terminated at the end of any slot. A frame structure is shown in the Figure 2.2. It shows that one slot is further divided into two half slots with the same structure. The total number of chips in one slot is 2048, which includes 192 chips for the pilots, 256 chips for the MAC layer, 1536 chips for the traffic data and 64 chips for the data preamble. The chip rate of this system can be calculated as $(1536 + 64 + 192 + 256) / 16.666 = 1.2288$ Mcps, which is the standard chip rate for CDMA20001x.

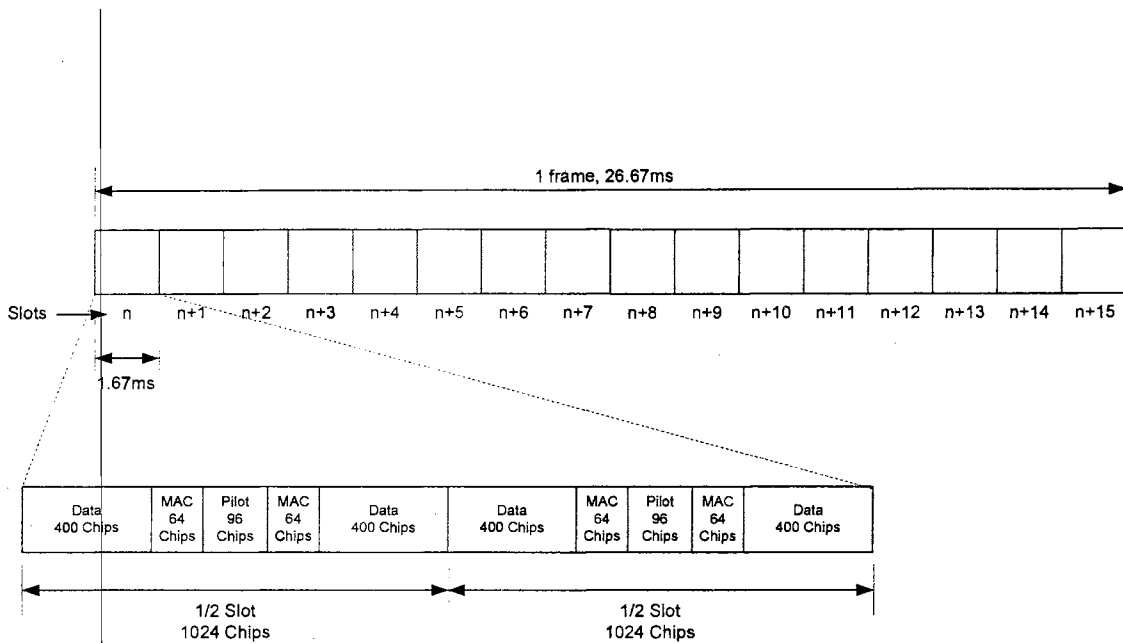


Figure 2.2 Frame structure in CDMA2000 1xEV-DO.

The nominal highest data rate in 1xEV-DO is realized by sending 4096 bits of data within one slot, i.e., $4096/1.666 = 2.457$ Mbps. This data stream goes through a 1/3 Turbo encoder and 16 QAM modulation. The number of symbols after that becomes $4096 \times 3 \times 1/4 = 3072$. These symbols are multiplied by the 1536 traffic chips with a rate of 2 bits/chip and multiplexed into the frame structure.

Besides putting more data into one time slot, other methods also have been used to increase the data rate in 1x EV-DO systems. Some of these methods are listed below [113]–[115].

- 1) Link adaptation: Allocating the transmission data rate (possibly power, code channels) in an efficient manner in response to channel variations. These parameters are decided before the packet transmission by considering the current channel condition and the data rate the MT requested, and are encoded in the packet for the MT to correctly decode the data.

- 2) Hybrid ARQ: Forward Error Correction (FEC) Turbo coding and Automatic Retransmission Request (ARQ) are implemented at the physical layer. Compared with higher-layer re-transmission schemes, a much shorter round-trip delay is achieved. Bit repetition, coding, and interleaving are used for the transmitted packet, so it is possible for the receiver to succeed in decoding the packet even before it is entirely received. In this case, at the end of this slot, the receiver can inform the sender to stop sending the remaining part of the packet. This early termination leads to a decrease of packet duration and consequently an increase of the data rate.
- 3) Multi-user diversity: In EV-DO networks, a time-division multiplexing (TDM) scheme is used to provide data access to a number of MT users. At a given time, the BS selects the MT based on the packet type requested by the MTs and the current channel condition to each MT. This diversity scheme takes advantage of uncorrelated channel variations of different MTs, and seeks to serve each user at a local peak of its channel fading process [114]. Therefore, the system overall throughput increases as the number of users increase in the system.

2.4.3 Discussion

From the above analysis, it is observed that the 2.457 Mbps nominal maximum data rate is the data rate of the overall system. If one MT is to receive a continuous 2 Mbps data stream, no other users can be supported anymore. In practical system applications, the individual user actual data rate will be less than 2.457 Mbps divided by the number of users simultaneously requesting high-speed data services. This is generally the case for

all multiple access schemes. But the 2.457 Mbps data rate still needs to be greatly improved in order to match the speeds of the wired networks. The future generation of wireless systems is targeted at 100 Mbps data rate in outdoor environments and 1 Gbps for indoor channels [116]. This goal is far beyond what can be achieved by the current technologies used in 3G systems.

Another observation in EV-DO is that for the 2.457 Mbps transmission, the bit rate of data is already faster than the 1.2288 Mcps chip rate. Generally speaking, very small or no spectrum spreading exists in 3G systems for its high data rate modes. This means that there is no processing gain and the transmitted signals are very susceptible to interference. Processing gain can be improved by allocating wider frequency bands and accordingly using faster chip codes. If the bandwidth is fixed, however, the only way to improve the processing gain will be to reduce the data symbol rate.

On one hand, a much higher data rate is needed to improve the user's experience and to support new multimedia services; on the other hand, a lower symbol rate is preferred to ensure the quality transmission. A high bandwidth-efficient modulation scheme is required for the future wireless communication systems. As the symbol constellation can not arbitrarily increase in the traditional QAM modulation, a new MIMO system structure is very promising in increasing the spectral efficiency. As mentioned in chapter I, MIMO systems create multiple spatial sub-channels and transmit multiple data streams simultaneously. Thus low data rate transmission can be used in each sub-channel while the overall high data rate can still be achieved. The MIMO system structure is already being considered for future specifications in 3GPP and 3GPP2 groups. For example, the

future specification release from 3GPP may use MIMO technology in HSPDA to support a data rate of up to 20 Mbps.

2.5 Summary

A review of the cellular communication system history is given in this chapter and the applied technology of each evolution is analyzed. Technology enhancements used in 3G systems are explained, and the methods to increase user capacity and data rate are investigated. While the current 3G standards were designed to provide high-speed data services, the original goals of these standards were set too low to integrate the wireless handsets into Internet and give MT users an experience comparable to the wired users. Therefore, new technologies that significantly improve the wireless link performance need to be exploited. MIMO technology, with its ability to provide unprecedented spectral efficiency, is widely expected to be used in future mobile systems. The theory and implementation issues of MIMO systems will be studied in detail in the following chapters.

CHAPTER III

BACKGROUND RESEARCH IN MIMO SYSTEMS

3.1 MIMO System Introduction

Fast fading is a common effect representing the microscopic aspect of the wireless channels. Due to the motion of the transmitter/receiver or the objects in the surrounding environment, the signals at the receiver side exhibit random changes. When the receiver is surrounded by rich scatters, different fading characteristics are usually observed over distances of about half the wavelength [4]. Traditionally, fading effect in wireless communications has been seen as a deteriorative factor. Many schemes, e.g. diversity, have been used to combat the fading effect and improve the system performance. However, the pioneering works shown in [1] by Foschini and [15] by Telatar proved that this effect can be used in MIMO systems to greatly improve the system capacity. In a MIMO communication link where both the transmitter and the receiver have multiple antennas, each transmit/receive antenna link has its own distinct fading characteristic. With the help of signal processing, multiple spatial sub-channels can be opened up between the transmitter and the receiver. Through these channels, parallel data streams can be simultaneously sent out at the transmitter and recovered at the receiver. In this way, the capacity increases linearly with the number of transmit and receive antennas.

The Shannon capacity equation gives the maximum possible throughput of a system and is computed by $C = B \log_2(1 + \text{SNR})$, where B is the channel bandwidth and SNR is the signal-to-noise power ratio [48], [49]. This equation shows several ways to improve the capacity of a communication system:

- 1) Increasing the SNR value: This can be done by increasing the transmission power or using diversity methods. There are two things to consider in regards of this. First, increasing the SNR value only gives a logarithmic increase in capacity. Second, the maximum transmission power is limited by the FCC regulations. Also, in an interference-limited system, increasing the transmission power will also increase the interference power. These two increments occurring together have a tendency to cancel out each other and give no performance gain to the system.
- 2) Increasing the bandwidth: Increasing the bandwidth allows higher data rates. However, the thermal noise power and its vulnerability to interfering signals will also increase. Thus the extent of this capacity increase is limited. Also this increase in the data rate will not increase the spectral efficiency. Furthermore, as mentioned above, the bandwidth for specific implementations are strictly defined by FCC regulations.

In MIMO systems, on the other hand, there is no need to increase the transmission power/bandwidth to increase the capacity of the channel. Since multiple antennas are used at both the transmitter and receiver, multiple space sub-channels can be opened up by signal processing techniques. So, theoretically the MIMO system capacity can be increased almost linearly with the number of antennas without limit. This potential capacity increase makes the MIMO system a very promising structure for future high-speed wireless communications.

3.2 MIMO System Capacity

Here we consider a point-to-point wireless channel with n_t antennas at the transmitter end and n_r antennas at the receiver end. Signals transmitted between different transmitter/receiver pairs are assumed to experience i.i.d. fading.

3.2.1 Capacity Derivation

In MIMO systems, the n_r -dimensional received signal vector \mathbf{y} can be expressed as:

$$\mathbf{y} = \mathbf{H}\mathbf{x} + \mathbf{n} \quad (3.1)$$

where \mathbf{x} is the n_t -dimensional desired signal from the transmitter, \mathbf{H} is the $n_r \times n_t$ channel matrix, and \mathbf{n} is the n_r -dimensional additive white Gaussian noise (AWGN) noise vector having a covariance of $\mathbf{Q}_n = E[\mathbf{nn}^*] = \sigma_n^2 \mathbf{I}$.

Let $\mathbf{Q}_x = E[\mathbf{xx}^*]$ and the total transmission power constraint is given by $\text{tr}(\mathbf{Q}_x) = P_t$.

For a given \mathbf{H} , the covariance of the received signal \mathbf{y} is

$$\begin{aligned} \mathbf{Q}_y &= E[(\mathbf{H}\mathbf{x} + \mathbf{n})(\mathbf{H}\mathbf{x} + \mathbf{n})^H] \\ &= \mathbf{H}\mathbf{Q}_x\mathbf{H}^H + \sigma_n^2 \mathbf{I} \end{aligned} \quad (3.2)$$

From information theory, the link spectral efficiency can be calculated in terms of the mutual information as

$$\begin{aligned} C &= I(\mathbf{x}; \mathbf{y}) \\ &= h(\mathbf{y}) - h(\mathbf{y} | \mathbf{x}) \\ &= h(\mathbf{y}) - h(\mathbf{n}) \\ &= \log_2 \det(\mathbf{Q}_y) - \log_2 \det(\mathbf{Q}_n) \\ &= \log_2 \det\left(\frac{\mathbf{H}\mathbf{Q}_x\mathbf{H}^H}{\sigma_n^2} + \mathbf{I}\right) \end{aligned} \quad (3.3)$$

where $I(\mathbf{x}; \mathbf{y})$ is the mutual information, $h(\cdot)$ stands for the entropy and $h(\mathbf{y} | \mathbf{x})$ is the conditional entropy [15].

A. Optimum power allocation strategy

When the transmitter knows the channel matrix \mathbf{H} , \mathbf{Q}_x can be selected according to this information to maximize the mutual information shown in (3.3). Applying singular value decomposition on matrix \mathbf{H} , we get $\mathbf{H} = \mathbf{U}_H \mathbf{D}_H \mathbf{V}_H^H$ where $n_r \times n_r$ matrix \mathbf{U}_H and $n_t \times n_t$ matrix \mathbf{V}_H are unitary matrices, $n_r \times n_t$ matrix \mathbf{D}_H has singular values s_k ($k = 1, \dots, n_{\min} = \min\{n_r, n_t\}$) in the (k, k) position and zeros elsewhere. The spectral efficiency becomes

$$\begin{aligned} C &= \log_2 \left[\det \left(\mathbf{I} + \mathbf{U}_H \mathbf{D}_H \mathbf{V}_H^H \frac{\mathbf{Q}_x}{\sigma_n^2} (\mathbf{U}_H \mathbf{D}_H \mathbf{V}_H^H)^H \right) \right] \\ &= \log_2 \left[\det \left(\mathbf{I} + \mathbf{D}_H \mathbf{V}_H^H \frac{\mathbf{Q}_x}{\sigma_n^2} \mathbf{V}_H \mathbf{D}_H^H \right) \right]. \end{aligned} \quad (3.4)$$

Applying singular value decomposition $\mathbf{Q}_x = \mathbf{U}_x \mathbf{D}_x \mathbf{U}_x^H$ and choose $\mathbf{U}_x = \mathbf{V}_H$, the capacity becomes

$$\begin{aligned} C &= \log_2 \left[\det(\mathbf{I} + \mathbf{D}_H \mathbf{D}_x \mathbf{D}_H^H) \right] \\ &= \log_2 \left[\det(\mathbf{I} + \mathbf{D}_x |\mathbf{D}_H|^2) \right] \\ &= \max_{\text{tr}(\mathbf{Q}_x) \leq P_t} \sum_{k=1}^{n_{\min}} \log_2 \left(1 + \frac{P_k}{\sigma_n^2} \lambda_k \right) \end{aligned} \quad (3.5)$$

where $\lambda_k = |s_k|^2$ is the k^{th} eigenvalue of $\mathbf{H}\mathbf{H}^H$.

The optimum power allocated to each sub-channel P_k ($k = 1, 2, \dots, n_{\min}$) that maximizes the system capacity can be found by the water-filling solution [8]

$$P_k = \left(\mu - \frac{\sigma_n^2}{\lambda_k} \right)^+$$

where $(x)^+$ denotes the larger number of 0 and x ; μ is chosen such that $\sum_{k=1}^{n_{\min}} P_k = P_t$.

B. Uniform power allocation strategy

When the transmitter does not have channel state information (CSI), the transmission power will be evenly distributed among all sub-channels, i.e., $\mathbf{Q}_x = P_t/n_t \cdot \mathbf{I}$.

Accordingly, the capacity becomes

$$\begin{aligned} C &= \log_2 \left[\det \left(\mathbf{I} + \frac{P_t}{n_t \sigma_n^2} |\mathbf{D}_H|^2 \right) \right] \\ &= \sum_{k=1}^{n_{\min}} \log_2 \left(1 + \frac{\rho}{n_t} \lambda_k \right) \end{aligned} \quad (3.6)$$

where $\rho = P_t/\sigma_n^2$.

For the system with $n_t = n_r = n$ and identical eigenvalues, the capacity becomes

$$C = \log_2 \det \left[\mathbf{I} + \frac{\rho}{n} \lambda \cdot \mathbf{I} \right] = n \log_2 \left[1 + \frac{\rho \lambda}{n} \right]. \quad (3.7)$$

3.2.2 Comparison with Other Diversity Systems

A. No diversity: $n_t = n_r = 1$.

When there is only 1 transmit antenna and 1 receive antenna, the capacity simply reduces to

$$C = \log_2 \det \left[1 + \frac{\rho}{1} |H|^2 \right] = \log_2 [1 + \rho \chi_2^2] \quad (3.8)$$

where χ_2^2 is chi-square distributed with two degrees of freedom (DOF).

B. Receiver diversity: $n_t = 1, n_r = n$.

In this system topology, if maximal ratio combining (MRC) is used to combine all the received signals, the capacity can be represented as,

$$\begin{aligned}
 C &= \log_2 \left[1 + \rho \sum_{i=1}^{n_r} |H_i|^2 \right] \\
 &= \log_2 \left[1 + \rho \sum_{i=1}^{n_r} (\text{Re}(H_i)^2 + \text{Im}(H_i)^2) \right] \\
 &= \log_2 (1 + \rho \chi_{2n_r}^2)
 \end{aligned} \tag{3.9}$$

where $\chi_{2n_r}^2$ is chi-square distributed with a DOF of $2n_r$.

C. Transmitter diversity: $n_t = n, n_r = 1$.

In this case, the channel matrix becomes a vector $\mathbf{H}_{1 \times n}$. The capacity can be shown as

$$\begin{aligned}
 C &= \log_2 \det \left[1 + \frac{\rho}{n} \mathbf{H} \mathbf{H}^H \right] \\
 &= \log_2 \left[1 + \frac{\rho}{n} \sum_{i=0}^{n_r-1} (\text{Re}(H_i)^2 + \text{Im}(H_i)^2) \right] \\
 &= \log_2 \left[1 + \frac{\rho}{n} \chi_{2n}^2 \right].
 \end{aligned} \tag{3.10}$$

D. Simulation

In the Monte-Carlo simulation, the outage capacities (10% outage) are calculated for three types of systems mentioned above: the receive diversity system, the transmit diversity system and the MIMO system. The parameters used in the simulation follow

those in [3] and they are listed in Table 3.1. In the simulation, it is assumed that the signals at different antennas are independent.

Antenna gain	15 dB
Bandwidth	$B = 5 \times 10^6$ Hz
Transmit power	$P_t = 10$ W
Noise figure	$F = 2$
Receiver temperature	$T = 300$ °K
Number of iterations	$N = 10^5$ times
Propagation exponent	3.5
Log-normal shadowing	8 dB standard derivation
Fast fading	Independent Rayleigh PDF

Table 3.1 Simulation parameters for capacity comparison.

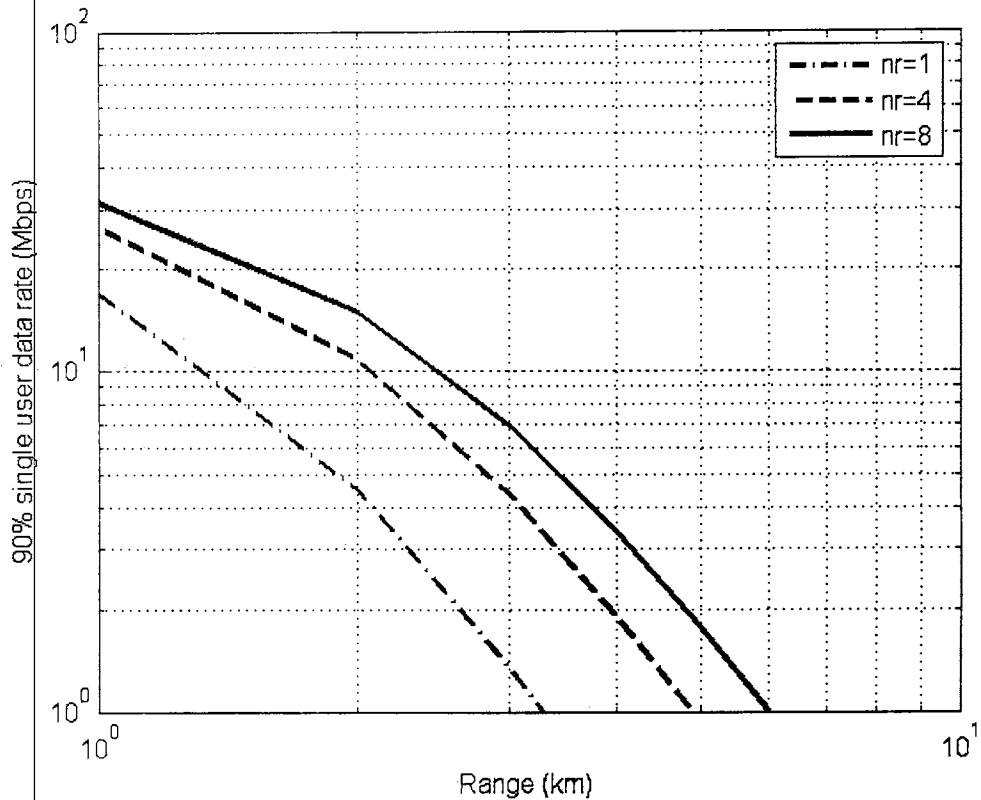


Figure 3.1 Capacity of the receiver diversity systems.

The simulation results of receiver diversity are shown in Figure 3.1. As the number of receiver antennas increases, more independent signals will be available at the receiver. Collecting and combining these signals increase the comprehensive receiver SNR. However, because of the logarithmic relationship between SNR and capacity, this receiver diversity scheme only gives limited capacity improvement.

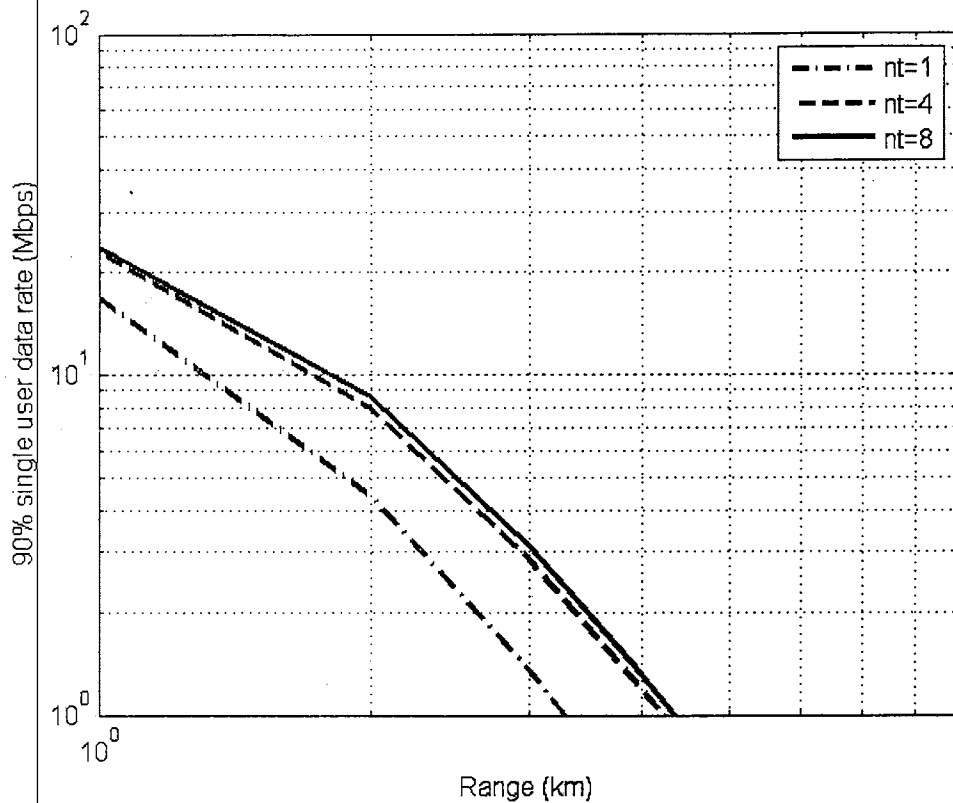


Figure 3.2 Capacity of the transmitter diversity systems.

Figure 3.2 shows the simulation result of the transmitter diversity. A comparison between capacity equations of (3.9) and (3.10) shows that the only difference between the receiver diversity and transmitter diversity is that in the later case, the transmission power is divided by the number of transmit antennas. This means that in a transmitter diversity system, the power of signals from individual transmit antennas is reduced. As shown in Figure 3.2, this property obviously limits the capacity increment of the transmitter diversity system. There is not much benefit in increasing the number of transmit antennas beyond 4.

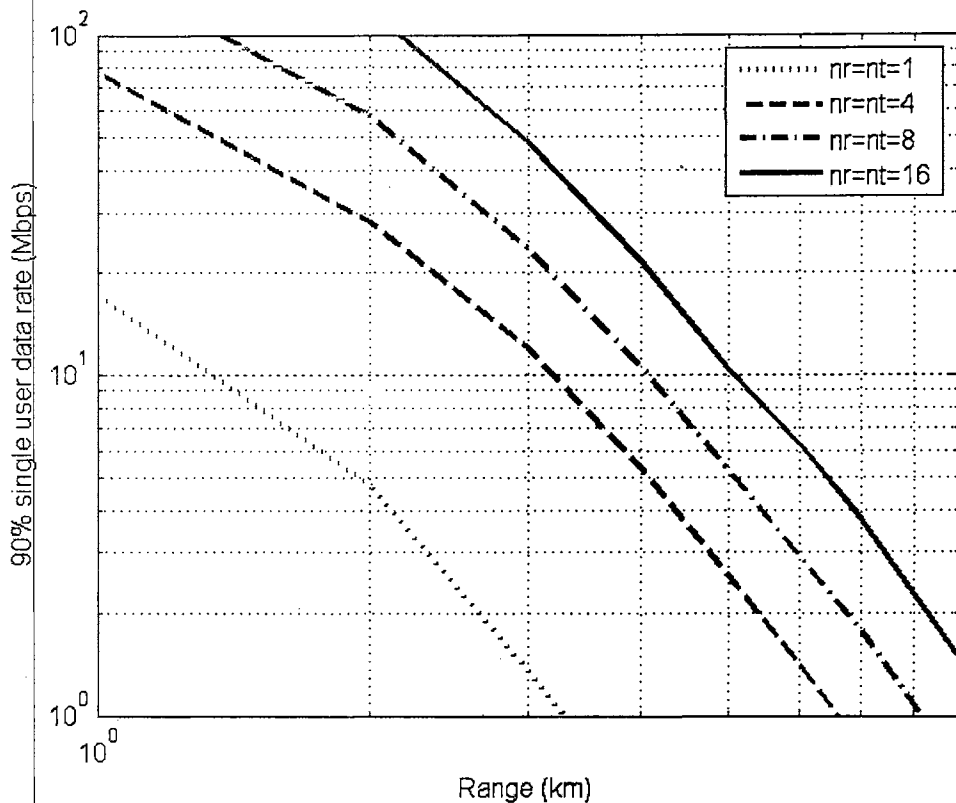


Figure 3.3 Capacity of MIMO systems.

The capacity of MIMO systems is shown in Figure 3.3. As predicted theoretically, increasing the number of both transmit and receive antennas opens extra spatial sub-channels and brings an extraordinary increase of the capacity. As long as more uncorrelated antennas can be incorporated to both the transmitter and receiver ends, the capacity growth will not saturate.

3.2.3 Effects of the Number of Antennas

In this section, we show the relative performance changes of MIMO systems with different $\{n_r, n_t\}$ pairs.

Monte-Carlo simulation is performed in a MIMO system where $n_r, n_t = 2, 4, 8, 16$. Without any loss of generality, the average SNR value ρ is set to one in the simulation. The mean capacity of MIMO systems is calculated and shown in Figure 3.4. As proved formerly in this chapter and in other literatures [1]-[4], [15], capacity grows linearly as n_r and n_t equally increase. When $n_r \neq n_t$, fixing one number and increasing the other gives a small increase in capacity that saturates quickly. As shown in equation (3.6), the number of available sub-channels equals $\min\{n_r, n_t\}$. Just increasing either n_r or n_t cannot further create additional sub-channels. The only thing it does is provide diversity. Comparing the cases of $n_r > n_t$ and $n_r < n_t$, it is shown that letting n_r to be the larger number provides more capacity than letting n_t to be the larger number.

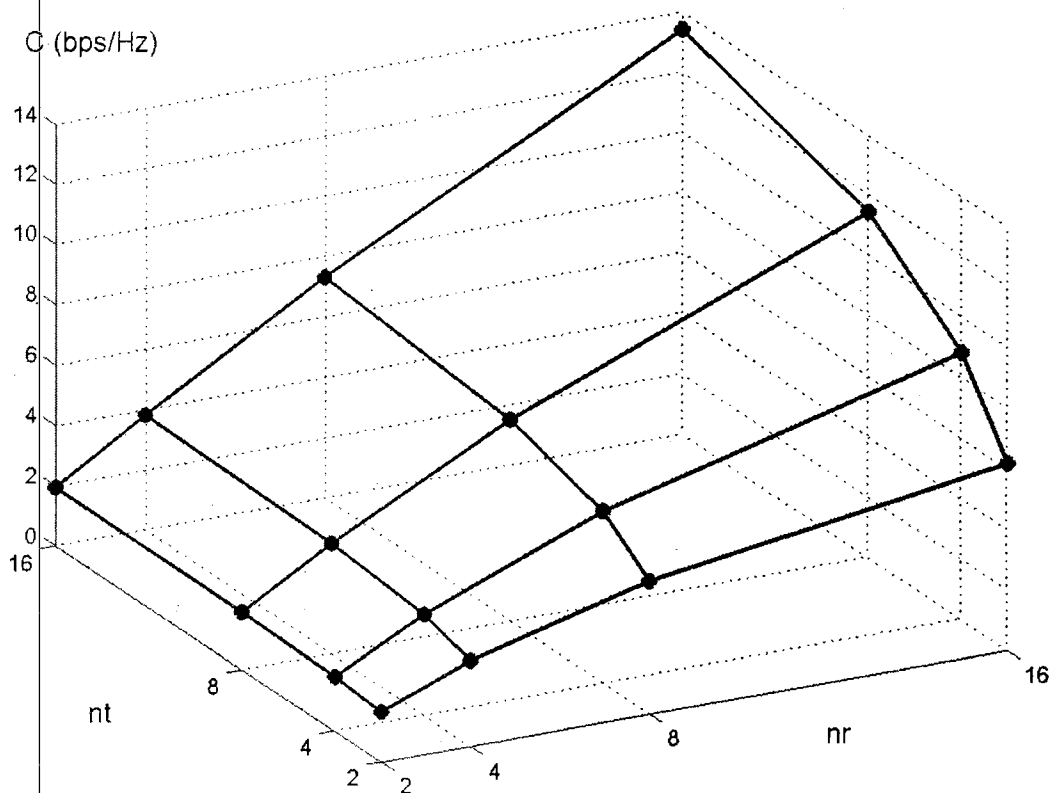


Figure 3.4 Capacity of MIMO systems with different $\{n_r, n_t\}$ pairs.

3.3 MIMO Systems in a Multi-cell Environment

3.3.1 Capacity Derivation

Consider MIMO systems in a multi-cell environment. For the down link, each MT will receive MIMO signals from co-channel BSs as well as from the local BS. This co-channel interference, together with the thermal noise, will degrade the link performance. We consider a multi-cell MIMO system with I co-channel BSs. When all BSs have the same number of antennas of n_t , the n_r -dimensional received signal vector \mathbf{y} can be expressed as:

$$\mathbf{y} = \mathbf{H}\mathbf{x} + \sum_{i=1}^I \mathbf{H}_i \mathbf{x}_i + \mathbf{n} \quad (3.11)$$

where \mathbf{x} is the desired signal from a local BS; $\mathbf{x}_1, \mathbf{x}_2, \dots, \mathbf{x}_I$ are the co-channel interference signals and all of them are n_t -dimensional vectors; \mathbf{H} and \mathbf{H}_i are the corresponding $n_r \times n_t$ channel matrices.

Let $\boldsymbol{\Sigma}_x = E[\mathbf{x}\mathbf{x}^H]$ with the total transmission power constraint of $\text{tr}(\boldsymbol{\Sigma}_x) = P_t$. The n_r -dimensional AWGN noise \mathbf{n} has a covariance of $\boldsymbol{\Sigma}_n = E[\mathbf{n}\mathbf{n}^H] = \sigma_n^2 \mathbf{I}$. The covariance of interference plus AWGN noise is

$$\mathbf{K}_n = E \left[\left(\sum_{i=1}^I \mathbf{H}_i \mathbf{x}_i + \mathbf{n} \right) \left(\sum_{i=1}^I \mathbf{H}_i \mathbf{x}_i + \mathbf{n} \right)^H \right]. \quad (3.12)$$

For channel matrices $\mathbf{H}_i, i = 1, 2, \dots, I$,

$$\mathbf{K}_n = \sum_{i=1}^I \mathbf{H}_i \boldsymbol{\Sigma}_{x_i} \mathbf{H}_i^H + \sigma_n^2 \mathbf{I}. \quad (3.13)$$

From information theory, it is shown in [2] that the link spectral efficiency is

$$C = I(\mathbf{x}; \mathbf{y}) = \log_2 \det(\mathbf{I} + \mathbf{H}\boldsymbol{\Sigma}_x \mathbf{H}^H \mathbf{K}_n^{-1}). \quad (3.14)$$

Since $\log \det(\mathbf{I} + \mathbf{A}\mathbf{B}) = \log \det(\mathbf{I} + \mathbf{B}\mathbf{A})$, the above equation can be expressed as

$$\begin{aligned} C &= \log_2 \det(\mathbf{I} + \mathbf{H}\boldsymbol{\Sigma}_x \mathbf{H}^H \mathbf{K}_n^{-1}) \\ &= \log_2 \det(\mathbf{I} + \mathbf{H}^H \mathbf{K}_n^{-1} \mathbf{H}\boldsymbol{\Sigma}_x). \end{aligned} \quad (3.15)$$

This expression is similar to that obtained in the single-cell environment case. Assuming no co-channel information is known at the local BS, the reasonable power allocation choice will be to uniformly allocate power among all the transmitters. So the signal covariance matrix will be $\boldsymbol{\Sigma}_x = \frac{P_t}{n_t} \mathbf{I}$. Accordingly, the link spectral efficiency is

$$C = \log_2 \left(\mathbf{I} + \frac{P_t}{n_t} \mathbf{H}\mathbf{K}_n^{-1} \mathbf{H}^H \right). \quad (3.16)$$

The situation of optimal power allocation in multi-cell environments is different from that in a single-cell environment. Intuitively, it seems like the optimal power allocation might be obtained by distributing the power according to the eigenvalues of $\mathbf{H}^H \mathbf{K}_n^{-1} \mathbf{H}$. But the problem is that the outcome of the optimal power allocation in one cell is determined by (and also determines) the power allocation of the other co-channel cells. So the optimization of one cell will require the re-optimization of all the other co-channel cells again. This is an iterative process and its convergence has not been conclusively proved [2].

So, as a sub-optimal strategy, the water-filling algorithm can be performed according to the local channel information only. The statistics of the co-channel interference will not be considered when allocating local transmit power among sub-channels.

3.3.2 Simulation Results

Simulations are conducted to show the performance of the MIMO system in multi-cell environments. The parameters used are summarized in Table 3.2.

The cell size is adjusted so that 90% of the cell has a SNR value above 25 dB and the system is interference limited. Simulation results are shown in Figure 3.5. Outage capacity is used in the illustration, where each point shows the probability of a MT having a capacity lower than the x -axis value corresponding to this point. The results show that MIMO capacity increases linearly in multi-cell environments. For example, the 10% outage capacity of a $n_t = n_r = 4$ system is 8 Mbps; while it is 17 Mbps for a $n_t = n_r = 8$ system and 34 Mbps for a $n_t = n_r = 16$ system.

Sectors per cell:	3
BS antenna:	120° perfect sectorization
MT antenna:	Omni-directional
Frequency reuse:	Universal
Path loss model:	Hata
Log-normal shadowing:	8 dB standard derivation
Fast fading:	Independent Rayleigh PDF
Total transmit power:	10 Watts
Bandwidth:	5 MHz
Noise figure:	2

Table 3.2 Simulation parameters for multi-cell environment.

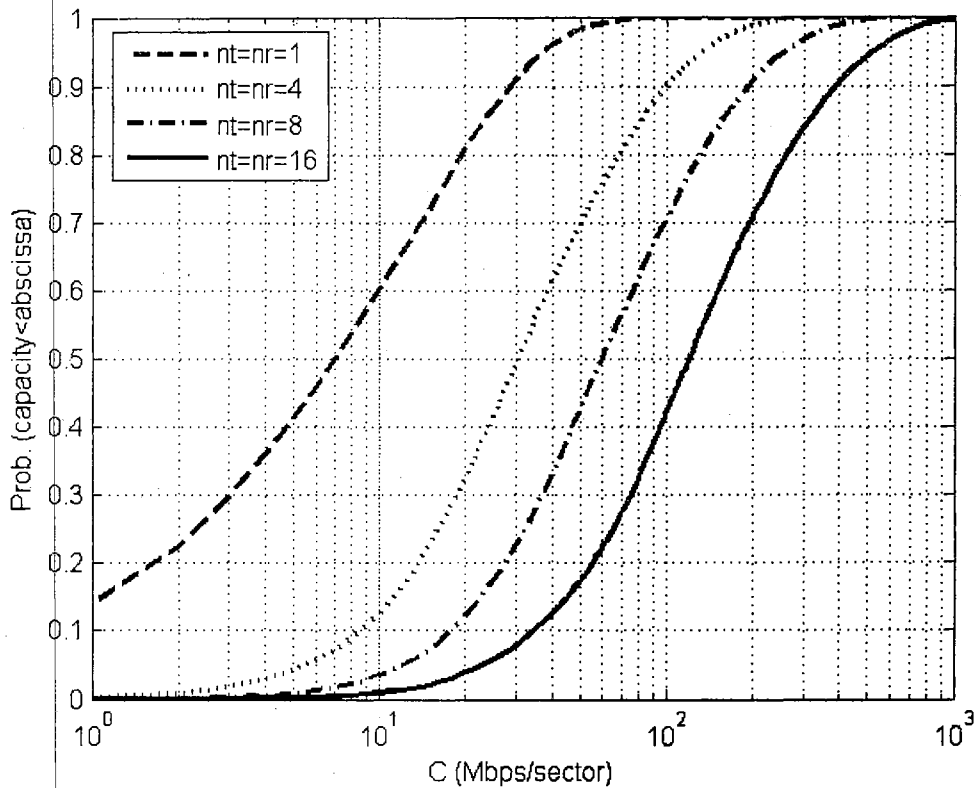


Figure 3.5 MIMO capacity in multi-cell environment.

3.4 Adaptive Modulation

After proving the capacity potentials of MIMO systems, the actual data rate that can be achieved will be derived in this chapter. Wireless channels randomly change with time. Most modulation schemes are not designed to change according to the channel fading conditions. In order to maintain robust transmission, the communication system needs to be designed according to the worst case channel conditions. When the channel is in a good condition, such that a much higher-rate modulation can be supported, use of the same modulation scheme is a waste of resources. Thus, fixed modulation schemes do not fully utilize the channel capacity.

When the CSI is known to the transmitter, transmission can be adaptively performed to maximize the system throughput. The CSI can be directly estimated at the transmitter in time division duplex (TDD) systems; or it can be estimated at the receiver and sent back to the transmitter through signaling channels. Many transmission parameters can be adjusted according to the CSI, including transmission power, symbol rate, symbol constellation, coding rate, and even instantaneous BER. In this chapter, we adapt the transmission power and symbol constellation along space sub-channels to maximize the throughput, while maintaining a fixed BER and transmission power in the time domain.

3.4.1 MIMO System Adaptive Modulation – Scheme 1

We consider an adaptive modulation MIMO system where the transmission power and modulation constellations are adjusted along the spatial domain. It is assumed that for all space sub-channels, the instantaneous SNR values γ_i ($i = 1, 2, \dots, n_{\min}$) and their PDF functions $f(\gamma_i)$ ($i = 1, 2, \dots, n_{\min}$) are known to the transmitter. Since most practical systems can only support a certain number of symbol constellations, a fixed rate set $\{k_j\}_{j=1}^{N_s}$ is applied where the rate k_{ij} is used for the i^{th} sub-channel when the SNR value for this sub-channel is between $[\rho_j, \rho_{j+1})$. The objective is to maximize the average data

rate $\sum_i \left[\sum_j k_{ij} \int_{\gamma_j}^{\gamma_{j+1}} f(\gamma_i) d\gamma_i \right]$ with the following constraints [32]:

$$1) \text{ Instantaneous-BER constraint } BER(\gamma) = \frac{\sum_i [BER(\gamma_i)k_i]}{\sum_i k_i} = BER.$$

2) Average power constraint $\int_{\gamma} \sum_i P_i(\gamma_i) f(\gamma) d\gamma = P_t$, where the SNR vector

$\gamma = [\gamma_1, \gamma_2, \dots, \gamma_{n_{\min}}]$. This constraint can be further simplified as

$$\sum_i \int_{\gamma_i} P_i(\gamma_i) f(\gamma_i) d\gamma_i = P_t.$$

This is a standard constraint optimization problem, which can be solved by Lagrange's method [24], [32]. The Lagrange equation can be written as

$$\begin{aligned} & J(\gamma_1, \gamma_2, \dots, \gamma_{n_{\min}}) \\ &= \sum_i \left[\sum_j k_{ij} \int_{\gamma_j}^{\gamma_{j+1}} f(\gamma_i) d\gamma_i \right] \\ &+ \lambda_1 \left\{ \frac{\sum_i [BER(\gamma_i) k_i]}{\sum_i k_i} - \overline{BER} \right\} + \lambda_2 \left\{ \sum_i \int_{\gamma_i} P_i(\gamma_i) f(\gamma_i) d\gamma_i - P_t \right\}. \end{aligned} \quad (3.17)$$

It should be noted that the instantaneous BER constraint can also be expressed as

$$\overline{BER} = \frac{\sum_i \left[\sum_j k_{ij} \int_{\gamma_j}^{\gamma_{j+1}} BER(\gamma_i) f(\gamma_i) d\gamma_i \right]}{\sum_i \left[\sum_j k_{ij} \int_{\gamma_j}^{\gamma_{j+1}} f(\gamma_i) d\gamma_i \right]}. \quad \text{Therefore, the throughput will be}$$

$$\sum_i \left[\sum_j k_{ij} \int_{\gamma_j}^{\gamma_{j+1}} f(\gamma_i) d\gamma_i \right] = \frac{\sum_i \left[\sum_j k_{ij} \int_{\gamma_j}^{\gamma_{j+1}} BER(\gamma_i) f(\gamma_i) d\gamma_i \right]}{\overline{BER}}. \quad (3.18)$$

Substituting (3.18) into the first term of (3.17), the Lagrange equation becomes

$$\begin{aligned}
& J(\gamma_1, \gamma_2, \dots, \gamma_{n_{\min}}) \\
&= \frac{\sum_i \left[\sum_j k_{ij} \int_{\gamma_j}^{\gamma_{j+1}} BER(\gamma_i) f(\gamma_i) d\gamma_i \right]}{\overline{BER}} \\
&+ \lambda_1 \left\{ \frac{\sum_i [BER(\gamma_i) k_i]}{\sum_i k_i} - \overline{BER} \right\} \\
&+ \lambda_2 \left\{ \sum_i \int_{\gamma_i} P_i(\gamma_i) f(\gamma_i) d\gamma_i - P_i \right\}.
\end{aligned} \tag{3.19}$$

From the BER expression in [32], $BER(\gamma_i) = c_1 \exp\left[\frac{-c_2 \gamma_i \frac{S(\gamma_i)}{\bar{S}}}{f(k_i(\gamma_i))}\right]$. Power allocation

can be expressed as $p(\gamma_i) = \frac{P_i f(k_i(\gamma_i)) \ln\left[\frac{BER(\gamma_i)}{c_1}\right]}{-c_2 \gamma_i}$. Therefore, the Lagrange equation

becomes

$$\begin{aligned}
& J(\gamma_1, \gamma_2, \dots, \gamma_{n_{\min}}) \\
&= \frac{\sum_i \left[\sum_j k_{ij} \int_{\gamma_j}^{\gamma_{j+1}} BER(\gamma_i) f(\gamma_i) d\gamma_i \right]}{\overline{BER}} \\
&+ \lambda_1 \left\{ \frac{\sum_i [BER(\gamma_i) k_i]}{\sum_i k_i} - \overline{BER} \right\} \\
&+ \lambda_2 \left\{ -\frac{P_i}{c_2} \sum_i \left[\sum_j f(k_{ij}) \int_{\gamma_j}^{\gamma_{j+1}} \frac{\ln\left(\frac{BER(\gamma_i)}{c_1}\right)}{\gamma_i} f(\gamma_i) d\gamma_i \right] - P_i \right\}.
\end{aligned} \tag{3.20}$$

The optimal rate regions $\gamma_1, \gamma_2, \dots, \gamma_{n_{\min}}$ can be obtained by taking partial derivatives with respect to $\gamma_1, \gamma_2, \dots, \gamma_{n_{\min}}$. First,

$$\frac{\partial J}{\partial \gamma_0} = \frac{-k_0 \overline{BER}(\gamma_0)}{\overline{BER}} \sum_i p(\gamma_{i0}) + \frac{\lambda_2 \overline{S} f(k_0) \ln \left[\frac{BER(\gamma_0)}{c_1} \right]}{c_2 k_0} \sum_i p(\gamma_{i0}) = 0. \quad (3.21)$$

The optimal value of γ_0 is

$$\gamma_0 = \frac{\lambda_2 \overline{S} f(k_0) \ln \left[\frac{BER(\gamma_0)}{c_1} \right] \overline{BER}}{c_2 k_0 \overline{BER}(\gamma_0)}. \quad (3.22)$$

For $j = 1, 2, \dots, N-1$, the optimal value of γ_j can be found as

$$\gamma_j = \frac{\lambda_2 \overline{S} [f(k_{j-1}) - f(k_j)] \ln \left[\frac{BER(\gamma_j)}{c_1} \right] \overline{BER}}{c_2 (k_{j-1} - k_j) \overline{BER}(\gamma_j)}. \quad (3.23)$$

3.4.2 MIMO System Adaptive Modulation – Scheme 2

It was shown in [32] that in an AWGN channel, the BER of square M -ary QAM with Gray bit mapping can be closely approximated as

$$BER(\gamma) \approx 0.2 \exp\left(\frac{-1.5\gamma}{M-1}\right) \quad (3.24)$$

where γ is the instantaneous SNR value at the receiver and M is the constellation size. This approximation is tight to within 1 dB for $k = \log_2 M \geq 2$ and $BER \leq 10^{-3}$. If the value of γ is known to the transmitter, the maximum constellation size to maintain a fixed BER at the receiver is

$$M = 1 + \frac{1.5\gamma}{-\ln(5BER)}. \quad (3.25)$$

Assuming the value of γ can be precisely measured at the receiver, and can be fed back to the transmitter without delay; the spectral efficiency can be maximized according to the estimated γ value as

$$\begin{aligned} k &= \log_2 M(\gamma) \\ &= \log_2 \left(1 + \frac{1.5\gamma}{-\ln(5BER)} \right) \\ &= \log_2(1 + \beta\gamma) \end{aligned} \quad (3.26)$$

where $\beta = \frac{1.5}{-\ln(5BER)}$. Comparing this with the Shannon capacity $C = \log_2(1 + \gamma)$, it can be seen that they have similar forms. Thus, data rate and capacity can be evaluated in a similar way. For a given BER requirement, k expressed in (3.26) is the maximum achievable adaptive rate. It should be noted that here we assume k to be any positive value. Thus equation (3.26) is the full adaptation according to the channel fading. In reality, only specific positive integers can be used at the transmitter. Equation (3.26) will be changed to $k = \lfloor \log_2(1 + \beta\lambda) \rfloor$, while $\lfloor x \rfloor$ means the biggest integer number equal to or smaller than x . Therefore, equation (3.26) can be seen as a upper bound of the adaptation data rate.

A. Uniform-Power Variable-Rate Adaptation.

1) Continuous Data Rate

In MIMO systems, CSI refers to all the eigenvalues of the channel matrix, i.e. $\lambda_i, i = 1, \dots, \min\{n_r, n_t\}$. Once CSI is known at the transmitter, it can be used to perform

adaptive modulation to maximize the transmission data rate under a given BER constraint. First, we consider the case where only the data rate is adapted according to the CSI. Transmission power is equally divided among all sub-channels. If we assume that the data rate can be continuously adapted, the maximum data rate will be

$$\begin{aligned}
D(BER) &= \sum_{i=1}^{n_{\min}} \log_2 \left(1 + \frac{1.5}{-\ln(5BER)} \frac{P_t}{n_i \sigma_n^2} \lambda_i \right) \\
&= \sum_{i=1}^{n_{\min}} \log_2 \left(1 + \frac{1.5}{-\ln(5BER)} \frac{\rho}{n_i} \lambda_i \right) \\
&= \sum_{i=1}^{n_{\min}} \log_2 \left(1 + \frac{\rho'}{n_i} \lambda_i \right)
\end{aligned} \tag{3.27}$$

where $\rho' = \frac{1.5\rho}{-\ln(5BER)}$ and $\rho = \frac{P_t}{\sigma_n^2}$. This expression of adaptive data rate is in the same form as the capacity expression shown in equation (3.6), except for the change of the average SNR value.

The average data rate of this adaptation scheme can be evaluated as

$$\begin{aligned}
&E[D(BER)] \\
&= \int \left[\sum_{i=1}^{n_{\min}} \log_2 \left(1 + \frac{1.5\lambda_i}{-\ln(5BER)} \frac{P_t}{n_i \sigma_n^2} \right) \right] P(\lambda_1, \lambda_2, \dots, \lambda_{n_{\min}}) d\lambda_1 d\lambda_2 \dots d\lambda_{n_{\min}} \\
&= \sum_{i=1}^{n_{\min}} \int \left[\log_2 \left(\frac{1.5\lambda_i}{-\ln(5BER)} \frac{P_t}{n_i \sigma_n^2} \right) \right] P(\lambda_i) d\lambda_i.
\end{aligned} \tag{3.29}$$

2) Discrete Data Rate

In real systems the allowable signal constellations are restricted, e.g., it must be 0, 2, 4, 8, 16, etc. Considering this restriction, the maximum data rate becomes

$$D(BER) = \sum_{i=1}^{n_{\min}} \left\lfloor \log_2 \left(1 + \frac{\rho'}{n_i} \lambda_i \right) \right\rfloor \tag{3.29}$$

where $\lfloor x \rfloor$ denotes the largest integer number less than or equal to x . Although this expression more accurately describes the real system, the operation $\lfloor \cdot \rfloor$ makes it difficult to be manipulated in derivations. Therefore, the continuous data rate equation (3.27) will be used in the following simulations and derivations.

B. Adaptive-Power Variable-Rate Adaptation.

When power is adaptively allocated among all sub-channels, the overall data rate of a MIMO system can be represented as

$$D(BER) = \sum_{i=1}^{n_{\min}} \log_2 \left(1 + \frac{1.5\lambda_i}{-\ln(5BER)} \frac{P_i}{\sigma_n^2} \right) \quad (3.30)$$

with the total power constraint of $\sum_{i=1}^{n_i} P_i = P_t$. By applying a water-filling algorithm to (3.30) to maximize the total data rate, we obtain,

$$P_i = \left[\mu - \frac{-\sigma_n^2 \ln(5BER)}{1.5\lambda_i} \right]^+. \quad (3.31)$$

Therefore, the maximal data rate under a certain BER becomes

$$D(BER) = \sum_{\substack{i=1 \\ P_i > 0}}^{n_{\min}} \log_2 \left(\mu \frac{1.5\lambda_i}{-\sigma_n^2 \ln(5BER)} \right). \quad (3.32)$$

The mean value of the maximal data rate can be calculated as

$$\begin{aligned} & E[D(BER)] \\ &= \int \left[\sum_{i=1}^{n_{\min}} \log_2 \left(\mu \frac{1.5\lambda_i}{-\sigma_n^2 \ln(5BER)} \right) \right] f(\lambda_1, \lambda_2, \dots, \lambda_{n_{\min}}) d\lambda_1 d\lambda_2 \dots d\lambda_{n_{\min}} \\ &= \sum_{i=1}^{n_{\min}} \int \left[\log_2 \left(\mu \frac{1.5\lambda_i}{-\sigma_n^2 \ln(5BER)} \right) \right] f(\lambda_i) d\lambda_i \end{aligned} \quad (3.33)$$

where $f(\lambda_1, \lambda_2, \dots, \lambda_{n_{\min}})$ is the joint eigenvalue PDF function, $f(\lambda_i)$ is the PDF function of the i th eigenvalue.

Example: A 2×2 MIMO system is used to show the effect of the adaptive power allocation. For different SNR values, the mean capacity is evaluated using both water-filling and uniform power allocation strategies. Simulation results are shown in Figure 3.6. Using the same simulation parameters, the mean value of the adaptive modulation data rate is evaluated for both power allocation strategies under the constraint of $\text{BER} = 10^{-3}$. The simulation results of adaptive modulation data rates are plotted in Figure 3.7.

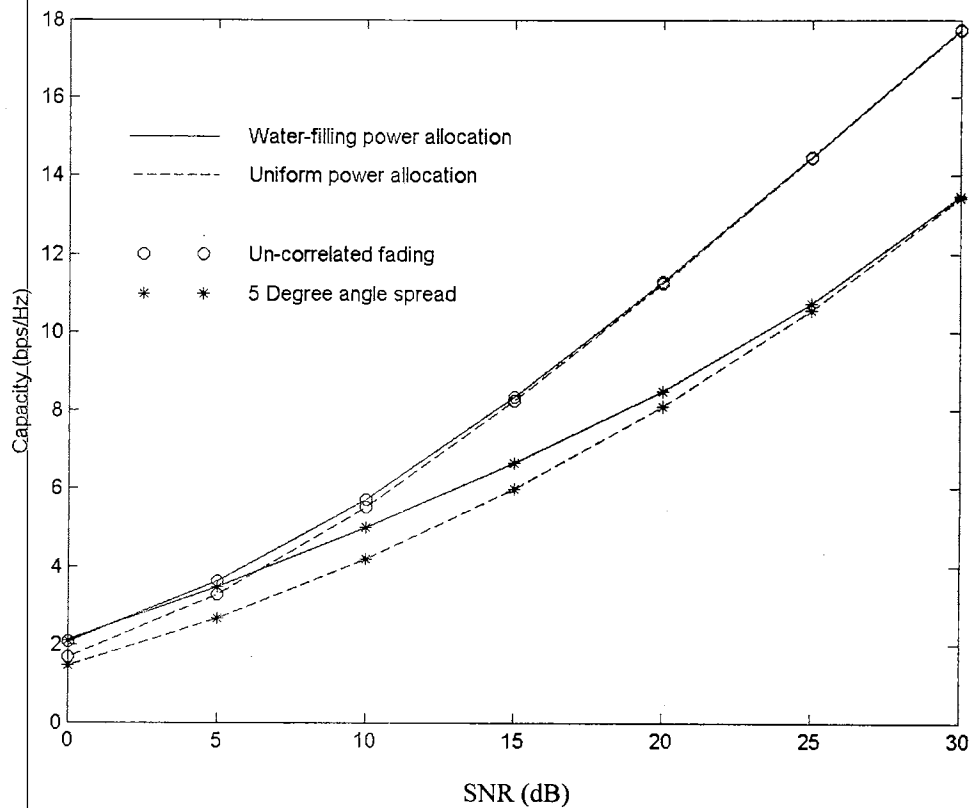


Figure 3.6 Channel capacity with/without power adaptation.

From Figures 3.6 and 3.7, we see that both capacity and data rate exhibit very similar characteristics. At the low SNR range, the MIMO system capacity/data rate is mainly

determined by the power allocation strategy, while at the high SNR range, the capacity/data rate is mainly determined by the correlation effects among antennas.

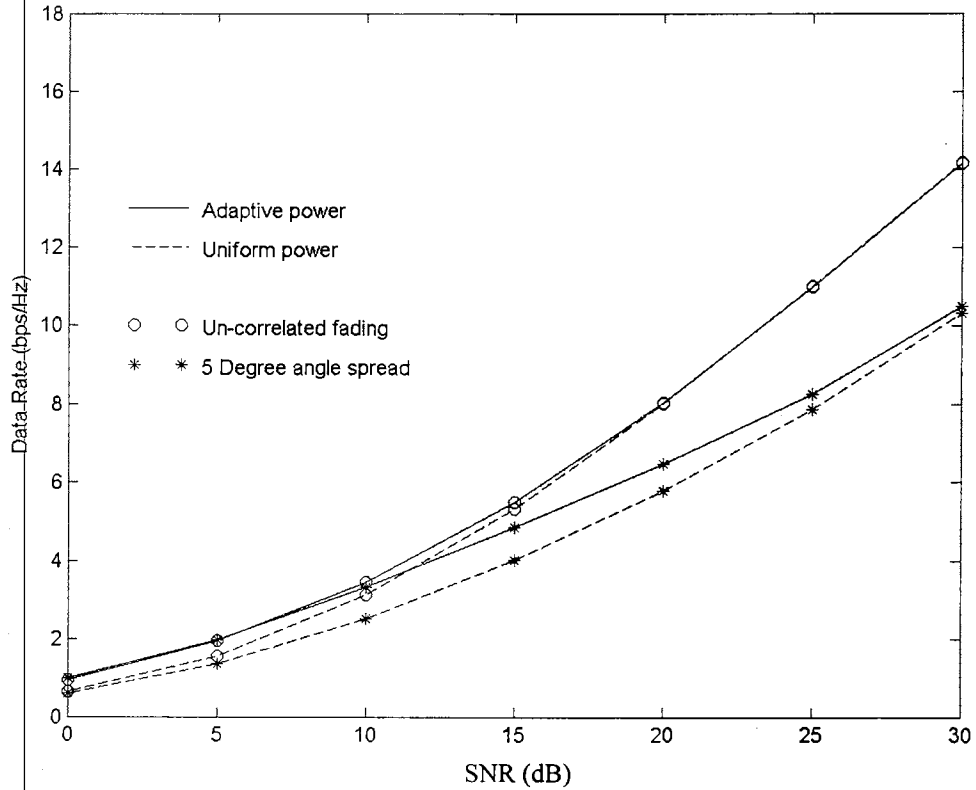


Figure 3.7 Adaptive modulation data rate with/without power adaptation ($BER = 10^{-3}$).

Adaptive power allocation is performed by using the water-filling algorithm among all spatial sub-channels, which is a lengthy iterative process. Uniform power allocation, on the other hand, is much simpler, and sometimes gives closed-form solutions. Therefore, when we investigate the performance of a system, uniform power allocation usually is first used. Then the benefit of power adaptation can be added in. For the purpose of investigating the correlation effects, we will focus on the moderate/high SNR

range. Within this range, there is very little performance difference between uniform power allocation and adaptive power allocation. So, the expressions get simplified.

3.5 Summary

In this chapter, the fundamentals of the research are exploited. First, the concept and mechanism of MIMO systems are introduced. The capacity equations are derived to show the linear increase in capacity with the number of antennas. This capacity of MIMO systems is compared with the capacities of the diversity systems, and the fundamental difference between these two systems is observed. The MIMO system capacity in multi-cell environments is also investigated. Then, adaptive modulation is used in MIMO systems to maximize the system throughput by adapting the transmission parameters according to the CSI. This chapter gives two approaches to maximize the MIMO system throughput by adaptively changing the symbol constellation for each sub-channel and adaptively allocating the transmission power among all sub-channels. Simulation results show that in the moderate and high SNR region, adapting both symbol constellation and power gives almost the same throughput as adapting symbol constellation only. Since adaptive power allocation requires an iterative water-filling algorithm, which is not easy to evaluate, in the following research, only symbol constellation adaptation will be considered.

CHAPTER IV

ANALYTICAL MODEL OF MIMO SYSTEMS

In this chapter, first channel models are introduced to reflect the correlation effect in MIMO systems. The performance deterioration of MIMO systems under correlated fading is demonstrated. Then by assuming a Gaussian distributed matrix for the channel model, the eigenvalue distribution of the channel matrix is derived for both the independent fading case and the correlated fading case. The results from this chapter will be applied to future research to improve the MIMO system performance in correlated fading environments.

4.1 Correlation Effect in MIMO Systems

A large amount of former MIMO research has been conducted under the assumption that transmissions between all pairs of transmitter-receiver antennas experience independent fading. However, in real propagation systems, the fades are correlated to each other due to insufficient antenna spacing or the lack of local scatters. It has been shown that in correlated fading environments, the capacity of MIMO systems can be significantly lower compared to independent fading. In [4], the authors used the exponential correlation to represent the correlation coefficients between any two individual fading channels. In [5] and [29], different correlation models are introduced to simulate the different propagation environments, and to investigate the effects of antenna correlations. In [30] and [31], the asymptotic capacity of correlated MIMO systems is investigated. All these investigations show that the correlation effect will reduce the

MIMO capacity to some extent. To implement MIMO systems, the correlation effect is a very important factor needing to be investigated, and if possible, mitigated.

There are different approaches to model the fading correlation effects. An overview of the spatial channel models is provided in [53]. One approach is the ray-tracing model. In this approach, the exact location and properties of the transmitter, receiver, and all the surrounding objects need to be measured. Received signals are obtained by calculating its propagation through all the possible paths. Another approach is to construct a scatter model that can provide a reasonable description of the propagation environment. The advantage of this approach is that with a simple and intuitive model, the essential characteristics of the channel can be clearly illuminated, and the insights obtained from the model can then be utilized in planning the detailed measurements and simulations [29].

We investigate MIMO systems in an outdoor cellular environment as shown in Figure 4.1. In this case, it is usually assumed that the MT is of the same height or is lower than its surrounding objects. Thus the MT immerses in its local scatters and receives reflected signals from all directions. The BS, however, is much higher than its surrounding objects. So the signals coming from the MT and its surrounding scatters come directly to the BS antennas. Therefore, the signal spread angle for the BS is quite limited.

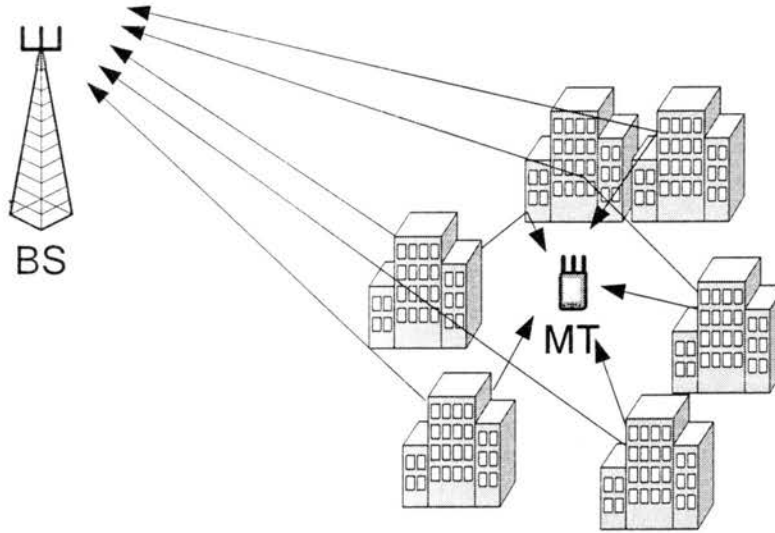


Figure 4.1 Outdoor cellular signal propagation environment.

4.1.1 Continuous Scatter One-Ring Model

The formerly discussed phenomenon is abstracted into a one-ring model [67] shown in Figure 4.2. For downlink signal transmissions, the BS antennas are the transmitters and the MT antennas are the receivers. A continuous ring of scatters is assumed around the MT. The parameters of this model include the distance D between the BS and the MT, the radius R of the scatter ring, the angle spread Δ at the BS, and the angle of arrival Θ at the BS. The one-ring model is basically a ray-tracing model [4]. It is shown that this model closely approximates outdoor cellular environments [29], [120].

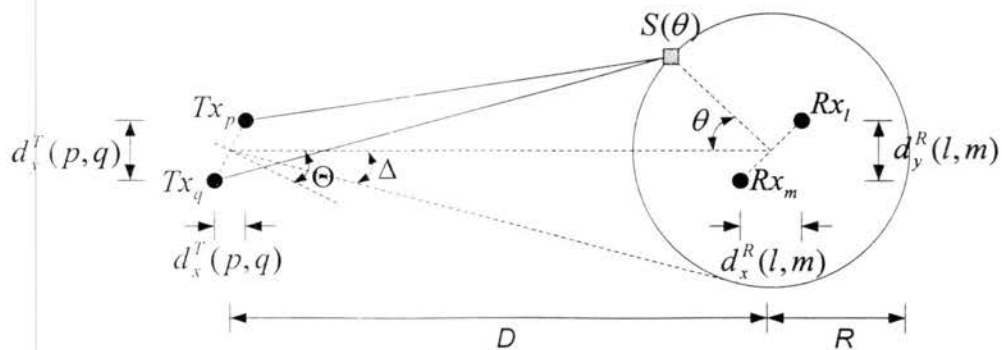


Figure 4.2 Continuous scatter one-ring model.

The following assumptions are usually made in this model [4], [28], [65]:

- a. Every actual scatter at an angle θ to the receiver is represented by a corresponding “effective scatter” located at the same angle on the scatter ring around the MT. The angle of actual scatters, and also effective scatters, are assumed uniformly distributed in $[0, 2\pi)$.
- b. Only rays that are reflected by scatters exactly once are considered.
- c. All rays that reach the receive antennas have equal power.

When there is an infinite number of scatters, the normalized complex path gain h_{lp} , which denotes the path going from the p^{th} transmit antenna to the l^{th} receive antenna, can be calculated as

$$h_{lp} = \frac{1}{\sqrt{2\pi}} \int_0^{2\pi} \exp \left[-j \frac{2\pi}{\lambda} (D_{Tx_p \rightarrow S(\theta)} + D_{S(\theta) \rightarrow Rx_l}) + j\phi(\theta) \right] d\theta \quad (4.1)$$

where $D_{X \rightarrow Y}$ is the distance from object X to object Y and λ is the wavelength. From central limit theory, h_{lp} constructed from (4.1) is complex $N(0, 1)$. Therefore, the channel constructed according to (4.1) is purely Rayleigh fading [75].

The covariance between two propagation channels h_{lp} and h_{mq} is

$$E[h_{lp} h_{mq}^*] = \frac{1}{\sqrt{2\pi}} \int_0^{2\pi} \exp \left[-j \frac{2\pi}{\lambda} (D_{Tx_p \rightarrow S(\theta)} - D_{Tx_q \rightarrow S(\theta)}) + (D_{S(\theta) \rightarrow Rx_l} + D_{S(\theta) \rightarrow Rx_m}) \right] d\theta. \quad (4.2)$$

When the BS angle spread is small, which is often the case in outdoor cellular systems, the following simplifications can be made:

$$D_{Tx_p \rightarrow S(\theta)} - D_{Tx_q \rightarrow S(\theta)} \approx d_x^T(p, q) \cos \Omega_\theta + d_y^T(p, q) \sin \Omega_\theta \quad (4.3)$$

$$\sin \Omega_\theta \approx (R/D) \sin \theta \approx \Delta \sin \theta$$

$$\cos \Omega_\theta \approx 1 - \frac{1}{2} (R/D)^2 \sin^2 \theta = 1 - \frac{1}{4} \Delta^2 + \frac{1}{4} \Delta^2 \cos 2\theta.$$

Therefore, the covariance of (4.2) can be approximated as

$$E[h_p h_{mq}] \approx \frac{1}{\sqrt{2\pi}} \int_0^{2\pi} \exp \left\{ -j \frac{2\pi}{\lambda} \left[d_x^T(p, q) \left(1 - \frac{\Delta^2}{4} + \frac{\Delta^2 \cos 2\theta}{4} \right) + \Delta d_y^T(p, q) \sin \theta + d_x^R(l, m) \sin \theta + d_y^R(l, m) \cos \theta \right] \right\} d\theta. \quad (4.4)$$

Since the MT is surrounded by local scatters, it has been shown that the correlation introduced by MT antennas is negligible if the antenna spacing is greater than half the wavelength [4]. In this case, the rows of channel matrix \mathbf{H} can be regarded as i.i.d. complex Gaussian row vectors with covariance matrix Σ , where $\Sigma_{pq} = E[h_{kp} (h_{kq})^H]$.

The covariance matrix of the channel matrix is then in the form of $\text{cov}[\text{vec}(\mathbf{H})] = \Sigma \otimes \mathbf{I}_{n_r}$.

Let $(\mathbf{B}\mathbf{B}^H)^T = \Sigma$, the following approximation can be used when analyzing the MIMO system capacity,

$$\mathbf{H} \sim \mathbf{H}_w \mathbf{B}^H \quad (4.5)$$

which means the distribution of \mathbf{H} is identical to the distribution of $\mathbf{H}_w \mathbf{B}^H$. This property is proved in [29].

4.1.2 Discrete Scatter One-Ring Model

Similar to the model proposed by Lee in [64], in the discrete scatter model, a finite number of effective scatters are evenly placed on a circle around the MT as shown in Figure 4.3. Each of these effective scatters represents many real scatters within a certain

region. The typical radius of the scatter ring is from 100 to 200 wavelengths. By using this model, the calculation of the covariance matrix can be numerically obtained more easily.

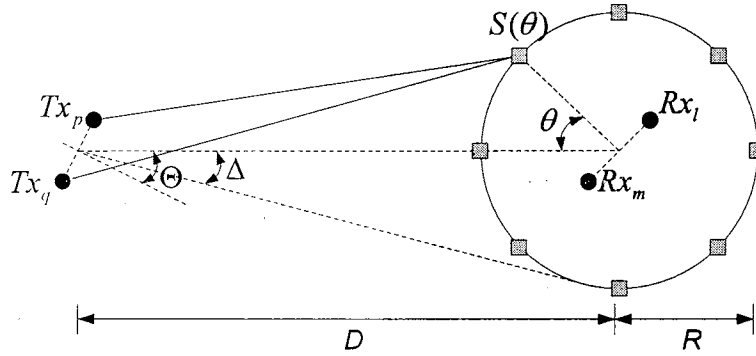


Figure 4.3 Discrete scatter one-ring model.

It must be observed that the models in the above figures are only suitable to evaluate spatial correlation. Some extensions have been proposed to incorporate the Doppler effect in this model [69], which will be investigated and used in the research.

4.1.3 Exponential Correlation Model

When an explicit way is needed to study the effects of correlation, i.e. the relationship between capacity and correlation, the exponential correlation model is commonly used [37], [91]. No physical parameter is needed to use this model. Instead, a correlation coefficient r will be chosen to compose the correlation matrix. For example, for the correlation occurring at the transmitter side, the correlation effect can be represented as

$$\Sigma = \left\{ r^{|i-j|} \right\}_{i,j=1,\dots,n_t}, \quad r \in [0, 1).$$

This model may not be an accurate model for specific real environments. But it is physically reasonable in the sense that the correlation decreases with increasing distance

between the antennas. Measurement results also show that this model provides reasonable conclusions when applied to MIMO systems [92]. The exponential correlation model can be easily used in the capacity vs. correlation analysis to get some insights about their relationship.

4.1.4 Correlation Effect

Monte-Carlo simulation is conducted to show the correlation effect by using a one-ring model. Capacity is calculated for different values of angle spread. The simulation parameters are shown in Table 4.1.

Antenna gain:	$G = 15$ dB
Bandwidth:	$B = 5 \times 10^6$ Hz
Transmit power:	$P_t = 10$ W
Noise figure:	$F = 2$
Receiver temperature:	$T = 300$ °K
Number of iterations:	$N = 10^4$ times
Propagation exponent:	3.5
Log-normal shadowing:	8 dB standard derivation
Fast fading:	Rayleigh PDF
Antenna array type:	Broadside antenna arrays
Antenna number:	$n_t = n_r = 5$
Correlation model:	One-ring model
Angle of arrival at BS:	90°

Table 4.1 Simulation parameters for correlation effects.

The result of the simulation is shown in Figure 4.4. For comparison purposes, the capacity of an independent MIMO system is also plotted. We can see that as the angle spread increases from 1° to 50° , the capacity of the correlated MIMO system increases gradually from 28 Mbps to 70 Mbps, which is almost the same as the capacity of the independent MIMO system. At the angle spread of 30° , the capacity difference between these two MIMO systems is only around 10%. Thus in the one-ring model, the correlation problem becomes significant only when the angle spread at the BS is very small, e.g., less than 20° . As the angle spread increases the correlated fading capacity approximates the independent fading capacity.

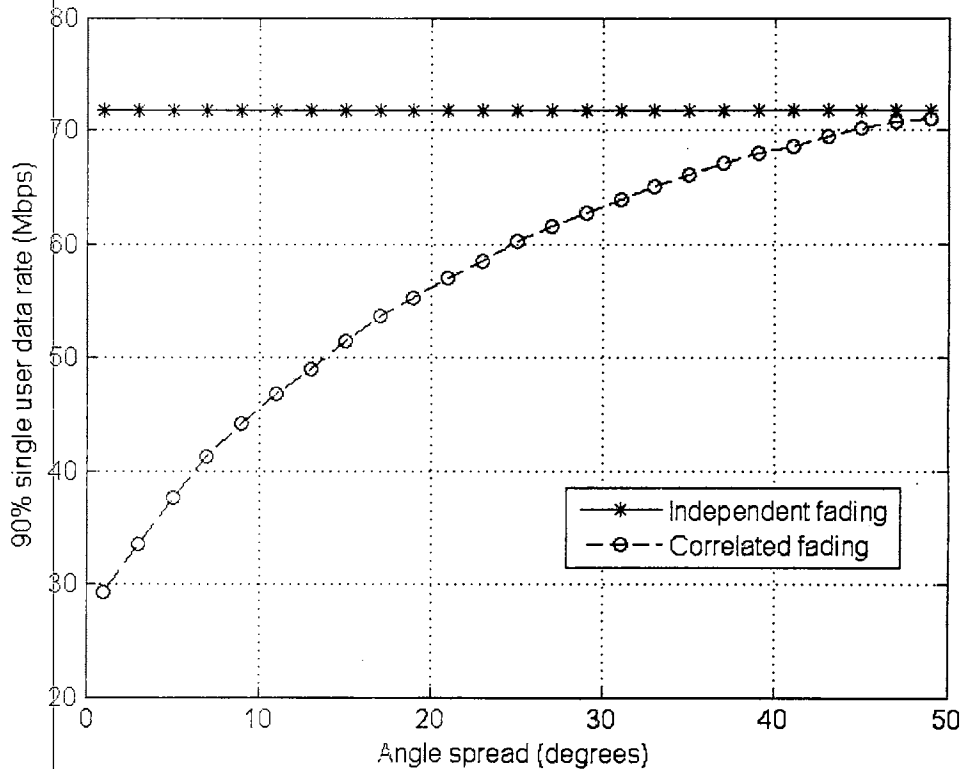


Figure 4.4 Correlation effect in MIMO systems.

4.2 Introduction to Random Matrix

For the multivariate analysis in this section and in the following sections of 4.3 and 4.4, a matrix \mathbf{H} with dimensions of $n \times m$ is used with $n \geq m$. This dimension notation is different from that used in the other part of this dissertation. It is used in here so that the equations can be read more easily.

4.2.1 Normally Distributed Random Matrix

If \mathbf{H} is a $n \times m$ matrix, then $\text{vec}(\mathbf{H})$ represents the $nm \times 1$ column vector formed by stacking the columns of \mathbf{H} under each other. For example, if the channel matrix is expressed as $\mathbf{H} = [\mathbf{h}_1 \quad \mathbf{h}_2 \quad \cdots \quad \mathbf{h}_m]$, where \mathbf{h}_j is $n \times 1$ vector for $j = 1, \dots, m$, then

$$\text{vec}(\mathbf{H}) = \begin{bmatrix} \mathbf{h}_1 \\ \mathbf{h}_2 \\ \vdots \\ \mathbf{h}_m \end{bmatrix}. \quad (4.6)$$

When we say a $n \times m$ matrix \mathbf{H} is complex Gaussian distributed, i.e., $\mathbf{H} \sim N(\boldsymbol{\mu}_H, \boldsymbol{\Psi})$, it is the same as saying $\text{vec}(\mathbf{H}) \sim N(\text{vec}(\boldsymbol{\mu}_H), \boldsymbol{\Psi})$, where the mean $\boldsymbol{\mu}_H = E(\mathbf{H})$, and $mn \times mn$ matrix $\boldsymbol{\Psi} = E\{[\text{vec}(\mathbf{H}) - \text{vec}(\boldsymbol{\mu}_H)] \cdot [\text{vec}(\mathbf{H}) - \text{vec}(\boldsymbol{\mu}_H)]^H\}$ is the covariance matrix. The covariance matrix is also the correlation matrix if \mathbf{H} has zero mean.

Usually, the correlation effects at the transmitter and receiver can be considered separately. Thus the matrix $\boldsymbol{\Psi}$ is decomposed into the transmitter correlation matrix $\boldsymbol{\Sigma}_m$ and the receiver correlation matrix $\boldsymbol{\Sigma}_n$. It can be further shown that the matrix $\boldsymbol{\Psi}$ can be represented in the form of a Kronecker product as $\boldsymbol{\Psi} = \boldsymbol{\Sigma}_m \otimes \boldsymbol{\Sigma}_n$, where $\boldsymbol{\Sigma}_m$ and $\boldsymbol{\Sigma}_n$ are $m \times m$ and $n \times n$ matrices. The density function of \mathbf{H} is

$$f(\mathbf{H}) = (2\pi)^{-mn/2} (\det \boldsymbol{\Sigma}_m)^{-m/2} (\det \boldsymbol{\Sigma}_n)^{-n/2} \text{etr} \left[-\frac{1}{2} \boldsymbol{\Sigma}_m^{-1} (\mathbf{H} - \boldsymbol{\mu}_H) \boldsymbol{\Sigma}_n^{-1} (\mathbf{H} - \boldsymbol{\mu}_H)^H \right] \quad (4.7)$$

where $\text{etr}(\mathbf{X})$ denotes $\exp[\text{trace}(\mathbf{X})]$. Notice that when the rows of \mathbf{H} are uncorrelated, $\boldsymbol{\Psi} = \boldsymbol{\Sigma}_m \otimes \mathbf{I}_n$. Similarly, when the columns of \mathbf{H} are uncorrelated, $\boldsymbol{\Psi} = \mathbf{I}_m \otimes \boldsymbol{\Sigma}_n$.

4.2.2 Special Case Normally Distributed Matrix

In the case where the $n \times m$ matrix \mathbf{H} is zero-mean, and has a correlation matrix $\boldsymbol{\Psi} = \mathbf{I} \otimes \boldsymbol{\Sigma}_n$ (the transmit antennas are uncorrelated), i.e., $\mathbf{H} \sim N(0, \mathbf{I} \otimes \boldsymbol{\Sigma}_n)$, the density function of \mathbf{H} is simplified as [36]

$$f(\mathbf{H}) = (2\pi)^{-mn/2} (\det \boldsymbol{\Sigma}_n)^{-n/2} \text{etr} \left(-\frac{1}{2} \boldsymbol{\Sigma}_n^{-1} \mathbf{H}^H \mathbf{H} \right). \quad (4.8)$$

4.2.3 Wishart Distribution

Let $\mathbf{A} = \mathbf{H}^H \mathbf{H}$, where $n \times m$ matrix $\mathbf{H} \sim N(0, \mathbf{I} \otimes \boldsymbol{\Sigma}_n)$, then $m \times m$ matrix \mathbf{A} is said to have the Wishart distribution with n degrees of freedom and a $m \times m$ covariance matrix $\boldsymbol{\Sigma}_m$. In the remaining parts of this chapter, we simply represent $\boldsymbol{\Sigma}_m$ as $\boldsymbol{\Sigma}$, i.e., the Wishart distribution will be written as $\mathbf{A} \sim W_m(n, \boldsymbol{\Sigma})$. The density function of \mathbf{A} is

$$f(\mathbf{A}) = \frac{1}{2^{mn/2} \Gamma_m(\frac{1}{2}n) (\det \boldsymbol{\Sigma})^{n/2}} \text{etr} \left(-\frac{1}{2} \boldsymbol{\Sigma}^{-1} \mathbf{A} \right) (\det \mathbf{A})^{(n-m-1)/2}. \quad (4.9)$$

4.3 Eigenvalue Distribution

4.3.1 Eigenvalue Distribution of Positive Definite Random Matrix

If \mathbf{A} is a $m \times m$ positive definite random matrix with density function $f(\mathbf{A})$, then the joint density function of the eigenvalues $\lambda_1, \dots, \lambda_m$ of \mathbf{A} is

$$f(\lambda_1, \dots, \lambda_m) = \frac{\pi^{m^2/2}}{\Gamma_m(\frac{1}{2}m)} \prod_{i < j} (\lambda_i - \lambda_j) \int_{O(m)} f(\mathbf{H}\mathbf{\Lambda}\mathbf{H}^H) d\mathbf{H} \quad (4.10)$$

where $\mathbf{\Lambda} = \text{diag}(\lambda_1, \dots, \lambda_m)$, $\lambda_1 > \lambda_2 > \dots > \lambda_m > 0$.

4.3.2 Eigenvalue Distribution of Wishart Random Matrix

If \mathbf{A} is $W_m(n, \mathbf{\Sigma})$ with $n \geq m$, the joint density function of the eigenvalues $\lambda_1, \dots, \lambda_m$ of \mathbf{A} can be represented as

$$\begin{aligned} f_W(\lambda_1, \dots, \lambda_m) \\ = \frac{\pi^{m^2/2} 2^{-mn/2} (\det \mathbf{\Sigma})^{-n/2}}{\Gamma_m(\frac{1}{2}m) \Gamma_m(\frac{1}{2}n)} \prod_{i=1}^m \lambda_i^{(n-m-1)/2} \prod_{i < j} (\lambda_i - \lambda_j) \int_{O(m)} \text{etr}\left(-\frac{1}{2} \mathbf{\Sigma}^{-1} \mathbf{H}\mathbf{\Lambda}\mathbf{H}^H\right) d\mathbf{H}. \end{aligned} \quad (4.11)$$

4.3.3 Hypergeometric Function Representation

A. Hypergeometric Function Notation

1) Generalized Hypergeometric Function

For given integer numbers p and q , the generalized hypergeometric function of matrix argument \mathbf{X} is

$${}_pF_q(a_1, \dots, a_p; b_1, \dots, b_q; \mathbf{X}) = \sum_{k=0}^{\infty} \sum_{\kappa} \frac{(a_1)_{\kappa} \cdots (a_p)_{\kappa}}{(b_1)_{\kappa} \cdots (b_q)_{\kappa}} \frac{C_{\kappa}(\mathbf{X})}{k!} \quad (4.12)$$

where \sum_{κ} denotes summation over all partitions $\kappa = (k_1, \dots, k_m)$, $k_1 \geq \dots \geq k_m \geq 0$, of k ,

$C_{\kappa}(\mathbf{X})$ is the zonal polynomial of \mathbf{X} corresponding to κ . The generalized

hypergeometric coefficient $(a)_{\kappa}$ is given by the equation $(a)_{\kappa} = \prod_{i=1}^m (a - \frac{1}{2}(i-1))_{k_i}$,

where each term $(a)_k = a(a+1)\cdots(a+k-1)$, $(a)_0 = 1$.

Therefore ${}_pF_q(a_1, \dots, a_p; b_1, \dots, b_q; \mathbf{X})$ is a function of the complex symmetric $m \times m$ matrix \mathbf{X} depending on the arbitrary complex numbers a_1, \dots, a_p and b_1, \dots, b_q . Many special cases exist for this hypergeometric function, e.g., ${}_0F_0(\mathbf{X}) = e^{\text{tr}(\mathbf{X})}$.

2) Hypergeometric Functions with Two Matrix Arguments.

Hypergeometric functions with two symmetric $m \times m$ matrix \mathbf{X} and \mathbf{Y} as arguments are given by

$${}_pF_q^{(m)}(a_1, \dots, a_p; b_1, \dots, b_q; \mathbf{X}, \mathbf{Y}) = \sum_{k=0}^{\infty} \sum_{\kappa} \frac{(a_1)_{\kappa} \cdots (a_p)_{\kappa}}{(b_1)_{\kappa} \cdots (b_q)_{\kappa}} \frac{C_{\kappa}(\mathbf{X})C_{\kappa}(\mathbf{Y})}{k! C_{\kappa}(\mathbf{I}_m)}. \quad (4.13)$$

Notice that if one of the argument matrices is the identity, this hypergeometric function reduces to the one-matrix function defined before, for example

$${}_pF_q^{(m)}(a_1, \dots, a_p; b_1, \dots, b_q; \mathbf{X}, \mathbf{I}_m) = {}_pF_q(a_1, \dots, a_p; b_1, \dots, b_q; \mathbf{X}). \quad (4.14)$$

B. Eigenvalue Distribution in Correlated Case

The matrix integration term in (4.11) can be changed to

$$\int_{O(m)} e^{\text{tr}\left(-\frac{1}{2}\Sigma^{-1}\mathbf{H}\Lambda\mathbf{H}^H\right)} d\mathbf{H} = \int_{O(m)} {}_0F_0\left(-\frac{1}{2}\Sigma^{-1}\mathbf{H}\Lambda\mathbf{H}^H\right) d\mathbf{H}. \quad (4.15)$$

From Theory 7.3.3 in [36], we have

$$\begin{aligned} & \int_{O(m)} {}_pF_q^{(m)}(a_1, \dots, a_p; b_1, \dots, b_q; \mathbf{X}\mathbf{H}\mathbf{Y}\mathbf{H}^H) d\mathbf{H} \\ &= {}_pF_q^{(m)}(a_1, \dots, a_p; b_1, \dots, b_q; \mathbf{X}, \mathbf{Y}) \end{aligned} \quad (4.16)$$

Therefore, equation (4.15) becomes

$$\int_{O(m)} {}_0F_0\left(-\frac{1}{2}\Sigma^{-1}\mathbf{H}\Lambda\mathbf{H}^H\right) d\mathbf{H} = {}_0F_0^{(m)}\left(-\frac{1}{2}\Sigma^{-1}, \Lambda\right) \quad (4.17)$$

Substituting (4.17) in the integration term of (4.11), the joint eigenvalue distribution of the Wishart matrix becomes

$$f_W(\lambda_1, \dots, \lambda_m) = \frac{\pi^{m^2/2} 2^{-mn/2} (\det \Sigma)^{-n/2}}{\Gamma_m(\frac{1}{2}m) \Gamma_m(\frac{1}{2}n)} {}_0F_0^{(m)}\left(-\frac{1}{2}\Sigma^{-1}, \Lambda\right) \prod_{i=1}^m \lambda_i^{(n-m-1)/2} \prod_{i<j}^m (\lambda_i - \lambda_j) \quad (4.18)$$

$$\lambda_1 > \lambda_2 \cdots > \lambda_m > 0.$$

C. Eigenvalue Distribution in Independent Case

In the non-correlated case, Wishart matrix \mathbf{A} has a distribution of $W_m(n, \sigma \cdot \mathbf{I}_m)$ with $n \geq m$, therefore the integration term in equation (4.11) is

$$\begin{aligned} & \int_{O(m)} \text{etr}\left(-\frac{1}{2}\Sigma^{-1}\mathbf{H}\Lambda\mathbf{H}^H\right) (d\mathbf{H}) \\ &= \int_{O(m)} \text{etr}\left(-\frac{1}{2\sigma}\mathbf{H}\Lambda\mathbf{H}^H\right) (d\mathbf{H}) \\ &= \text{etr}\left(-\frac{1}{2\sigma}\Lambda\right) \int_{O(m)} (d\mathbf{H}) \\ &= \exp\left(-\frac{1}{2\sigma} \sum_{i=1}^m \lambda_i\right). \end{aligned} \quad (4.19)$$

Therefore, the joint density function of the eigenvalues $\lambda_1, \dots, \lambda_m$ of \mathbf{A} becomes

$$f_W(\lambda_1, \dots, \lambda_m) = \frac{\pi^{m^2/2} (2\sigma)^{-mn/2}}{\Gamma_m(\frac{1}{2}m) \Gamma_m(\frac{1}{2}n)} \exp\left(-\frac{1}{2\sigma} \sum_{i=1}^m \lambda_i\right) \prod_{i=1}^m \lambda_i^{(n-m-1)/2} \prod_{i<j}^m (\lambda_i - \lambda_j) \quad (4.20)$$

for the eigenvalues $\lambda_1 > \lambda_2 \cdots > \lambda_m > 0$.

D. Complex Normal Distribution

In the case where matrix \mathbf{H} is a complex $n \times m$ matrix, i.e., $\mathbf{H} = \mathbf{H}_r + j\mathbf{H}_i$, the eigenvalues distribution of $\mathbf{A} = \mathbf{H}\mathbf{H}^H$ is [35]

$$f_{IV}(\lambda_1, \dots, \lambda_m) = \frac{\pi^{m(m-1)} 2^{-mn/2} (\det \Sigma)^{-n}}{\Gamma_m(m) \Gamma_m(n)} {}_0F_0^{(m)}(-\Sigma^{-1}, \mathbf{A}) \prod_{i=1}^m \lambda_i^{(n-m)} \prod_{i < j}^m (\lambda_i - \lambda_j)^2 \quad (4.21)$$

$$\lambda_1 > \lambda_2 > \dots > \lambda_m > 0$$

where $\tilde{\Gamma}_m(\alpha) = \pi^{m(m-1)/2} \sum_{i=1}^m \Gamma(\alpha - i + 1)$ is the complex multivariate gamma function.

${}_0\tilde{F}_0(\mathbf{A}) = e^{tr(\mathbf{A})}$ is the special case complex hypergeometric function.

$$\begin{aligned} {}_0\tilde{F}_0(-\Sigma^{-1}, \mathbf{A}) &\stackrel{def}{=} \int_{\mathcal{O}(m)} \exp(-tr \Sigma^{-1} \mathbf{X} \mathbf{A} \mathbf{X}^H) d\mathbf{X} \\ &= \det(\Sigma)^\alpha e^{-tr \mathbf{A}} \sum_{k=0}^{\infty} \sum_{\kappa} \frac{C_{\kappa}(\mathbf{I} - \Sigma) L_{\kappa}^{(\alpha - (m+1)/2)}(\mathbf{A})}{C_{\kappa}(\mathbf{I}) k!} \end{aligned} \quad (4.22)$$

4.4 Evaluation of Eigenvalue Distribution

4.4.1 Truncated Summation Approach

Among the terms in equation (4.21), the two-matrix-argument hypergeometric function ${}_0\tilde{F}_0(-\Sigma^{-1}, \mathbf{A})$ can be expressed as

$${}_0\tilde{F}_0(-\Sigma^{-1}, \mathbf{A}) = \sum_{k=0}^{\infty} \sum_{\kappa} \frac{C_{\kappa}(-\Sigma^{-1}) C_{\kappa}(\mathbf{A})}{C_{\kappa}(\mathbf{I}_m) k!}. \quad (4.23)$$

To numerically evaluate this term, summation to infinity needs to be replaced by an big-enough number β

$${}_0\tilde{F}_0(-\Sigma^{-1}, \mathbf{A}) = \sum_{k=0}^{\beta} \sum_{\kappa} \frac{C_{\kappa}(-\Sigma^{-1}) C_{\kappa}(\mathbf{A})}{C_{\kappa}(\mathbf{I}_m) k!} \quad (4.24)$$

where the $C_{\kappa}(\mathbf{I}_m)$ term can be evaluated as

$$C_{\kappa}(\mathbf{I}_m) = 2^{2k} k! \left(\frac{1}{2} m\right)_{\kappa} \frac{\prod_{i < j}^p (2k_i - 2k_j - i + j)}{\prod_{i=1}^p (2k_i + p - i)!}. \quad (4.25)$$

For the general case of zonal polynomial, there is no known formula [36]. However, it can be evaluated as a monomial expansion of $M_\lambda(\mathbf{A})$

$$C_\kappa(\mathbf{A}) = \sum_{\lambda < \kappa} c_{\kappa,\lambda} M_\lambda(\mathbf{A}) \quad (4.26)$$

where $c_{\kappa,\lambda}$ is a constant and the summation is over all partitions λ of k with $\lambda \leq \kappa$, i.e., λ is below or equal to κ in the lexicographical ordering. Coefficients $c_{\kappa,\lambda}$ can be calculated in an iterative way as

$$c_{\kappa,\lambda} = \sum_{\lambda < \mu \leq \kappa} \frac{[(l_i + t) - (l_i - t)]}{\rho_\kappa - \rho_\lambda} c_{\kappa,\mu} \quad (4.27)$$

where $\lambda = (l_1, \dots, l_m)$ and $\mu = (l_1, \dots, l_i + t, \dots, l_j - t, l_m)$ for $t = (1, \dots, l_j)$ such that, when the parts of the partition μ are arranged in descending order, μ is above λ and below or equal to κ in the lexicographical ordering. It can be seen that this is an iterative equation. It determines all coefficients in the expansion of $C_\kappa(\mathbf{A})$ except for the coefficient $c_{\kappa,\kappa}$. It is known that $c_{(k),(k)} = 1$. For other $c_{\kappa,\kappa}$ values, James proves that [35]

$$c_{\kappa,\kappa} = \frac{2^{2k} k!}{(2k)!} \chi_{[2\kappa]}(1) \prod_{l=1}^p \prod_{i=1}^l \left(\frac{1}{2} l - \frac{1}{2} (i-1) + k_i - k_l \right)_{k_i - k_l + 1} \quad (4.28)$$

where $\chi_{[2\kappa]}(1)$ is given as

$$\chi_{[2\kappa]}(1) = \frac{(2k)! \prod_{i < j}^p (2k_i - 2k_j - i + j)}{\prod_{i=1}^p (2k_i + p - i)!} \quad (4.29)$$

where p is the number of nonzero parts in the partition κ . The monomial symmetric function

$$M_\kappa(\mathbf{A}) = \sum \dots \sum \lambda_{i_1}^{k_1} \lambda_{i_2}^{k_2} \dots \lambda_{i_p}^{k_p}. \quad (4.30)$$

The summation above is over the distinct permutations of p different integers from the integers $1, 2, \dots, m$.

This eigenvalue distribution involves the evaluation of hypergeometric function with matrix arguments, which is expressed in terms of zonal polynomials. No closed-form equation can be obtained for this expression. Also the numerical evaluation method has been proven to converge very slowly for strongly correlated MIMO channels.

4.4.2 Closed-Form Expression

In reference [37], the authors provide an alternative expression for joint eigenvalue distribution in correlated MIMO channels. This method provides closed-form PDF functions for the channel eigenvalues in a correlated environment. Under the restriction that eigenvalues of a correlation matrix are all distinct, the hypergeometric function with matrix argument ${}_0\tilde{F}_0(-\Sigma^{-1}, \mathbf{A})$ can be expressed in terms of determinants of matrices whose elements are hypergeometric functions of scalar arguments:

$${}_0\tilde{F}_0(-\Sigma^{-1}, \mathbf{A}) = \zeta_{n_{\min}} \frac{|\mathbf{F}(\boldsymbol{\lambda}, \boldsymbol{\sigma})|}{|\mathbf{V}_1(\boldsymbol{\lambda})| |\mathbf{V}_2(\boldsymbol{\sigma})|} \quad (4.31)$$

where $\boldsymbol{\sigma} = [\sigma_1, \sigma_2, \dots, \sigma_{n_{\min}}]$ with $\sigma_1 > \sigma_2 > \dots > \sigma_{n_{\min}}$ denotes the ordered eigenvalues of

correlation matrix Σ ; $\zeta_{n_{\min}} = \prod_{j=1}^{n_{\min}} (j-1)!$ is a constant value; $\mathbf{F}(\mathbf{x}, \boldsymbol{\sigma})$ is a matrix of scalar-

argument hypergeometric functions defined in (4.32).

$$\mathbf{F}(\boldsymbol{\lambda}, \boldsymbol{\sigma}) = \begin{bmatrix} {}_0\tilde{F}_0(-\lambda_1 / \sigma_1) & {}_0\tilde{F}_0(-\lambda_2 / \sigma_1) & \cdots & {}_0\tilde{F}_0(-\lambda_{n_{\min}} / \sigma_1) \\ {}_0\tilde{F}_0(-\lambda_1 / \sigma_2) & {}_0\tilde{F}_0(-\lambda_2 / \sigma_2) & \cdots & {}_0\tilde{F}_0(-\lambda_{n_{\min}} / \sigma_2) \\ \vdots & \vdots & \ddots & \vdots \\ {}_0\tilde{F}_0(-\lambda_1 / \sigma_{n_{\min}}) & {}_0\tilde{F}_0(-\lambda_2 / \sigma_{n_{\min}}) & \cdots & {}_0\tilde{F}_0(-\lambda_{n_{\min}} / \sigma_{n_{\min}}) \end{bmatrix} \quad (4.32)$$

$\mathbf{V}_1(\boldsymbol{\lambda})$ is a Vandermonde matrix defined by

$$\mathbf{V}_1(\boldsymbol{\lambda}) = \begin{bmatrix} 1 & 1 & \cdots & 1 \\ \lambda_1 & \lambda_2 & \cdots & \lambda_{n_{\min}} \\ \vdots & \vdots & \ddots & \vdots \\ \lambda_1^{n_{\min}-1} & \lambda_2^{n_{\min}-1} & \cdots & \lambda_{n_{\min}}^{n_{\min}-1} \end{bmatrix}. \quad (4.33)$$

$\mathbf{V}_2(\boldsymbol{\sigma})$ is also a Vandermonde matrix defined by

$$\mathbf{V}_2(\boldsymbol{\sigma}) = \mathbf{V}_1(-[\sigma_1^{-1}, \dots, \sigma_{n_{\min}}^{-1}]). \quad (4.34)$$

Therefore, the joint eigenvalue distribution becomes

$$f(\lambda_1, \dots, \lambda_{n_{\min}}) = K_{\Sigma} |\mathbf{F}(\boldsymbol{\lambda}, \boldsymbol{\sigma})| |\mathbf{V}_1(\boldsymbol{\lambda})| \prod_{i=1}^{n_{\min}} \lambda_i^{(n_{\max}-n_{\min})} \quad (4.35)$$

where the normalizing constant $K_{\Sigma} = K_{\xi_{n_{\min}}} \cdot \frac{|\boldsymbol{\Sigma}|^{-n_{\max}}}{|\mathbf{V}_2(\boldsymbol{\sigma})|}$ only depends on matrix $\boldsymbol{\Sigma}$ through its eigenvalues. Thus, the functions of matrices are changed to matrices of scalar arguments. This will simplify the following capacity derivations.

The marginal probability density function of λ_k , $1 \leq k \leq n_{\min}$ can be calculated as

$$p_k(\lambda_k) = \int_{\lambda_k}^{\infty} d\lambda_{k-1} \cdots \int_{\lambda_3}^{\infty} d\lambda_2 \int_{\lambda_2}^{\infty} d\lambda_1 \int_0^{\lambda_k} d\lambda_{k+1} \cdots \int_0^{\lambda_{n_{\min}-2}} d\lambda_{n_{\min}-1} \int_0^{\lambda_{n_{\min}-1}} f(\lambda_1, \dots, \lambda_{n_{\min}}) d\lambda_{n_{\min}}.$$

Notice that this calculation is a two-way process: The integrations of all eigenvalues less than λ_k is from 0 to the next larger eigenvalue; while the integrations of all eigenvalues larger than λ_k is from the next less eigenvalue to infinity ∞ . This is because that in PDF function $f_{\lambda}(\lambda_1, \dots, \lambda_m)$, eigenvalues are in order.

Example: For a 2×2 complex Gaussian channel matrix \mathbf{H} with correlation matrix Σ , the eigenvalue distribution is

$$f(\lambda_1, \lambda_2) = K_\Sigma \left(e^{-\frac{\lambda_1}{\sigma_1} - \frac{\lambda_2}{\sigma_2}} - e^{-\frac{\lambda_1}{\sigma_2} - \frac{\lambda_2}{\sigma_1}} \right) (\lambda_1 - \lambda_2)$$

where $K_\Sigma = \frac{1}{\sigma_1 \sigma_2 (\sigma_1 - \sigma_2)}$.

The marginal PDF functions of λ_1 and λ_2 can be found as

$$f(\lambda_1) = \int_0^{\lambda_1} f_\lambda(\lambda_1, \lambda_2) d\lambda_2$$

$$f(\lambda_2) = \int_{\lambda_2}^{\infty} f_\lambda(\lambda_1, \lambda_2) d\lambda_1.$$

Eigenvalue distribution functions of uncorrelated MIMO channel and MIMO channels with angle spread of 30° and 10° are plotted below for comparison.

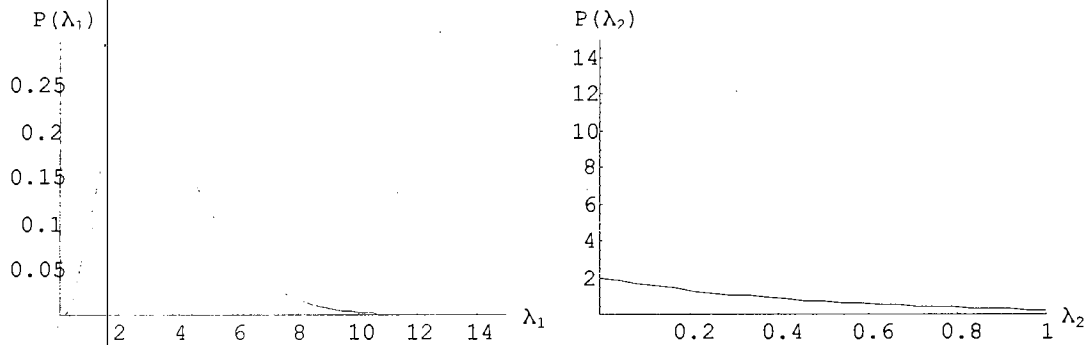


Figure 4.5 Eigenvalue distributions for 2×2 uncorrelated MIMO systems.

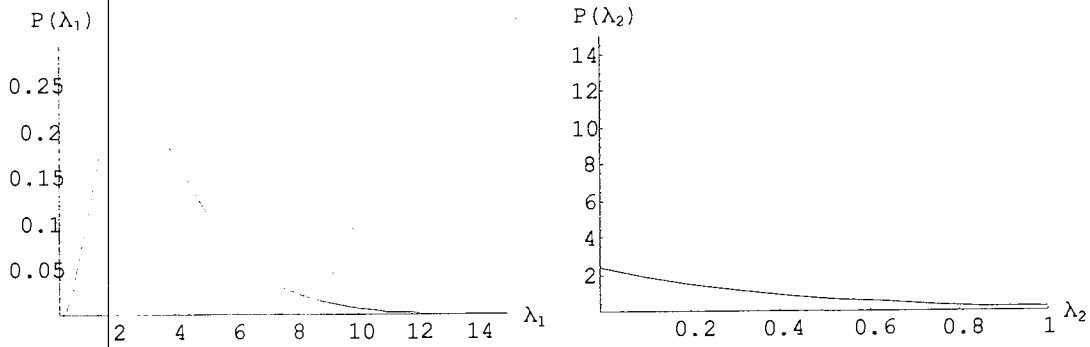


Figure 4.6 Eigenvalue distributions for 2×2 correlated MIMO systems
(30° angle spread).

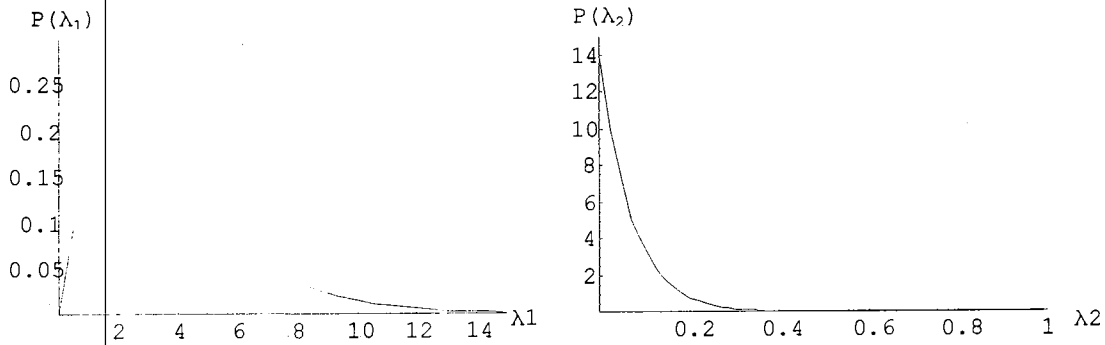


Figure 4.7 Eigenvalue distributions for 2×2 correlated MIMO systems
(10° angle spread).

4.5 Characteristic Function (c.f.) Method for MIMO System Throughput

In this section, we use the c.f. method to evaluate the correlation effect on the adaptive modulation data rate. It has been shown in chapter III that the expression of adaptive modulation data rate is similar to that of the capacity, with the only difference being in the modified SNR value. Thus, the observations in this section will also apply to the system capacity.

4.5.1 Characteristic Function Method

Assuming that the data rate is continuously adapted and the transmit power is uniformly allocated among all spatial sub-channels, the data rate of a MIMO system has been shown in equation (3.27) as

$$D = \sum_{i=1}^{n_{\min}} \log_2 \left(1 + \frac{\rho'}{n_t} \lambda_i \right) \quad (4.38)$$

where $\rho' = \frac{1.5\rho}{-\ln(5BER)}$. Then the c.f. of the data rate can be expressed as

$$\begin{aligned} \phi_D(z) &= E_D \left[e^{j2\pi Dz} \right] \\ &= \int_D e^{j2\pi Dz} f(D) dD \\ &= \int_{\lambda} e^{j2\pi z \sum_i \log_2 \left(1 + \frac{\rho'}{n_t} \lambda_i \right)} f_{\lambda}(\lambda) d\lambda \\ &= \int_{\lambda} \left[\prod_i \left(1 + \frac{\rho'}{n_t} \lambda_i \right) \right]^{\frac{j2\pi z}{\ln 2}} f_{\lambda}(\lambda) d\lambda \end{aligned} \quad (4.39)$$

where \int_{λ} is the ordered integration $\int_{\lambda_1} \int_{\lambda_2} \dots \int_{\lambda_{n_{\min}}}$. By inserting the PDF function of (4.35),

the c.f. becomes

$$\begin{aligned} \phi_D(z) &= \int_{\lambda} \prod_{i=1}^{n_{\min}} \left(1 + \frac{\rho'}{n_t} \lambda_i \right)^{\frac{j2\pi z}{\ln 2}} \cdot K_{\Sigma} \cdot \det[\mathbf{E}(\lambda, \boldsymbol{\sigma})] \cdot \det[\mathbf{V}_1(\lambda)] \cdot \prod_{i=1}^{n_{\min}} (\lambda_i)^{n_{\max} - n_{\min}} d\lambda \\ &= K_{\Sigma} \int_{\lambda} \det[\mathbf{E}(\lambda, \boldsymbol{\sigma})] \cdot \det[\mathbf{V}_1(\lambda)] \cdot \prod_{i=1}^{n_{\min}} \left[\left(1 + \frac{\rho'}{n_t} \lambda_i \right)^{\frac{j2\pi z}{\ln 2}} \cdot (\lambda_i)^{n_{\max} - n_{\min}} \right] d\lambda. \end{aligned} \quad (4.40)$$

The identity in [37] indicates that

$$\begin{aligned}
& \int_{x_1} \cdots \int_{x_N} \det \mathbf{\Phi}(\mathbf{x}) \cdot \det \mathbf{\Psi}(\mathbf{x}) \cdot \prod_{k=1}^N \xi(x_k) dx \\
& = \det \left[\int_a^b \Phi_i(x) \Psi_j(x) \xi(x) dx \right]_{i,j=1,\dots,N}
\end{aligned} \tag{4.41}$$

where $\mathbf{\Phi}(\mathbf{x})$ and $\mathbf{\Psi}(\mathbf{x})$ are arbitrary square matrices; $\xi(x_k)$ is an arbitrary function; and the multiple integral is over $\{b \geq x_1 \geq x_2 \geq \cdots \geq x_N \geq a\}$. Let

$$\mathbf{\Phi}(\mathbf{x}) = \mathbf{E}(\boldsymbol{\lambda}, \boldsymbol{\sigma}) \tag{4.42}$$

$$\mathbf{\Psi}(\mathbf{x}) = \mathbf{V}_1(\boldsymbol{\lambda})$$

$$\xi(x_k) = \left(1 + \frac{\rho'}{N} \lambda_i\right)^{\frac{j2\pi z}{\ln 2}} \cdot (\lambda_i)^{n_{\max} - n_{\min}}.$$

Equation (4.40) can be changed to

$$\begin{aligned}
\phi_D(z) &= K_{\Sigma} \det \left[\int_0^{\infty} e^{-\frac{x}{\sigma_l}} \cdot (x)^{m-1} \cdot \left(1 + \frac{\rho'}{n_l} \omega x\right)^{\frac{j2\pi z}{\ln 2}} \cdot \left(\frac{x}{\omega}\right)^{n_{\max} - n_{\min}} dx \right]_{l,m=0,\dots,n_{\min}} \\
&= K_{\Sigma} \det \left[\int_0^{\infty} e^{-\frac{x}{\sigma_l}} \cdot (x)^{n_{\max} - n_{\min} + m - 1} \cdot \left(1 + \frac{\rho'}{n_l} x\right)^{\frac{j2\pi z}{\ln 2}} dx \right]_{l,m=0,\dots,n_{\min}}.
\end{aligned} \tag{4.43}$$

Reference [37] shows the following equation is valid for $\text{Re}\{a\} > 0$, $n \geq 0$,

$\arg\{b\} \neq \pi$, where

$$\begin{aligned}
& \int_0^{\infty} x^n (1 + bx)^y e^{-\frac{x}{a}} dx \\
& = \frac{n! \Gamma(-1 - n - y) {}_1F_1\left(1 + n, n + y + 2, \frac{1}{ab}\right)}{b^{n+1} \Gamma(-y)} + a^{n+1+y} b^y \Gamma(n + 1 + y) {}_1F_1\left(-y, -n - y, \frac{1}{ab}\right)
\end{aligned} \tag{4.44}$$

In which $\Gamma(\cdot)$ is gamma function and ${}_1F_1(\cdot, \cdot, \cdot)$ is hypergeometric function. Let

$$n = n_{\max} - n_{\min} + m - 1 \quad (4.45)$$

$$a = \sigma_l$$

$$b = \frac{\rho^l}{n_l}$$

$$y = \frac{-j2\pi z}{\ln 2}.$$

A compact form of the inner part of the $\phi_D(z)$ expression can be obtained as

$$\phi_D(z) = K_{\Sigma} \det \left[\begin{array}{c} \left\{ \frac{n! \Gamma(-1-n-y) {}_1F_1\left(1+n, n+y+2, \frac{1}{ab}\right)}{\omega^n b^{n+1} \Gamma(-y)} \right. \\ \left. + \frac{a^{n+1+y} b^y \Gamma(n+1+y) {}_1F_1\left(-y, -n-y, \frac{1}{ab}\right)}{\omega^n} \right\}_{l,m=0,\dots,n_{\min}} \end{array} \right] \quad (4.46)$$

Now the data rate PDF function can be obtained by doing FFT transformation as

$$f_D(x) = \int_{-\infty}^{\infty} \phi_D(z) e^{-j2\pi x z} dz. \quad (4.47)$$

The expression of the data rate cumulative distribution function (CDF) function can be obtained as

$$\begin{aligned}
F_D(x) &= \int_0^x f_D(\alpha) d\alpha \\
&= \int_0^x \int_{-\infty}^{\infty} \phi_D(z) e^{-j2\pi z \alpha} dz d\alpha \\
&= \int_{-\infty}^{\infty} \phi_D(z) dz \cdot \int_0^x e^{-j2\pi z \alpha} d\alpha \\
&= \int_{-\infty}^{\infty} \phi_D(z) \left(\frac{1 - e^{-j2\pi z x}}{j2\pi z} \right) dz.
\end{aligned} \tag{4.48}$$

4.5.2 Results and Analysis

A 2×2 MIMO system is used in this section to verify the results of the c.f. method. Here only small-scale fading is considered. Assuming a one-ring correlation model with correlation at the receiver end only, the outage capacity performance curves are obtained using the method introduced in this section. Situations ranging from independent fading to 5° angle spread are considered and results are drawn in Figure 4.8. To show the validity of this method, Monte-Carlo simulation results for the same situations are also plotted. It can be seen that these two methods give identical results in all situations.

As shown in other literature, as the angle spread decreases, the whole outage capacity curve moves to the left side, i.e., capacities at all outage levels are reduced. This is because the phases and amplitudes of the signals received by different antennas are more likely to be similar to each other. Thus, these received signals are more correlated to each other and less multiplexing gain can be exploited. If we take a look at the lower tail which is the region of interest, the 10% outage capacity is seen to decrease from 3.9 bps/Hz in the independent fading case to 2.75 bps/Hz in the 5° angle spread case. This represents a 30% reduction in the outage capacity.

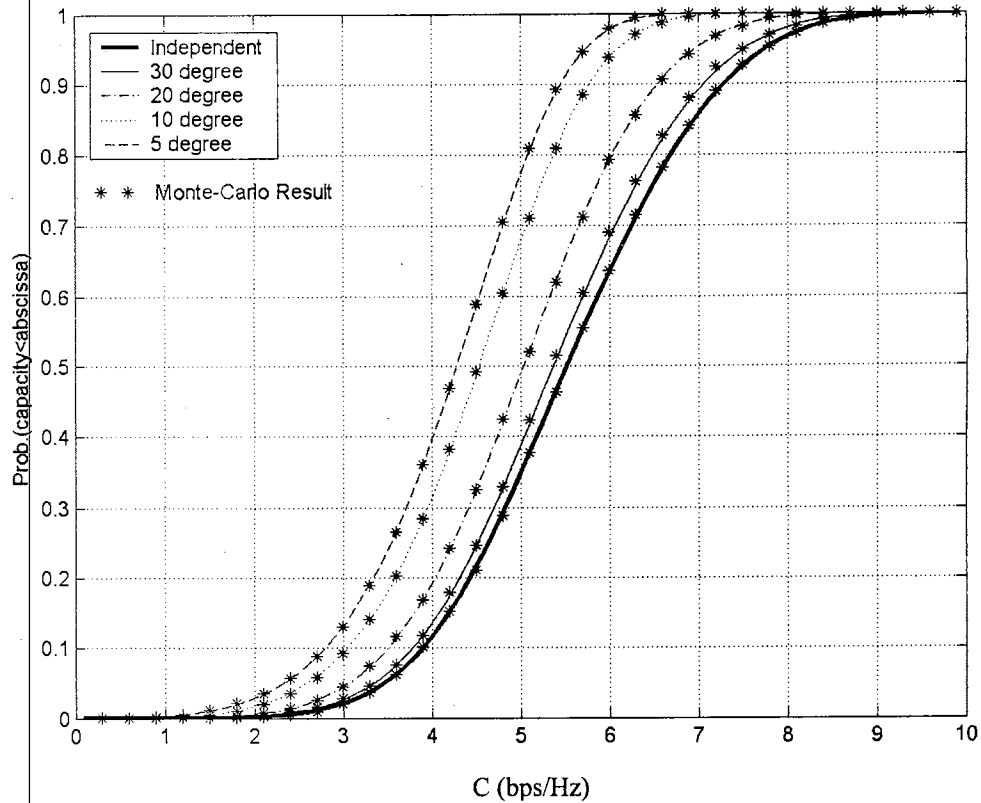


Figure 4.8 Outage capacity in different correlation situations.

4.6 Summary

In practical environments, the correlation effects limit the capacity increase of MIMO systems. Different correlation models are investigated and the appropriate model is selected for this research. By using the one-ring model, the results from the Monte-Carlo simulation show that the correlation effect can greatly reduce the MIMO capacity when the angle spread is small. This problem will be further investigated in the following chapter and solutions will be proposed.

The effects of correlation in MIMO systems are analyzed through the eigenvalues of the channel matrix. The eigenvalue distributions function is derived by assuming the channel matrix to be Gaussian distributed. While the distribution function is manageable for independent MIMO systems, it becomes too complicated to be used in correlated MIMO systems even for a small system configuration. Numerical method has been applied to approximate the correlated distribution by calculating zonal polynomials and truncating the summations. However, this method converges too slowly to approximate the correct results, especially for the highly correlated MIMO systems. Thanks to the work of Chiani *et al.* [37], the hypergeometric function with matrix arguments is converted into a matrix of hypergeometric functions with scalar arguments. Thus, along with the characteristic function method, the MIMO system capacity can be exactly calculated in both independent and correlated systems. This capacity calculation method is verified by Monte-Carlo simulation and it will be used in the research of the following chapter.

CHAPTER V

MACROSCOPIC DIVERSITY MIMO SYSTEM

Methods of using macroscopic diversity to combat the large-scale shadowing effect have been investigated in numerous papers. In this chapter, the effect of macroscopic diversity in MIMO systems is studied. By placing antennas at different BSs, these antennas will experience different shadowing components and it will be very unlikely that their shadowing factors are correlated to each other [119]. Thus a large-scale shadowing diversity gain is obtained. By deriving and evaluating the upper-bound of the system capacity, this chapter shows that implementing macroscopic diversity in MIMO systems can significantly improve the capacity at the lower tail of a capacity CDF curve, which is the region of most interest.

5.1 Introduction to Shadowing Effect

In addition to multipath correlation, the received signal is degraded by large scale physical obstacles in the propagation path, resulting in a phenomenon called shadowing. Usually, in a MIMO system the transmitted directional signals from a BS to a MT are under a common shadowing influence even though the multipath signal scattering profile may be uncorrelated. In such a system, there would be significant reductions in obtainable channel capacity despite of an ample scattering profile.

Space diversity techniques have been investigated extensively in order to combat multipath Rayleigh fading as well as the shadowing effects in mobile communication. A few representative examples are discussed in the following. A majority of the early ideas

are well organized in [67] by Jakes, which deals with both multiple base-station diversity to combat shadowing, and small scale diversity techniques to overcome Rayleigh fading. The term macrodiversity was first used in [18] by Yeh, Wilson, and Schwartz. In [19] and [46], Turkmani provides a theoretical analysis of composite microscopic plus MSD combining within continuous phase modulation (CPM) systems. In [17], Haas and Li introduce the multiply-detected macrodiversity (MDM) scheme, which utilizes the maximum-likelihood bit-by-bit decision criterion on the combined information. The MDM scheme is based on postdetection combining of information rather than predetection combining techniques.

Diversity schemes have also been applied in MIMO systems research. In [87], the channel capacity as well as its upper and lower bounds are derived for MIMO-based macroscopic diversity combining systems applying selection diversity and stochastic water filling in composite fading environments. In [89], a performance analysis based on computer simulation was conducted for MIMO distributed antenna systems. Commonly, macroscopic diversity is applied to overcome shadowed regions, improve the bit error rate over fixed data rate channels, reduce the signal outage, and/or simply increase the number of user channels through multiplexing more channels into the cell area.

5.2 System Model

We consider the case where each element in the channel matrix experiences both Rayleigh fading and shadowing effect. According to [9], a composite fading-shadowing component can be expressed as the product of the short term multipath fading and the long term shadow fading, and they are an independent random process. Following this approach, the element representing the channel attenuation from the j^{th} transmitter to the

i^{th} receiver, which is a composite Rayleigh fading – lognormal shadowing component, can be represented as $(h_c)_{ij} = h_{ij}\omega_{ij}^{1/2}$ where h_{ij} is a zero-mean, unit-variance complex Gaussian random variable representing the Rayleigh fading part and $\omega_{ij}^{1/2}$ is the shadowing part. The power ω_{ij} follows a log-normal distribution. We use $\mathbf{H}_c = \mathbf{\Omega}^{1/2}\mathbf{H}$ to represent the composite fading channel matrix. Thus the MIMO system capacity is in the form of $C = \log_2 \det\left(\mathbf{I} + \frac{\rho}{n_t} \mathbf{H}_c \mathbf{H}_c^H\right)$.

In this section, uplink cellular communication is studied, which is generally considered as the performance-limiting link due to the limited power at the MT. We consider the case where $n_r = n_t$. But for the clarity of the derivation, the symbols n_r and n_t will still be used in the following equations of this chapter.

5.2.1 Standard MIMO System

In standard MIMO systems, all receive antennas are located at the same BS. Therefore all channels experience the same shadowing effect. The channel matrix can be expressed as

$$\begin{aligned} \mathbf{H}_c &= \omega^{1/2} \mathbf{H} \\ &= \begin{bmatrix} \omega^{1/2} h_{11} & \omega^{1/2} h_{12} & \cdots & \omega^{1/2} h_{1n_t} \\ \omega^{1/2} h_{21} & \omega^{1/2} h_{22} & & \vdots \\ \vdots & & \ddots & \\ \omega^{1/2} h_{n_r,1} & \cdots & & \omega^{1/2} h_{n_r,n_t} \end{bmatrix}. \end{aligned} \quad (5.1)$$

Assuming a rich scattering environment, all Rayleigh fading components h_{ij} of matrix \mathbf{H} are totally uncorrelated. However, the log-normal shadowing components ω are identical, i.e., totally correlated. No macroscopic diversity can be exploited in this

system. This situation is related to the ‘keyhole’ analysis in [10]. In this system, although all the elements in \mathbf{H} are uncorrelated, they have only one DOF from the shadowing point of view. So the capacity achieved by this channel matrix is limited.

5.2.2 Macroscopic Diversity MIMO System

The ideal macroscopic diversity MIMO system is one where each BS antenna is located at a different location far away from each other so that their shadowing effects are uncorrelated. This is also called the distributed antenna system. The channel matrix with uncorrelated shadowing components can be expressed as

$$\begin{aligned}
 \mathbf{H}_c &= \mathbf{\Omega}^{1/2} \mathbf{H} \\
 &= \begin{bmatrix} \omega_1^{1/2} & & & \\ & \omega_2^{1/2} & 0 & \\ & 0 & \ddots & \\ & & & \omega_{n_r}^{1/2} \end{bmatrix} \times \begin{bmatrix} h_{11} & h_{12} & \cdots & h_{1n_t} \\ h_{21} & h_{22} & & \vdots \\ \vdots & & \ddots & \\ h_{n_r,1} & \cdots & & h_{n_r,n_t} \end{bmatrix} \\
 &= \begin{bmatrix} \omega_1^{1/2} h_{11} & \omega_1^{1/2} h_{12} & \cdots & \omega_1^{1/2} h_{1n_t} \\ \omega_2^{1/2} h_{21} & \omega_2^{1/2} h_{22} & & \vdots \\ \vdots & & \ddots & \\ \omega_{n_r}^{1/2} h_{n_r,1} & \cdots & & \omega_{n_r}^{1/2} h_{n_r,n_t} \end{bmatrix}
 \end{aligned} \tag{5.2}$$

This channel matrix has a DOF of n_r . Both macroscopic and microscopic diversity can be exploited. Higher capacity is expected compared to the first one.

5.3 Capacity Upper Bound

5.3.1 Capacity Comparison

A. Standard MIMO system

In standard MIMO systems, the channel matrix multiplication is

$$\begin{aligned}
\mathbf{H}_c(\mathbf{H}_c)^H &= (\omega^{1/2} H)(\omega^{1/2} H)^H \\
&= |\omega| \cdot \begin{bmatrix} \sum_i^{n_r} |h_{i1}|^2 & & \dots \\ & \sum_i^{n_r} |h_{i2}|^2 & \\ \dots & & \ddots \\ & & & \sum_i^{n_r} |h_{in_r}|^2 \end{bmatrix}
\end{aligned} \tag{5.3}$$

We observe that the diagonal elements are Chi-square distributed positive large value random variables (RVs) with degree of freedom of $2n_r$; while the non-diagonal elements are zero mean small value RVs. It will be shown later that these small value non-diagonal elements can be ignored in the capacity upper bound evaluation.

The MIMO capacity calculation can be simplified as

$$\begin{aligned}
C &= \log_2 \det \left[\mathbf{I} + \frac{\rho}{n_t} \mathbf{H}_c(\mathbf{H}_c)^H \right] \\
&= \log_2 \det \left(\mathbf{I} + \frac{\rho}{n_t} \omega \cdot \mathbf{H}\mathbf{H}^H \right).
\end{aligned} \tag{5.4}$$

Here our interest is to estimate the effect of macroscopic diversity to the MIMO system capacity. This effect is decided by the shadowing components to different BSs. Therefore, we will average out the microscopic effect in the following analysis. By taking an expectation with respect to the small scale fading, the mean capacity becomes

$$\begin{aligned}
C &= E_H \left[\log_2 \det \left(\mathbf{I} + \frac{\rho}{n_t} \omega \cdot \mathbf{H}\mathbf{H}^H \right) \right] \\
&\leq \log_2 \det \left[\mathbf{I} + \frac{\rho}{n_t} \omega \cdot E_H(\mathbf{H}\mathbf{H}^H) \right] \\
&= \log_2 \det \left[\mathbf{I} + \frac{\rho}{n_t} \omega \cdot n_t \cdot \mathbf{I} \right] \\
&= n_r \log_2(1 + \rho\omega)
\end{aligned} \tag{5.5}$$

where the second step is due to the Jensen's inequality. This agrees with the result in [23], which is obtained by assuming $n_t \rightarrow \infty$. It can be seen from here that this result is actually the capacity upper bound of a MIMO system. Let $\omega' = 1 + \rho\omega$ in equation (5.5), we have $C \leq n_r \log_2(\omega')$. Since ω is a log-normal RV for $\omega > 0$ with mean μ and standard deviation σ , ω' is also a log-normal RV for $\omega' > 1$ with mean $\mu_1 = 1 + \rho\mu$ and standard deviation of $\sigma_1 = \rho\sigma$. After applying a base-2 logarithm, we obtain a RV with a Gaussian distribution. The mean and standard deviation of the Gaussian RV $\log_2(\omega')$ can be calculated as

$$\begin{aligned}
\mu'_{dB} &= \frac{1}{10 \log_{10} 2} \frac{1}{\xi} \ln \left[\frac{\mu_1}{\sqrt{\left(\frac{\sigma_1}{\mu_1}\right)^2 + 1}} \right] \\
&= \frac{1}{10 \log_{10} 2} \frac{1}{\xi} \ln \left(\frac{1 + \rho\mu_0}{\sqrt{\left(\frac{\rho\sigma_0}{1 + \rho\mu_0}\right)^2 + 1}} \right) \\
\sigma'_{dB} &= \frac{1}{10 \log_{10} 2} \frac{1}{\xi} \sqrt{\ln \left[\left(\frac{\sigma_1}{\mu_1}\right)^2 + 1 \right]} \\
&= \frac{1}{10 \log_{10} 2} \frac{1}{\xi} \sqrt{\ln \left[\left(\frac{\rho\sigma_0}{1 + \rho\mu_0}\right)^2 + 1 \right]}
\end{aligned} \tag{5.6}$$

where $\xi = \ln(10)/10$.

In conventional MIMO systems, the term $\log_2(\omega')$ will be multiplied by n_r as shown in equation (5.5). Corresponding, mean and standard deviation values will be multiplied by n_r .

$$\mu'' = n_r \mu'_{dB} = \frac{n_r}{10 \log_{10} 2} \frac{1}{\xi} \ln \left(\frac{1 + \rho \mu_0}{\sqrt{\left(\frac{\rho \sigma_0}{1 + \rho \mu_0} \right)^2 + 1}} \right) \quad (5.7)$$

$$\sigma'' = n_r \sigma'_{dB} = \frac{n_r}{10 \log_{10} 2} \frac{1}{\xi} \sqrt{\ln \left[\left(\frac{\rho \sigma_0}{1 + \rho \mu_0} \right)^2 + 1 \right]}$$

Therefore, the shadowing-dependent channel capacity upper bound follows the Gaussian distribution as $C \sim N(\mu'', \sigma''^2)$.

B. Macroscopic diversity MIMO system

Following the same procedure, an expectation is taken with respect to small scale fading to the macroscopic diversity MIMO system capacity,

$$\begin{aligned} C_{Mac} &= E_H \left[\log_2 \det \left(\mathbf{I} + \frac{\rho}{n_t} \mathbf{H}_c (\mathbf{H}_c)^H \right) \right] \\ &= E_H \left[\log_2 \det \left(\mathbf{I} + \frac{\rho}{n_t} \mathbf{\Omega}^{1/2} \mathbf{H} (\mathbf{\Omega}^{1/2} \mathbf{H})^H \right) \right] \\ &= E_H \left[\log_2 \det \left(\mathbf{I} + \frac{\rho}{n_t} \mathbf{H} \mathbf{H}^H \mathbf{\Omega} \right) \right] \\ &\leq \log_2 \det \left[\mathbf{I} + \frac{\rho}{n_t} \cdot E_H (\mathbf{H}^H \mathbf{H}) \mathbf{\Omega} \right] \\ &= \log_2 \det \left[\mathbf{I} + \frac{\rho}{n_t} \mathbf{\Omega} \cdot n_t \mathbf{I} \right] \\ &= \sum_i^{n_r} \log_2 (1 + \rho \omega_i). \end{aligned} \quad (5.8)$$

This is a summation of n_r independent Gaussian distributed RVs. Therefore, it is also a Gaussian RV with $\mu = \sum_i^{n_r} \mu(i)$ and $\sigma^2 = \sum_i^{n_r} \sigma^2(i)$. The mean value and standard

deviation of each RV can be calculated as above. Finally, the summation follows a Gaussian distribution with

$$\mu''_{Mac} = \frac{1}{10 \log_{10} 2} \frac{1}{\xi} \sum_i^{n_r} \ln \left(\frac{1 + \rho \mu_0(i)}{\sqrt{\left(\frac{\rho \sigma_0(i)}{1 + \rho \mu_0(i)} \right)^2 + 1}} \right) \quad (5.9)$$

$$\sigma''_{Mac} = \frac{1}{10 \log_{10} 2} \frac{1}{\xi} \sqrt{\sum_i^{n_r} \ln \left[\left(\frac{\rho \sigma_0(i)}{1 + \rho \mu_0(i)} \right)^2 + 1 \right]}.$$

To simplify the analysis, we assume all shadowing components are i.i.d. Thus they have the same mean and variance values. Equations in (5.9) can be simplified as

$$\mu''_{Mac} = n_r \mu'_{dB} = \frac{n_r}{10 \log_{10} 2} \frac{1}{\xi} \ln \left(\frac{1 + \rho \mu_0}{\sqrt{\left(\frac{\rho \sigma_0}{1 + \rho \mu_0} \right)^2 + 1}} \right) \quad (5.10)$$

$$\sigma''_{Mac} = \sqrt{n_r} \sigma'_{dB} = \frac{\sqrt{n_r}}{10 \log_{10} 2} \frac{1}{\xi} \sqrt{\ln \left[\left(\frac{\rho \sigma_0(i)}{1 + \rho \mu_0(i)} \right)^2 + 1 \right]}.$$

Therefore, for the macroscopic diversity MIMO system considering the shadowing effect, the channel capacity upper bound follows a Gaussian distribution as

$$C_{Mac} \sim N(\mu''_{Mac}, (\sigma''_{Mac})^2).$$

Comparing these two upper bounds C and C_{Mac} , it can be seen that they have the same mean value. However, the variance of C_{Mac} is much smaller than that of C . This means that in macroscopic environments, the distribution of the channel capacity is more centered at its mean capacity value. The probability that very low capacity occurs is

much lower than the standard MIMO system, i.e., the outage probability can be reduced in that region.

C. Comparison

1) *Upper Bound.* The outage capacity comparison is made to show the benefits of applying macroscopic diversity in MIMO systems. In the comparison, the average receiver SNR is assumed to be 18 dB independent of the number of antennas. Also all shadowing components have the same mean value, and the standard deviation is 8 dB.

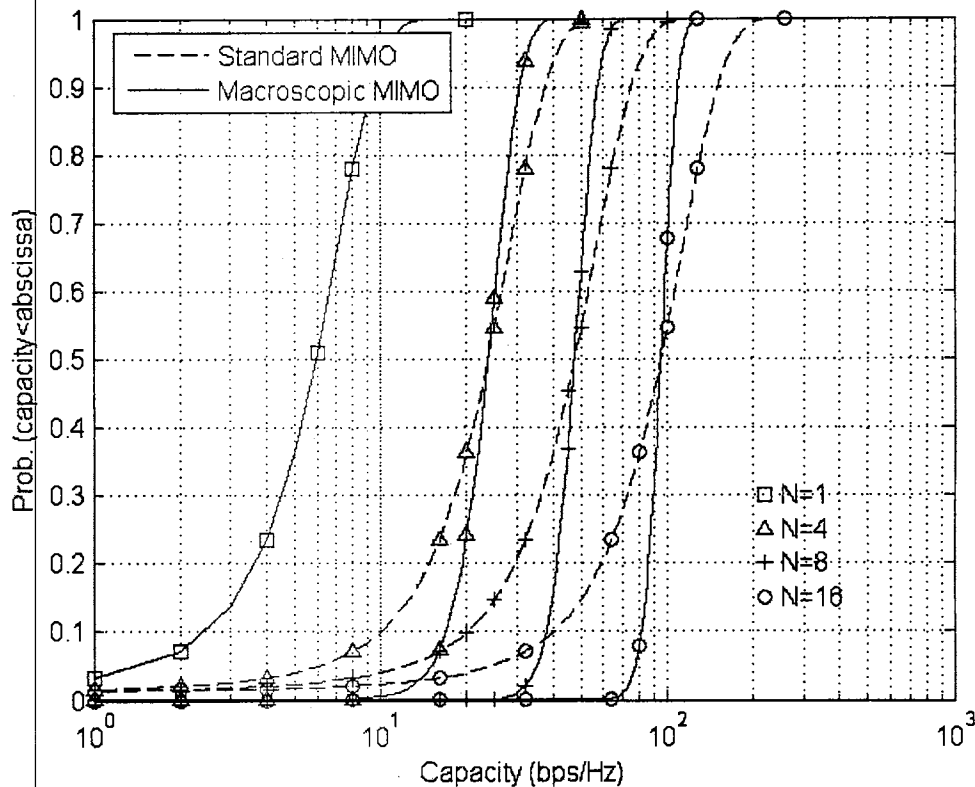


Figure 5.1 Capacity upper bound comparison.

The lower-tail capacity improvement mentioned in the former section can be clearly seen in this figure. If we look at the 10% outage capacity, 50% more capacity can be

achieved when 4 antennas are used; 90% more capacity can be achieved when 8 antennas are used; when 16 antennas are used, the capacity is more than doubled by the introduction of macroscopic diversity. In this evaluation, all BS antennas are assumed to be mounted at different BS locations.

2) *Numerical Verification.* The former comparison is made by evaluating the upper bound of the MIMO system capacity. To verify the observation obtained from this method, Monte-Carlo simulation is performed using the same system configuration and parameters. Simulation results are shown in Figure 5.2.

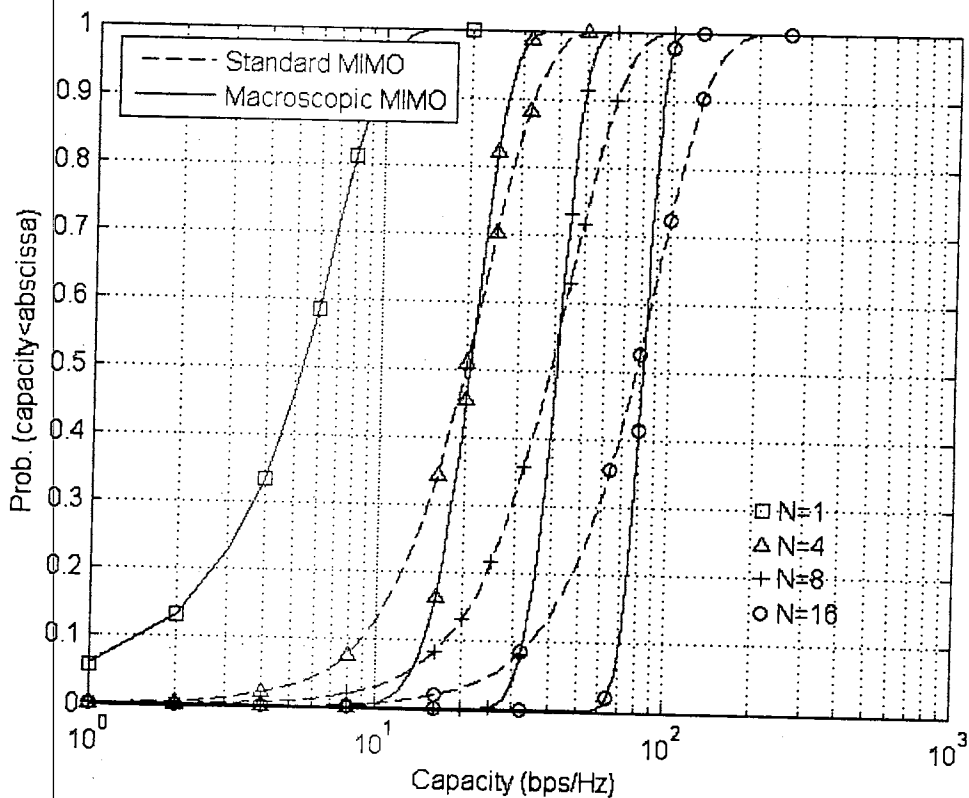


Figure 5.2 Monte-Carlo simulation verification.

It can be observed that the simulation shows almost the same result as shown in Figure 5.1. As predicted by the upper bound analysis, because of the macroscopic diversity, the 10% outage capacity is increased by more than 50%, more than 90%, and more than doubled compared to the standard MIMO systems when 4 antennas, 8 antennas, and 16 antennas are used respectively.

Comparing Figures 5.1 and 5.2 reveals that the Monte-Carlo simulation results have around 10% less capacity compared with the upper bound, and the trends of all curves are exactly the same. Therefore, the upper bound capacity approach proposed in this chapter is an effective way to analyze the macroscopic effects in MIMO systems.

5.3.2 Simulation Results

Monte-Carlo simulation is conducted to compare the capacities of macroscopic diversity MIMO systems and standard MIMO systems. In the simulations, the number of MT antennas is fixed as three, while the total number of BS antennas increases from 3 to 6, 12 and 24. In standard MIMO systems, all these BS antennas are mounted at the center of the hexagonal cell. In macroscopic diversity MIMO systems, these BS antennas are evenly distributed among three BSs along the edges of the cell. In the macroscopic diversity MIMO system, 120° perfect sectorization is assumed for BS antennas. Totally 10^4 uniformly-distributed user locations are randomly generated within a cell. Simulation parameters are summarized in Table 5.1. The simulation results are shown in Figure 5.3.

MT antenna:	Omni-directional
Frequency reuse:	Universal
Propagation exponent:	3.5
Log-normal shadowing:	8 dB standard deviation
Fast fading:	Independent Rayleigh PDF
Total transmit power:	10 Watts
Total antenna gain:	15 dBi
Bandwidth:	5 MHz
Noise figure:	2
Cell radius:	10 km

Table 5.1 Simulation parameters for macroscopic diversity MIMO systems.

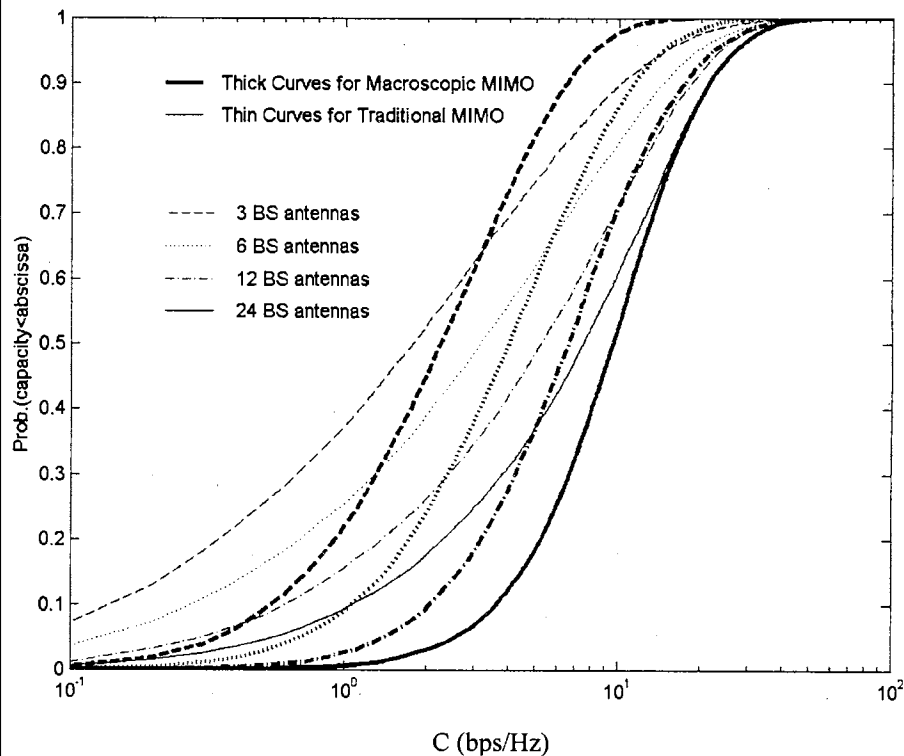


Figure 5.3 Capacity comparison of standard MIMO vs. macroscopic diversity MIMO systems.

As shown in Figure 5.3, the simulation results agree with those predicted by the upper bounds. By applying macroscopic diversity in MIMO systems, it shows that the capacity distribution is more centered at the mean capacity value and both extremely low capacity and extremely high capacity cases are reduced. The lower tails of these curves are of most interest for system designers. If we look at the 10% outage rate, it can be seen that macroscopic diversity MIMO systems provide a capacity more than 3 times compared to the standard MIMO systems.

It is noticed that the former upper-bound analysis shows that the macroscopic diversity does not improve the capacity median value (i.e., 50% outage capacity); while in this simulation, the median values are actually improved. This improvement is due to the advantage of the edge-excited cell structure. Since there are three BSs serving one cell, the MTs are more likely to come close to one of the BSs than in the standard MIMO case. Therefore, the MTs are more likely to get stronger signals compared with the situations in standard MIMO systems.

The curves of 10% outage capacity and 50% outage capacity are depicted in Figure 5.4 for both systems. When fixing n_t as 3 and increasing n_r from 3 to 6, 12 and 24, the following observations can be obtained:

- 1) 50% outage capacity increases logarithmically. The macroscopic diversity system provides a moderate improvement compared to the standard system (around 20% increases). As mentioned above, this increase is actually due to the edge-excited cell structure, not macroscopic diversity. Therefore, macroscopic diversity does not help much to improve the MIMO system mean capacity.

2) Because of the receiver diversity gain, the 10% outage capacity increases almost linearly for both macroscopic and standard MIMO systems. Notice that as n_r increases even larger, the increase will eventually become logarithmic. However, because macroscopic diversity has a special advantage at the lower distribution tail, it provides significant improvement (3 times) compared with the standard system.

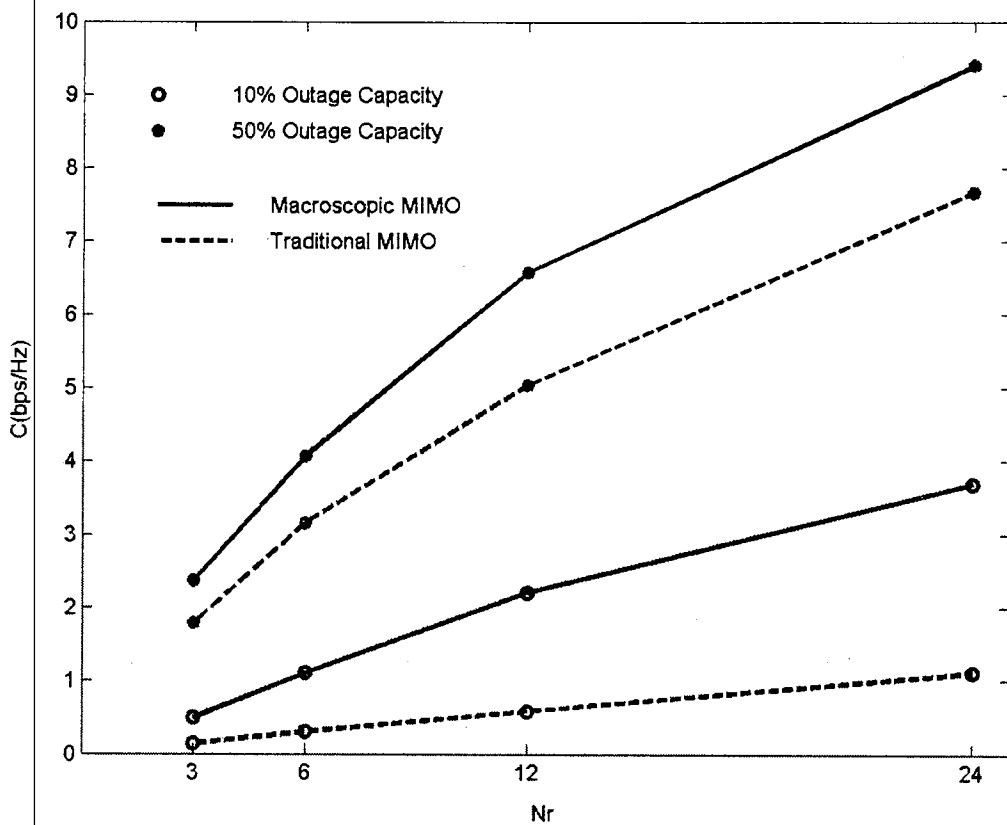


Figure 5.4 Capacity comparison of standard MIMO vs. macroscopic diversity MIMO systems (10% outage and 50% outage).

Another comparison is made between macroscopic diversity MIMO systems and standard MIMO systems in terms of the 5% outage capacity in Figure 5.5. Because of the

lower tail advantage, more capacity gain is expected from macroscopic systems. This expectation is verified from the simulation results showing that more than 4 times capacity can be obtained by using the macroscopic structure.

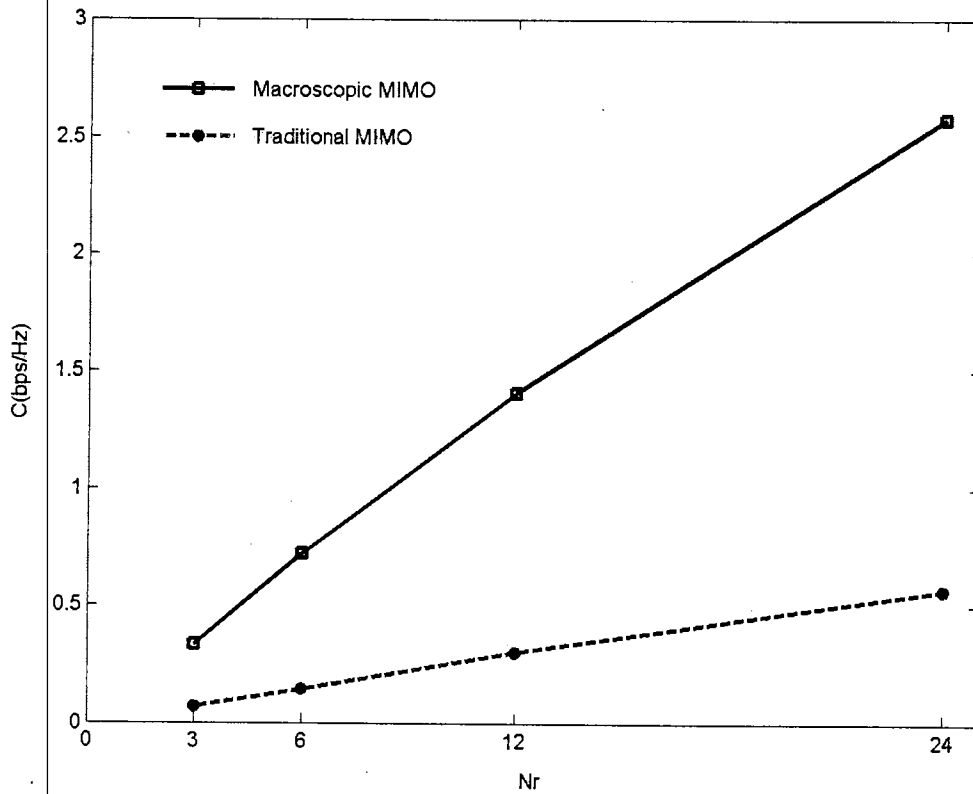


Figure 5.5 Capacity comparison of standard MIMO vs. macroscopic diversity MIMO systems (5% outage).

5.4 Summary

Macroscopic diversity MIMO systems are introduced and their performance is evaluated. In order to show the effects of multiple shadowing components, the capacity upper bound is derived and verified. This bound shows that using multiple BS in MIMO systems can dramatically increase the capacity at the lower-tail part of the capacity

distribution curves. Significant capacity gain is also demonstrated by the Monte-Carlo simulation results. In macroscopic diversity MIMO systems, while the mean capacity only has a moderate increment, the performance at the 10% and 5% outage capacity levels (which are the values of interest) are increased more than three times compared with those of standard MIMO systems. The potential of the macroscopic diversity MIMO system is thus clearly demonstrated.

CHAPTER VI

EXACT CAPACITY OF MSD-MIMO SYSTEM

In this chapter, it is shown that compared to the small-scale fading only environment, the capacity of a MIMO system is severely degraded when shadowing is present on the propagation channels, even in the optimal case where the multipath channel components are statistically uncorrelated. Macroscopic Selection Diversity (MSD), which is well-known as a scheme for combating deep shadowing effects [19], is implemented in MIMO systems to overcome this capacity degradation. The applied MSD topology enables the MTs and BSs to maximize the spatial multiplexing gain while combating the shadowing phenomena. Exact capacity representations of MSD-MIMO systems are derived. Two BS selection algorithms are presented in this chapter. The first algorithm is optimal in the sense of giving the highest capacity, but requires high-levels of computation. The second algorithm presented is suboptimal, but requires much less complexity. The proofs of optimality and suboptimality are provided along with a performance comparison of the two algorithms.

6.1 Capacity of MSD-MIMO Systems

6.1.1 Shadowing Effects in Correlated MIMO Systems

It has been shown that MIMO capacity in composite fading environment can be represented as

$$\begin{aligned}
C &= \log_2 \det \left(\mathbf{I} + \frac{\rho\omega}{n_t} \mathbf{H}\mathbf{H}^H \right) \\
&= \log_2 \det \left(\mathbf{I} + \frac{\rho\omega}{n_t} |\mathbf{D}_H|^2 \right) \\
&= \sum_{k=1}^{n_{\min}} \log_2 \left(1 + \frac{\rho}{n_t} \omega \lambda_k \right) \\
&= \sum_{k=1}^{n_{\min}} \log_2 \left(1 + \frac{\rho}{n_t} \lambda'_k \right)
\end{aligned} \tag{6.1}$$

where $\lambda'_k = \omega \lambda_k$, $k = 1, \dots, n_{\min}$, are the composite eigenvalues including both small-scale and large-scale components. For simplicity, in this chapter, we assume $n_r = n_t = n$. The large scale shadowing statistics, known to be log-normally distributed, has the probability density function (PDF) of

$$f_{\omega}(\omega) = \frac{1}{\omega \sigma_{\omega}^{\xi} \sqrt{2\pi}} \exp \left[-\frac{(10 \log_{10} \omega - \mu_{\omega(dBm)})^2}{2\sigma_{\omega}^2} \right]$$

where $\xi = \ln 10 / 10$; $\mu_{\omega(dBm)}$ and σ_{ω}^2 are respectively the local mean power and variance of Gaussian RV $\omega_{(dBm)} = 30 + 10 \log_{10} \omega$ [9].

Equation (6.1) shows that the capacity of a MIMO system depends on the distribution of multipath channel gain matrix and shadowed fading. Extensive research has been conducted on MIMO systems in multipath fading channels [1]-[5]. It has been observed that the capacity of MIMO systems under independent multipath fading channels increase linearly as the number of antennas at both ends increase. However, this improvement is degraded when the multipath channels are correlated. Figure 6.1 illustrates the degradation of capacity outage probability along with spatial correlation considering multipath fading only. In the simulation, a simple exponential model was used, which is explained in chapter II, to model the spatial correlation among multipath channels.

Monte-Carlo simulation is conducted to show the effect of correlation on the capacity in a 3×3 MIMO system when only small-scale fading is considered. In the simulation, the average SNR ratio is 10 dB. As shown in Figure 6.1, the capacity outage decreases as the correlation between the multipath fading channels increase.

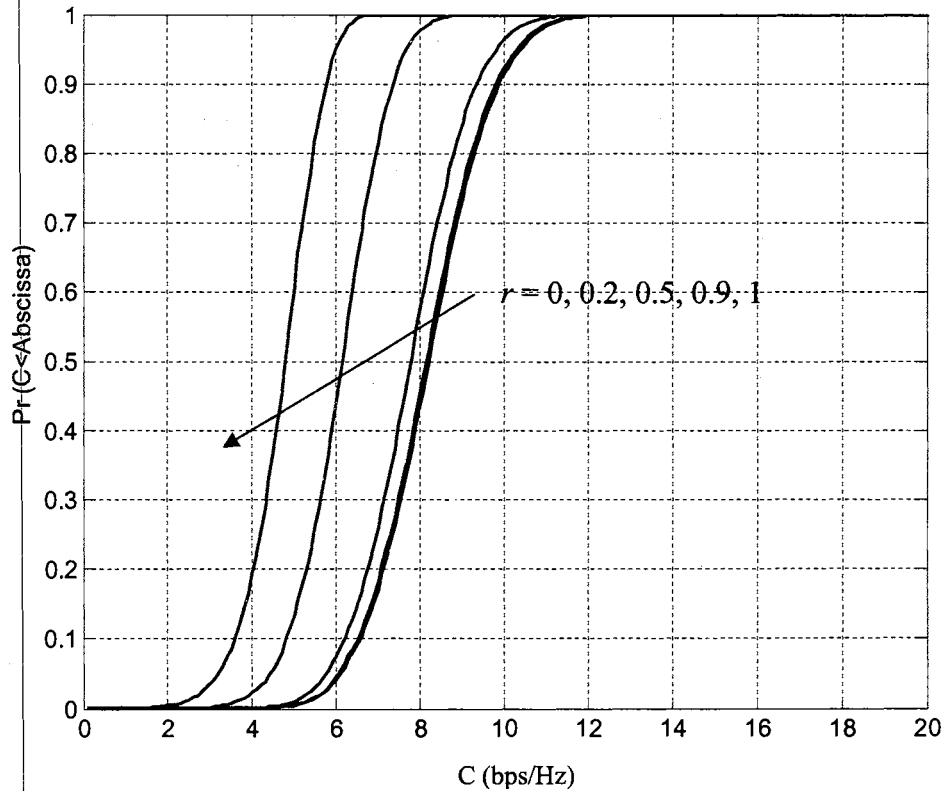


Figure 6.1 Capacity outage probability of a MIMO system for a multipath fading channel.

Then the shadowing effect is incorporated into the simulation with a standard deviation of $\sigma_{\omega} = 8$ dB. Results are shown in Figure 6.2. It shows that when shadowing is considered the capacity barely increases over the low outage probability region of interest (i.e., below the 10% outage region) even as the multipath fading correlation decreases. Compared with the small-scale fading only case, the capacity outage probability degrades

severely in this region. This is due to the fact that the received signal strength caused by shadowing is not enough to take advantage of the spatial multiplexing. This implies that shadowing is responsible for the capacity outage degradation, rather than the correlation of the multipath fading.

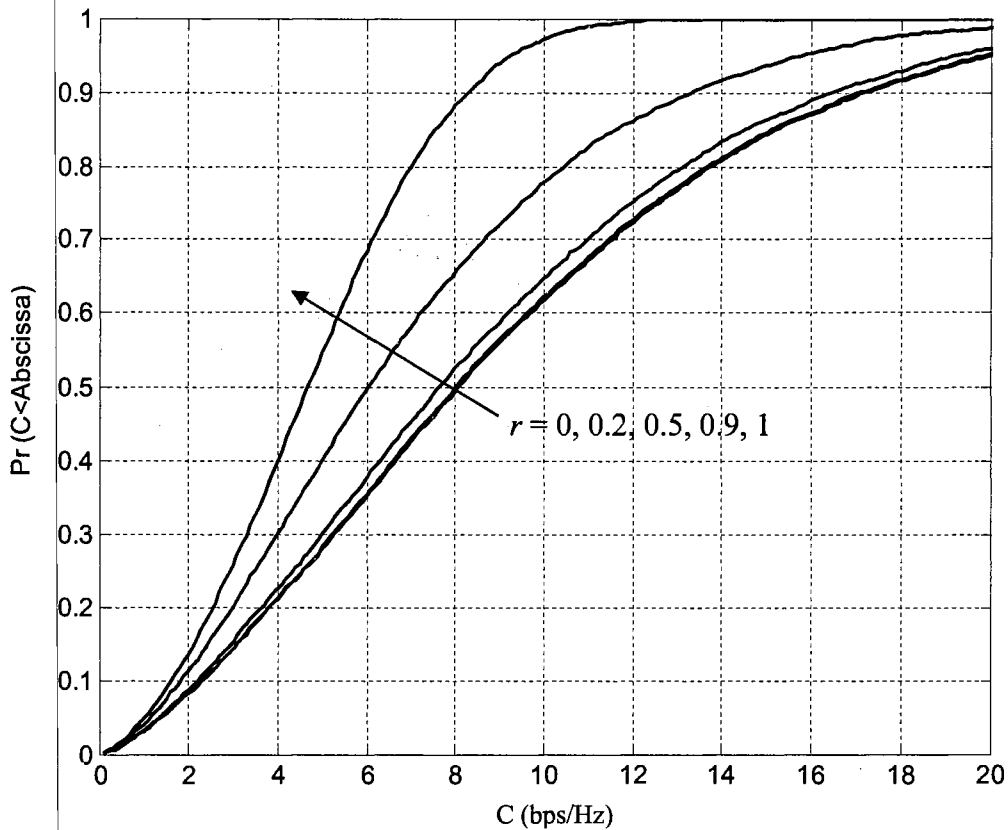


Figure 6.2 Capacity outage probability of a MIMO system for a composite fading channel ($\sigma_{\omega} = 8$ dB).

6.1.2 Characteristics of MSD-MIMO Systems

Macroscopic selection diversity has been known to be an efficient scheme to overcome the shadowing phenomenon in cellular communications [17], [67]. In MSD schemes, a BS is selected among a number of BSs. Figure 6.3 illustrates the configuration

of a (M, n_t, n_r) MDS-MIMO system, where M BSs cover a cellular area, n_t represents the number of transmitter antennas at the BS, and n_r represents the number of receiver antennas at the MT.

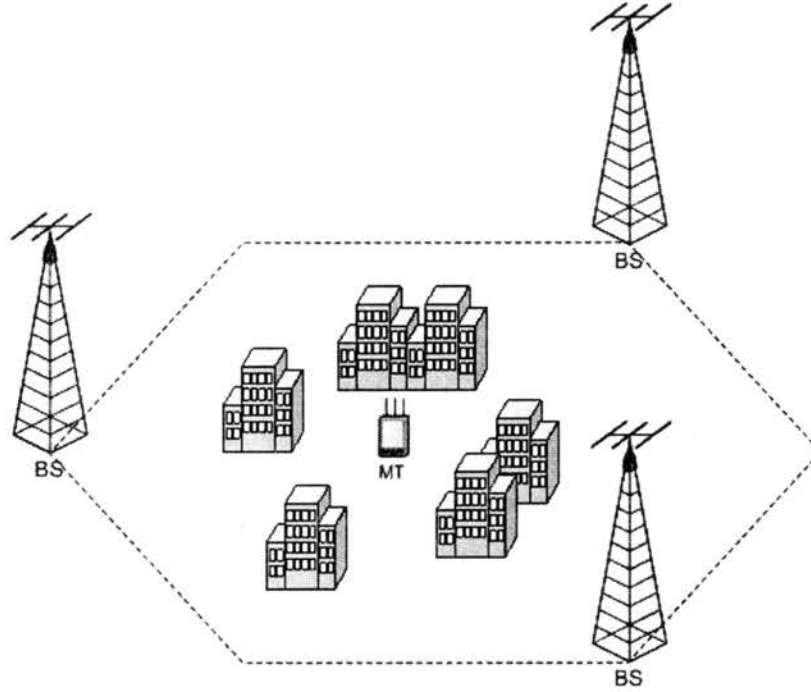


Figure 6.3 Illustration of the (M, n_t, n_r) MSD-MIMO system with $M = 3, n_t = n_r = 3$.

In this system, the optimal selection scheme is to select the BS that provides the largest capacity, i.e.,

$$C = \max[C_1 \quad C_2 \quad \cdots \quad C_M] \quad (6.2)$$

where $C_l, l = 1, \dots, M$, as given in (6.1), is the capacity of the communication link between the MT and the l th BS. The capacity outage probability of a (M, n_t, n_r) MDS-MIMO system is

$$\begin{aligned} \Pr(C \leq C_{Th}) &= F_C(C_{Th}) \\ &= \Pr[\max(C_1, C_2, \dots, C_M) \leq C_{Th}] \\ &= F_C(C_{Th}, C_{Th}, \dots, C_{Th}) \end{aligned} \quad (6.3)$$

where $F_C(C_{Th})$ is the CDF of RV $C = \max(C_1, C_2, \dots, C_M)$; $F_C(C_{Th}, C_{Th}, \dots, C_{Th}) = P(C_1 \leq C_{Th}, C_2 \leq C_{Th}, \dots, C_M \leq C_{Th})$ is the joint CDF of RVs C_1, C_2, \dots, C_M .

As shown in (6.1), the capacity of the communication link between the MT and the l th BS C_l is determined by the distribution of the shadowing term (ω_l) and multipath gain matrix H_l . We assume that the configuration of the local scatters at the MT site is symmetric. In other words, the geographical configuration of local scatters seen at any BS is identical. Thus, ω_l and H_l for all l is assumed to be i.i.d., thereby, C_l is also i.i.d.

With this assumption, the capacity outage probability can be simplified to

$$\begin{aligned}
& \Pr(C \leq C_{Th}) \\
&= F_C(C_{Th}, C_{Th}, \dots, C_{Th}) \\
&= P(C_1 \leq C_{Th}, C_2 \leq C_{Th}, \dots, C_M \leq C_{Th}) \\
&= \prod_{l=1}^M P(C_l \leq C_{Th}) \\
&= [F_{C_l}(C_{Th})]^M
\end{aligned} \tag{6.4}$$

where $F_{C_l}(C_{Th})$ is the outage probability of the l th link given as $F_{C_l}(C_{Th}) = \Pr(C_l \leq C_{Th})$, and l can be arbitrarily chosen from 1 to M . From (6.4), the following theory is obtained.

Theory 1: In wireless communication configurations where the local scatters at the mobile terminal are symmetric and the shadowed fading from the base stations are i.i.d., a macroscopic selection diversity system with 2 or more base stations will always have a lower capacity outage probability compared to a single base station communication topology.

Proof: The CDF of a random variable (or random vector) is upper bounded by 1, i.e. $0 \leq F(x) \leq 1$. Therefore, by applying (6.4) we obtain $F_C(C_{Th}) = [F_{C_i}(C_{Th})]^M \leq F_{C_i}(C_{Th})$.

An extension of Theory 1 leads to the following lemma.

Lemma 1: The difference between $F_{C_i}(C_{Th})$ and $F_C(C_{Th})$ becomes larger as $F_{C_i}(x)$ decreases.

Proof: The capacity outage CDF of two independent random variables (or random vectors) are defined as $F_C^{C_1}(C_{Th}) = [F_{C_1}(C_{Th})]^M$ and $F_C^{C_2}(C_{Th}) = [F_{C_2}(C_{Th})]^M$. For $M \geq 2$, for the condition of $F_{C_1}(C_{Th}) < F_{C_2}(C_{Th})$ it results that $(F_{C_1}(C_{Th}) - F_C^{C_1}(C_{Th})) > (F_{C_2}(C_{Th}) - F_C^{C_2}(C_{Th}))$.

It is worthy to note that Theory 1 not only applies to MIMO systems, but applies to general macroscopic selection diversity wireless communication topologies. The importance of Theory 1 is based on the fact that the outage capacity improvement of MSD-MIMO systems over standard MIMO systems is guaranteed, while Lemma 1 assures a significant improvement over low outage probability regions, which is the area of interest. This implies that the MSD scheme will be most effective at the low outage region.

6.2 Outage Probability of MSD-MIMO Systems

In this section, we provide exact expressions of capacity outage probability for the MSD-MIMO system. First, we provide an exact expression of the capacity outage

probability for the l th link, $F_{C_l}(C_{Th})$, using the c.f. Then, the capacity outage probability of a MSD-MIMO system is obtained as the product of $F_{C_l}(C_{Th})$ as shown in (6.4).

We present and analyze two BS selection algorithms as follows.

Algorithm 1: Optimal MSD Algorithm — Based on the criteria of achieving maximum channel capacity, an optimal MSD base station selection algorithm for a MIMO system is one that will result in selecting the base station that can provide the largest channel capacity.

Proof of Optimality: Consider a MT that detects signals from M independent BSs. Suppose that the MIMO system channel capacity at time t of the i th BS to the MT is denoted as $C_{BS_i}(t)$ (for $i = 1, \dots, M$), then at time t an optimal MSD base station selection algorithm will be one that selects the BS that maximizes its capacity, therefore the BS selection criteria will be $\max(C(t)) = \sup_{t \geq 0} (C_{BS_1}(t), C_{BS_2}(t), \dots, C_{BS_M}(t))$.

Algorithm 2: Suboptimal MSD Algorithm — Based on the criteria of achieving maximum channel capacity, a MSD algorithm that selects the BS that suffers the least shadowing will be suboptimal.

Proof of Suboptimality: Consider a MT that detects signals from M independent BSs. Suppose that the MIMO system channel capacity at time t of the i th BS to the MT is denoted as $C_{BS_i}(t)$ (for $i = 1, \dots, M$). Correspondingly, the MIMO system's average SNR at time t of the i th BS to the MT is denoted as $\rho_{BS_i}(t)$ (for $i = 1, \dots, M$). As proved in Algorithm 1, at time t , an optimal MSD base station selection algorithm will be one that

selects the BS that maximizes its capacity, i.e., the selection criteria will be $\max(C(t)) = \sup_{t \geq 0} (C_{BS1}(t), C_{BS2}(t), \dots, C_{BSM}(t))$. A MSD algorithm that selects the BS that suffers the least shadowing will make its decision based on the BS that satisfies $\sup_{t \geq 0} (\rho_{BS1}(t), \rho_{BS2}(t), \dots, \rho_{BSM}(t))$, where it is assumed that the BS that is selected from this maximum SNR criteria is denoted as $C_{\max(\rho_{BSi})}(t)$. Since $\max(C(t)) \geq C_{\max(\rho_{BSi})}(t)$, the BS that is selected from this maximum SNR criteria will be suboptimal, since it can not guarantee that the maximum channel capacity base station will be selected.

The base station selection scheme of Algorithm 1 is optimum in the sense that it maximizes the capacity by selecting the BS with the highest link capacity. However, this scheme requires an estimation of multipath channel gains and shadowing terms for all links involved in the communications. In this section, we also consider a simple BS selection scheme. As shown in section 6.1, the shadowing effect severely degrades the capacity outage performance. Thus, one might think of a BS selection scheme based on the shadowing term only, i.e., selecting the BS that suffers the least shadowing. Although this scheme is a suboptimal selection method, it will be demonstrated in the following section that this scheme shows an impressive capacity outage performance, very close to the performance of the optimal case. In addition, to its advantage, the suboptimum BS selection scheme does not require a computationally massive channel estimation for all links compared to the optimum selection method.

6.2.1 MSD-MIMO Systems with Optimum BS Selection Scheme

The c.f. of capacity for the l th link is given as:

$$\begin{aligned}
 \phi_{C_l}(z) &= E_{C_l} \left[e^{j2\pi C_l z} \right] \\
 &= E_{\lambda'} \left[e^{j2\pi z \sum_i \log_2 \left(1 + \frac{\rho}{n} \lambda'_i \right)} \right] \\
 &= E_{\lambda'} \left[\prod_{i=1}^n \left(1 + \frac{\rho}{n} \lambda'_i \right)^{\frac{j2\pi z}{\ln 2}} \right] \\
 &= \int \prod_{i=1}^n \left(1 + \frac{\rho}{n} \lambda'_i \right)^{\frac{j2\pi z}{\ln 2}} f_{\lambda'}(\lambda') d\lambda'
 \end{aligned} \tag{6.5}$$

where $E_{\alpha}[\cdot]$ is an expectation taken with respect to the random variable α ; $f_{\lambda'}(\cdot)$ is the

joint PDF of the composite eigenvalue vector λ' ; $\int_{\lambda'}$ is the ordered integration $\int_{\lambda'_1} \int_{\lambda'_2} \dots \int_{\lambda'_n}$.

Substitute the shadowing PDF equation into (6.5),

$$\begin{aligned}
 \phi_{C_l}(z) &= \int \prod_{i=1}^n \left(1 + \frac{\rho}{n} \lambda'_i \right)^{\frac{j2\pi z}{\ln 2}} \int_0^{\infty} \frac{1}{\omega^n} f_{\lambda} \left(\frac{\lambda'}{\omega} \right) f_{\omega}(\omega) d\omega \cdot d\lambda' \\
 &= \int_0^{\infty} \frac{1}{\omega^n} f_{\omega}(\omega) d\omega \int \prod_{i=1}^n \left(1 + \frac{\rho}{n} \lambda'_i \right)^{\frac{j2\pi z}{\ln 2}} f_{\lambda} \left(\frac{\lambda'}{\omega} \right) d\lambda' \\
 &= \int_0^{\infty} \frac{1}{\omega^n} f_{\omega}(\omega) \cdot \Theta(\omega, z) d\omega.
 \end{aligned} \tag{6.6}$$

The inner integral part of equation (6.6) is

$$\Theta(\omega, z) = \int \prod_{i=1}^n \left(1 + \frac{\rho}{n} \lambda'_i \right)^{\frac{j2\pi z}{\ln 2}} f_{\lambda} \left(\frac{\lambda'}{\omega} \right) d\lambda' \tag{6.7}$$

where $f_{\lambda}(\cdot)$ is the joint PDF of the eigenvalue vector λ and the integral is taken over the ordered statistics.

The capacity outage probability of the l th link is obtained from its c.f.:

$$\begin{aligned}\Pr[C_l \leq C_{Th}] &= F_{C_l}(C_{Th}) = \int_0^{C_{Th}} \int_{-\infty}^{\infty} \phi_{C_l}(z) e^{-j2\pi z C_l} dz dC_l \\ &= \int_{-\infty}^{\infty} \phi_{C_l}(z) \left[\frac{1 - e^{-j2\pi z C_{Th}}}{j2\pi z} \right] dz.\end{aligned}\quad (6.8)$$

By substituting (6.8) into (6.4), the capacity outage probability of the (M, n_t, n_r) MDS-MIMO system can be expressed as

$$\Pr[C \leq C_{Th}] = [F_{C_l}(C_{Th})]^M = \left\{ \int_{-\infty}^{\infty} \phi_{C_l}(z) \left[\frac{1 - e^{-j2\pi z C_{Th}}}{j2\pi z} \right] dz \right\}^M. \quad (6.9)$$

Numerical evaluation techniques such as inverse fast Fourier transform can be applied to evaluate (6.8).

A. The Uncorrelated Multipath fading case

Evaluation of (6.6) involves a $(n+1)$ th order integral, which usually increases the computational complexity. Chiani *et al.* provide a simpler form to evaluate the inner integral of $\Theta(\omega, z)$. Using corollary 2 in the appendix of [37], the c.f. of the l th link can be simplified as

$$\begin{aligned}\phi_{C_l}(z) &= \int_0^{\infty} \frac{1}{\omega^n} f_{\omega}(\omega_l) \cdot \Theta(\omega, z) d\omega \\ &= K \int_0^{\infty} \frac{1}{\omega^n} f_{\omega}(\omega) \cdot \det[\mathbf{U}] d\omega\end{aligned}\quad (6.10)$$

where \mathbf{U} is a Hankel matrix with the ij th element given by

$$u_{i,j} = \int_0^{\infty} \left(\frac{x}{\omega} \right)^{i+j-2} \cdot e^{-\frac{x}{\omega}} \cdot \left(1 + \frac{\rho}{n} x \right)^{\frac{j2\pi z}{\ln 2}} dx \quad (6.11)$$

and $K = \frac{\pi^{n(n-1)}}{[\tilde{\Gamma}_n(n)]^2}$ with $\tilde{\Gamma}_\alpha(\beta) = \pi^{\alpha(\alpha-1)/2} \prod_{i=1}^{\alpha} (\beta-i)!$.

B. The Correlated Multipath fading case

When the small-scale channel gains are correlated, the inner integral of the c.f. function shown in (6.6) can be obtained using corollary 2 in the appendix of [37]:

$$\Theta(\omega, z) = K_\Sigma \det[\mathbf{G}] \quad (6.12)$$

where the ij th element of the matrix \mathbf{G} is given by

$$g_{i,j} = \int_0^{\infty} \left(\frac{x}{\omega} \right)^{j-1} \cdot e^{-\frac{x}{\sigma_i \omega}} \cdot \left(1 + \frac{\rho}{n} x \right)^{\frac{j2\pi z}{\ln 2}} dx \quad (6.13)$$

and the normalizing constant is given by:

$$K_\Sigma = K \cdot \prod_{j=1}^n (j-1)! \cdot \frac{|\Sigma|^n}{|\mathbf{V}_2(\boldsymbol{\sigma})|} \quad (6.14)$$

where Σ is correlation matrix of small-scale fading with ordered eigenvalues of

$\boldsymbol{\sigma} = [\sigma_1, \sigma_2, \dots, \sigma_n]$, and $\mathbf{V}_2(\boldsymbol{\sigma})$ is a Vandermonde matrix given by

$$\mathbf{V}_2(\boldsymbol{\sigma}) = \begin{bmatrix} 1 & 1 & \dots & 1 \\ -\sigma_1^{-1} & -\sigma_2^{-1} & \dots & -\sigma_n^{-1} \\ \vdots & \vdots & \ddots & \vdots \\ -\sigma_1^{1-n} & -\sigma_2^{1-n} & \dots & -\sigma_n^{1-n} \end{bmatrix}$$

Note that (14) and (16) can be evaluated in a compact closed form using the identity

$$\begin{aligned}
& \int_0^{\infty} x^n (1+bx)^y e^{-\frac{x}{a}} dx \\
&= \frac{n! \Gamma(-1-n-y) {}_1F_1(1+n, n+y+2, 1/ab)}{b^{n+1} \Gamma(-y)} + a^{n+1+y} b^y \Gamma(n+1+y) {}_1F_1(-y, -n-y, 1/ab)
\end{aligned} \tag{6.15}$$

where $\Gamma(\cdot)$ is the Gamma function and ${}_1F_1(\cdot, \cdot)$ is the hypergeometric function [97]. This identity is valid for $R\{a\} > 0$, $n \geq 0$, $\arg\{b\} \neq \pi$.

6.2.2 MSD-MIMO Systems with Suboptimum BS Selection Scheme

If the distribution of \mathbf{H} for all BSs are identical (i.e., the configuration of the local scatters is symmetric) the selection of the BS to maximize capacity might be comparable to the capacity of the BS which suffers the least amount of shadowing. Thus, the capacity is given as

$$C = \sum_{i=1}^n \log_2 \left[1 + \frac{\rho}{n} \lambda_i \omega_{\max} \right] = \sum_{i=1}^N \log_2 \left[1 + \frac{\rho}{n} \lambda'_i \right] \tag{6.16}$$

where $\omega_{\max} = \max(\omega_1, \omega_2, \dots, \omega_M)$, and $\lambda'_i = \lambda_i \omega_{\max}$.

The distribution function of the shadowed fading component is given by [19]

$$F_{\omega_{\max}}(\omega) = \prod_{k=1}^M Q \left(\frac{10 \log_{10} \omega - \mu_{\omega}}{\sigma_{\omega}^2} \right) \tag{6.17}$$

where $Q(x) = \int_x^{\infty} \frac{1}{\sqrt{2\pi}} e^{-t^2/2} dt$. By differentiating (6.17), the PDF of the shadowing component can be simply obtained as in [19]

$$f_{\omega_{\max}}(\omega) = \frac{M}{\omega \sigma_{\omega}^{\xi} \sqrt{2\pi}} \exp\left[-\frac{(10 \log_{10} \omega - \mu_{\omega})^2}{2\sigma_{\omega}^2}\right] \times \left[\operatorname{erf}\left(\frac{10 \log_{10} \omega - \mu_{\omega}}{\sigma_{\omega}}\right) \right]^{M-1} \quad (6.18)$$

where $\xi = \ln 10 / 10$. In a similar fashion as in the optimal selection scheme, the capacity outage probability is represented as

$$\Pr[C \leq C_{Th}] = \int_{-\infty}^{\infty} \phi_C(z) \left[\frac{1 - e^{-j2\pi C_{Th} z}}{j2\pi z} \right] dz. \quad (6.19)$$

The c.f. in (6.19) is

$$\begin{aligned} \phi_C(z) &= E_C[e^{j2\pi Cz}] = E_{\mathbf{X}} \left[\prod_{i=1}^N \left(1 + \frac{\rho}{N} x_i \right)^{\frac{j2\pi z}{\ln 2}} \right] \\ &= \int_{\mathbf{X}} f_{\mathbf{X}}(x_1, \dots, x_N) \prod_{i=1}^N \left(1 + \frac{\rho}{N} x_i \right)^{\frac{j2\pi z}{\ln 2}} d\mathbf{X} \\ &= \int_0^{\infty} \frac{1}{\omega^N} f_{\omega_{\max}}(\omega) \cdot \Theta(\omega, z) d\omega \end{aligned} \quad (6.20)$$

where $\Theta(\omega, z)$ is given in (6.7).

6.2.3 Numerical Results

In this section, we provide numerical results of the capacity outage probability. As shown in (6.1), the capacity of MIMO systems is determined by large-scale shadowing and multipath fading. In wireless environments, the signals can be correlated to each other due to many reasons, which include insufficient antenna spacing or the lack of local scatters. It has been shown that in correlated fading environments, the capacity of MIMO systems can be significantly lower, compared to independent fading.

For downlink transmission, the distribution of a multipath channel gain matrix \mathbf{H} can be approximated as [5]

$$\mathbf{H} \sim \mathbf{H}_W \mathbf{\Sigma}^{1/2} \quad (6.21)$$

where \mathbf{H}_W is a complex Gaussian matrix whose elements are *i.i.d.* complex Gaussian $CN(0, 1)$, and $\mathbf{\Sigma}$ is channel correlation matrix whose elements represent spatial correlation of the multipath profile among the antennas. To model the channel correlation matrix $\mathbf{\Sigma}$, two correlation models are considered herein, the exponential model and the one-ring model. In our evaluation model, we assume $n_t = n_r = 3$, $\rho = 10$ dB, and $\sigma_\omega = 8$ dB.

A. Exponential Correlation Model

For a linear antenna array, the correlation among antennas decreases as the distance between antenna elements increases. In [68], exponential correlation was used to model the spatial correlation between any two individual fading channels for a uniform linear antenna array. The correlation matrix using this model is given $\mathbf{\Sigma} = \left\{ r^{|i-j|} \right\}_{i,j=1,\dots,n}$ with $r \in [0, 1)$.

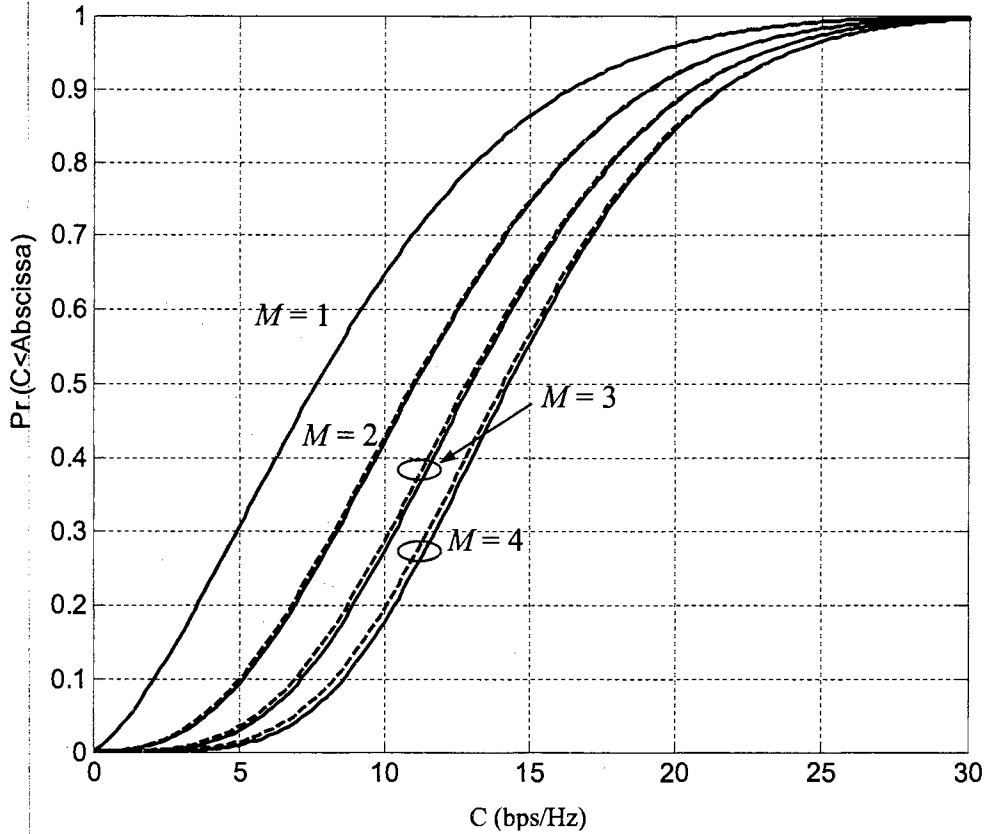


Figure 6.4 Outage Capacity of $(M, 3, 3)$ MSD-MIMO system for different number of BSs ($r = 0.5$). Note that the solid curves are the capacity outage probabilities for the optimum selection scheme, while the dashed curves are those for the suboptimum selection scheme.

Figure 6.4 shows the capacity outage probability of MSD-MIMO systems for different number of BSs. The results show that the mean capacity can be substantially improved by employing multiple BSs. The largest improvement occurs between M equals 1 and 2 where at the 10% outage level an approximate 120% capacity gain is obtained, and at the 5% outage level an approximate 180% capacity gain is obtained. Comparing Figure 6.4 to the uncorrelated case ($r = 0$) of Figure 6.1, the mean capacity is not degraded greatly even for $r = 0.5$. This means that the comparable spatial correlation in

small scale fading does not degrade the mean capacity. Rather, the capacity is much affected by the shadowing effect. Regarding the difference between the suboptimal to optimal selection methods, despite M increasing, the capacity difference is less than 4%. Since the suboptimal selection method performance is so close to the optimal method, and can be obtained at a fraction of the computation complexity, the suboptimal selection method becomes a natural preference, and therefore its performance is further illustrated in the following figures.

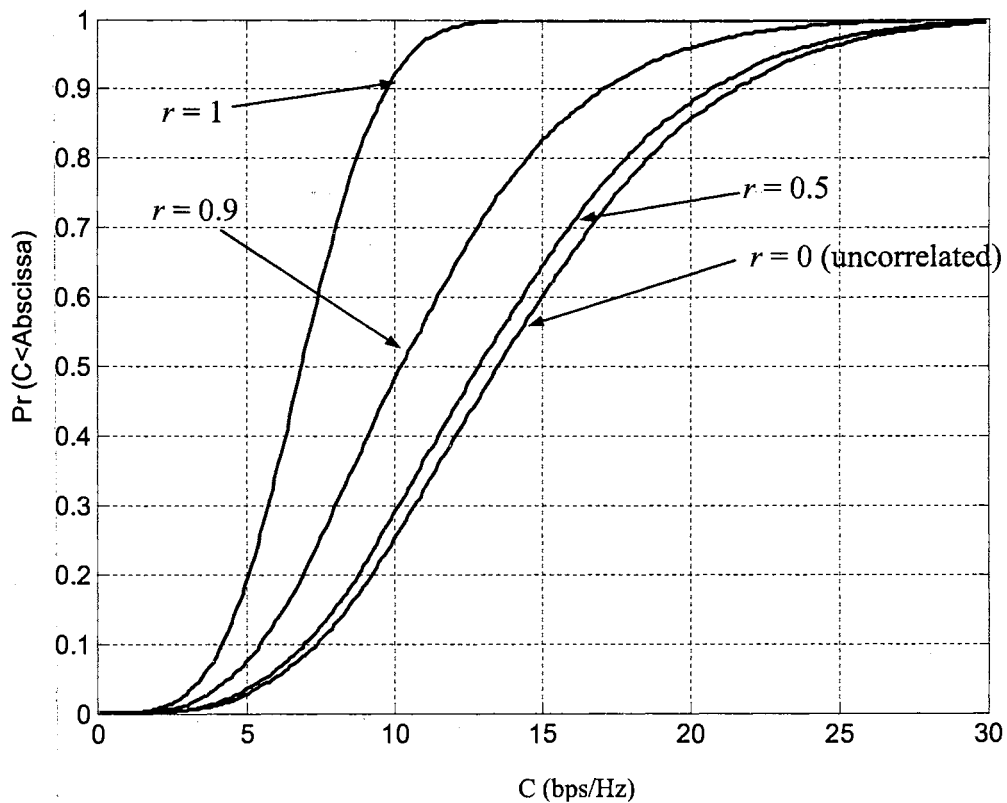


Figure 6.5 Outage Capacity of (3, 3, 3) MSD-MIMO system for different multipath correlation values (the suboptimum BS scheme is applied).

Figure 6.5 shows the outage capacity of a (3, 3, 3) MSD-MIMO system applying suboptimal selection for different spatial correlation values. It is observed that the outage

capacity degradation of the MSD-MIMO system at $r = 0.5$ is approximately 10%. In addition, Figure 6.6 shows the effect of SNR to the 10% capacity outage performance for a (3, 3, 3) MSD-MIMO communication topology. As the SNR level (in dB) increases the capacity outage increment factor is larger than 0.27 bps/Hz/dB for the uncorrelated and correlated cases. Comparing the uncorrelated case ($r = 0$) to the $r = 0.5$ correlated case, a less than 5% loss in outage capacity occurs for a wide range of SNR levels. This demonstrates the level of robustness the MSD-MIMO scheme has against composite fading environments. For a fixed value of correlation, this improvement owes to base station diversity. Thus, the benefit of diversity increases logarithmically as the diversity order increases.

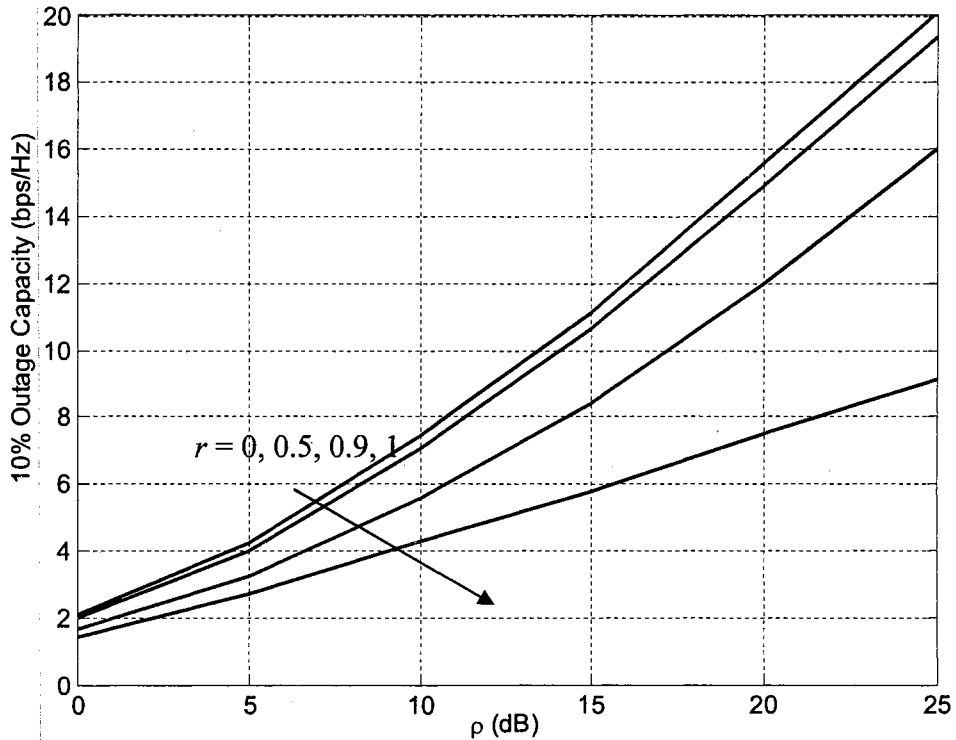


Figure 6.6 10%-Capacity outage of (3, 3, 3) MSD-MIMO system for different multipath correlation values (the suboptimum BS scheme is applied).

It is important to note that the results also apply if the channel model is reversed (i.e., if the transmitter and receiver role is reversed in the communication model) due to the channel reciprocal properties.

B. One-ring model

One-ring model is used to evaluate the system performance. Figures 6.7, 6.8, and 6.9 respectively show the capacity outage performance for the angle spread (Θ) of 10° , 30° , and 50° . In each graph the $(M, 3, 3)$ MSD-MIMO topology performance is illustrated for the cases of M equaling 1, 2, 3, and 4. Comparing Figure 6.7 to 6.8, for each corresponding case of $M = 2, 3,$ and 4 an approximate 27% gain in capacity is obtained at the 10% outage level. Next, comparing Figure 6.8 to 6.7, for the corresponding cases of $M = 2, 3,$ and 4 an approximate 5–10% gain in capacity is obtained at the 10% outage level. These results are complimentary to the results observed in Figures 6.4–6.6 showing the effects of correlation to the capacity outage performance based on the one ring model. As the angle spread increases from $10^\circ, 30^\circ,$ to 50° the correlation decreases resulting in an increment in the obtainable capacity. As the angle spread reaches 50° the signals become almost uncorrelated resulting in a capacity outage performance near to the saturated level.

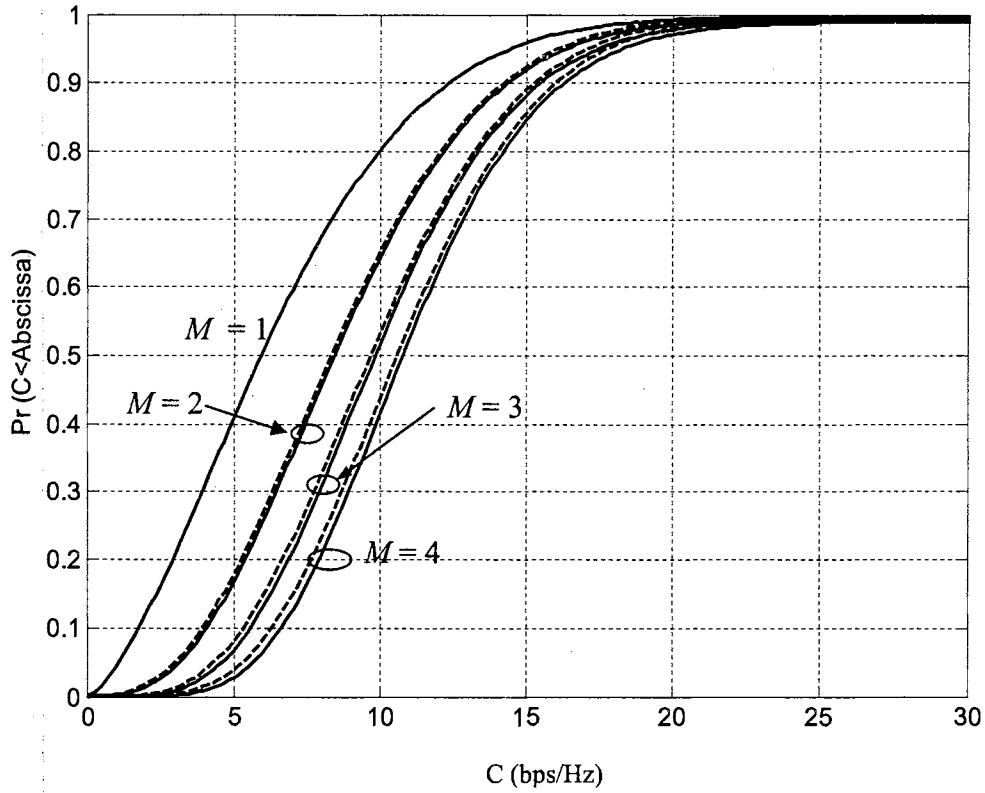


Figure 6.7 Capacity outage probability of $(M, 3, 3)$ MSD-MIMO system for a different number of BSs. Angle spread of 10 degree is used. Note that the solid curves are the capacity outage probabilities for the optimum selection scheme, while the dashed curves are those for the suboptimum selection scheme.

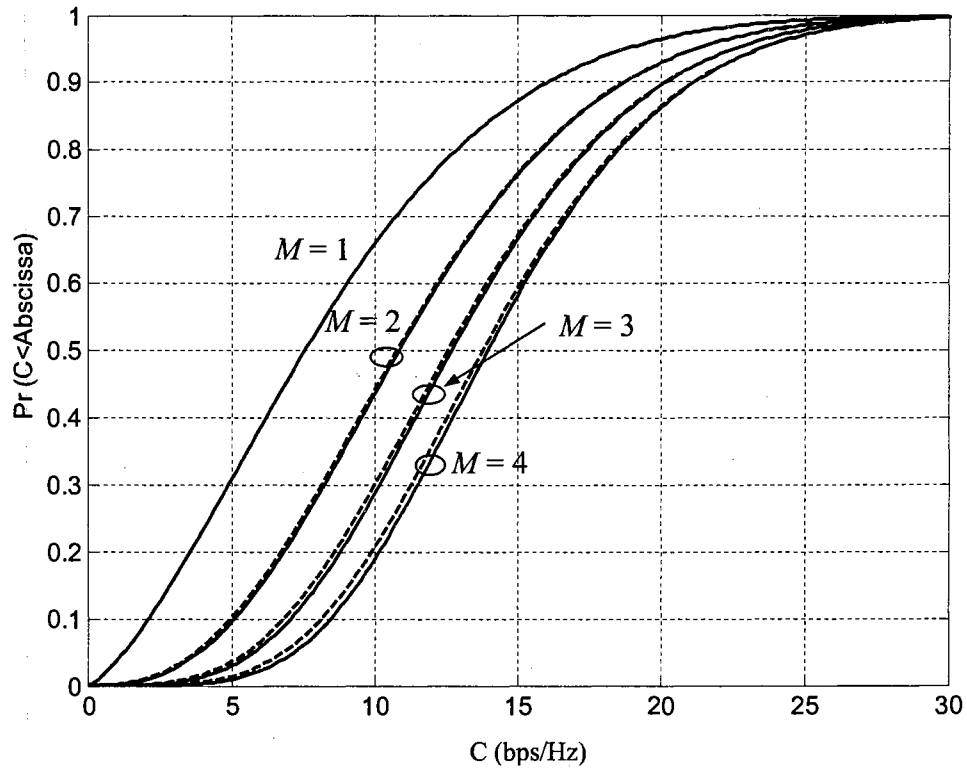


Figure 6.8 Capacity outage probability of $(M, 3, 3)$ MSD-MIMO system for different number of BSs. Angle spread of 30 degree is used. Note that the solid curves are the capacity outage probabilities for the optimum selection scheme, while the dashed curves are those for the suboptimum selection scheme.

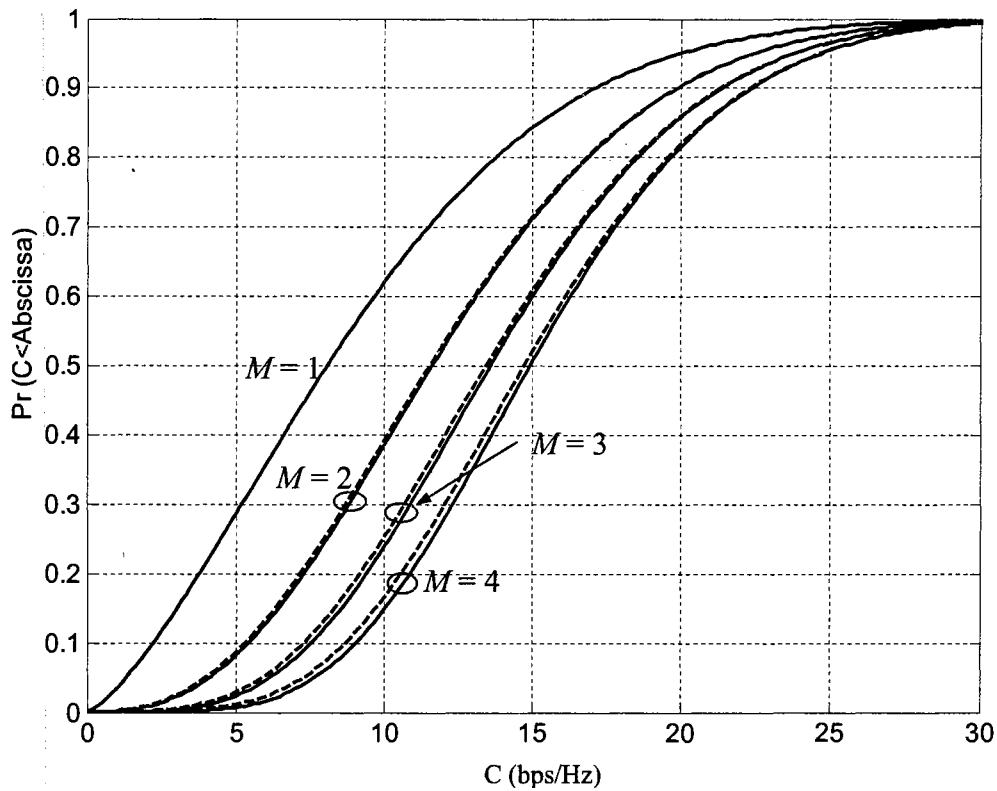


Figure 6.9 Capacity outage probability of $(M, 3, 3)$ MSD-MIMO system for different number of BSs. Angle spread of 50 degree is used. Note that the solid curves are the capacity outage probabilities for the optimum selection scheme, while the dashed curves are those for the suboptimum selection scheme.

6.3 Mean Capacity of MSD-MIMO Systems

6.3.1 Mean Capacity of MIMO Systems in Composite Fading

A. Uncorrelated Case

It has been shown in [37] that the distribution of eigenvalue vector λ in the uncorrelated fading case is

$$f_{\lambda}(\lambda) = K |\mathbf{V}_1(\lambda)|^2 \prod_{i=1}^{n_{\min}} e^{-\lambda_i} \lambda_i^{(n_{\max} - n_{\min})} \quad (6.22)$$

where $K = \frac{\pi^{n_{\min}(n_{\min}-1)}}{\tilde{\Gamma}_{n_{\min}}(n_{\max}) \cdot \tilde{\Gamma}_{n_{\min}}(n_{\min})}$, and $\tilde{\Gamma}_{n_{\min}}(x) = \pi^{n_{\min}(n_{\min}-1)/2} \prod_{i=1}^{n_{\min}} (x-i)!$.

Letting $n_{\max} = n_{\min} = n_t = n_r = n$, the above equation is further simplified as

$$f_{\lambda}(\lambda) = K |\mathbf{V}_1(\lambda)|^2 \prod_{i=1}^{n_{\min}} e^{-\lambda_i} \quad (6.23)$$

where matrix $\mathbf{V}_1(\lambda)$ is defined in equation (4.33). Mean capacity of the system can be obtained by averaging all the possible small-scale fading and large-scale fading values.

$$\begin{aligned} E[C] &= E \left[\sum_{i=1}^{n_t} \log_2 \left(1 + \frac{P_t}{n_t \sigma_n^2} \lambda_i' \right) \right] \\ &= \int \sum_{\lambda'} \log_2 \left(1 + \frac{P_t}{n_t \sigma_n^2} \lambda_i' \right) f_{\lambda'}(\lambda') d\lambda' \\ &= \int \sum_{\lambda'} \log_2 \left(1 + \frac{P_t}{n_t \sigma_n^2} \lambda_i' \right) \cdot \left[\int_0^{\infty} \frac{1}{\omega^{n_t}} f_{\lambda} \left(\frac{\lambda'}{\omega} \right) f_{\omega}(\omega) d\omega \right] d\lambda' \\ &= \int \sum_{\lambda'} \log_2 \left(1 + \frac{P_t}{n_t \sigma_n^2} \lambda_i' \right) \cdot \left[\int_0^{\infty} \frac{1}{\omega^{n_t}} K |\mathbf{V}_1 \left(\frac{\lambda'}{\omega} \right)|^2 \prod_{i=1}^{n_t} e^{-\lambda_i/\omega} f_{\omega}(\omega) d\omega \right] d\lambda' \\ &= \int_0^{\infty} \frac{1}{\omega^{n_t}} f_{\omega}(\omega) d\omega \int_{\lambda'} K |\mathbf{V}_1 \left(\frac{\lambda'}{\omega} \right)|^2 \prod_{i=1}^{n_t} e^{-\lambda_i/\omega} \cdot \sum_{i=1}^{n_t} \log_2 \left(1 + \frac{P_t}{n_t \sigma_n^2} \lambda_i' \right) d\lambda'. \end{aligned} \quad (6.24)$$

Using the identity in the appendix of [37], the inner integral can be evaluated as

$$\begin{aligned} & \int_{\lambda'} K |\mathbf{V}_1 \left(\frac{\lambda'}{\omega} \right)|^2 \prod_{i=1}^{n_t} e^{-\lambda_i/\omega} \cdot \sum_{i=1}^{n_t} \log_2 \left(1 + \frac{P_t}{n_t \sigma_n^2} \lambda_i' \right) d\lambda' \\ &= K_{\Sigma} \sum_{k=1}^{n_t} \det \left\{ \int_0^{\infty} \left(\frac{\lambda'}{\omega} \right)^{2(j-1)} \cdot e^{-\frac{\lambda'}{\omega}} \cdot U_{k,j} \left(\log_2 \left(1 + \frac{\rho \lambda'}{n_t} \right) \right) d\lambda' \right\}_{i,j=1,\dots,n_t} \end{aligned} \quad (6.25)$$

where $U_{k,j}(x) = \begin{cases} x, & k = j \\ 1, & k \neq j. \end{cases}$

B. Correlated Case

The distribution of the ordered eigenvalues $f_\lambda(\lambda)$ in the correlated fading case has been shown in chapter IV as

$$f_\lambda(\lambda) = K_\Sigma |\mathbf{F}(\lambda, \boldsymbol{\sigma})| |\mathbf{V}_1(\lambda)| \prod_{i=1}^{n_{\min}} \lambda_i^{(n_{\max} - n_{\min})}. \quad (6.26)$$

When $n_{\max} = n_{\min} = n_t = n_r = n$, the above equation is further simplified as

$$f_\lambda(\lambda) = K_\Sigma |\mathbf{F}(\lambda, \boldsymbol{\sigma})| |\mathbf{V}_1(\lambda)|. \quad (6.27)$$

Mean capacity can be obtained by averaging all the possible small-scale fading and large-scale fading values.

$$\begin{aligned} E[C] &= E \left[\sum_{i=1}^{n_t} \log_2 \left(1 + \frac{P_t}{n_t \sigma_n^2} \lambda_i' \right) \right] \\ &= \int \sum_{\lambda'}^{n_t} \log_2 \left(1 + \frac{P_t}{n_t \sigma_n^2} \lambda_i' \right) f_{\lambda'}(\lambda') d\lambda' \\ &= \int \sum_{\lambda'}^{n_t} \log_2 \left(1 + \frac{P_t}{n_t \sigma_n^2} \lambda_i' \right) \cdot \left[\int_0^\infty \frac{1}{\omega^{n_t}} p_\lambda \left(\frac{\lambda'}{\omega} \right) f_\omega(\omega) d\omega \right] d\bar{\lambda}' \\ &= \int \sum_{\lambda'}^{n_t} \log_2 \left(1 + \frac{P_t}{n_t \sigma_n^2} \lambda_i' \right) \cdot \left[\int_0^\infty \frac{1}{\omega^{n_t}} K_\Sigma \left| \mathbf{F} \left(\frac{\lambda'}{\omega}, \boldsymbol{\sigma} \right) \right| \cdot \left| \mathbf{V}_1 \left(\frac{\lambda'}{\omega} \right) \right| f_\omega(\omega) d\omega \right] d\lambda' \\ &= \int_0^\infty \frac{1}{\omega^{n_t}} f_\omega(\omega) d\omega \int_{\lambda'} K_\Sigma \left| \mathbf{F} \left(\frac{\lambda'}{\omega}, \boldsymbol{\sigma} \right) \right| \cdot \left| \mathbf{V}_1 \left(\frac{\lambda'}{\omega} \right) \right| \cdot \sum_{i=1}^{n_t} \log_2 \left(1 + \frac{P_t}{n_t \sigma_n^2} \lambda_i' \right) d\lambda' \end{aligned} \quad (6.28)$$

Using the identity in the appendix of [37], the inner integral can be evaluated as

$$\begin{aligned}
& \int_{\lambda'} K_{\Sigma} \left| \mathbf{F} \left(\frac{\lambda'}{\omega}, \sigma \right) \right| \cdot \left| \mathbf{V}_1 \left(\frac{\lambda'}{\omega} \right) \right| \cdot \sum_{i=1}^{n_i} \log_2 \left(1 + \frac{P_i}{n_i \sigma_n^2} \lambda'_i \right) d\lambda' \\
& = K_{\Sigma} \sum_{k=1}^{n_i} \det \left\{ \int_0^{\infty} \left(\frac{\lambda'}{\omega} \right)^{j-1} \cdot e^{-\frac{\lambda'}{\omega \sigma_i}} \cdot U_{k,j} \left(\log_2 \left(1 + \frac{\rho \lambda'}{n_i} \right) \right) d\lambda' \right\}_{i,j=1,\dots,N_{\min}}
\end{aligned} \tag{6.29}$$

where $U_{k,j}(x) = \begin{cases} x, & k = j \\ 1, & k \neq j. \end{cases}$

Figure 6.10 shows the mean capacity calculation results of a 2×2 standard MIMO system in a composite fading environment. For verification purpose, Monte-Carlo simulation result is also plotted for comparison. It is shown that the numerical calculations perfectly match the results of the Monte-Carlo simulation.

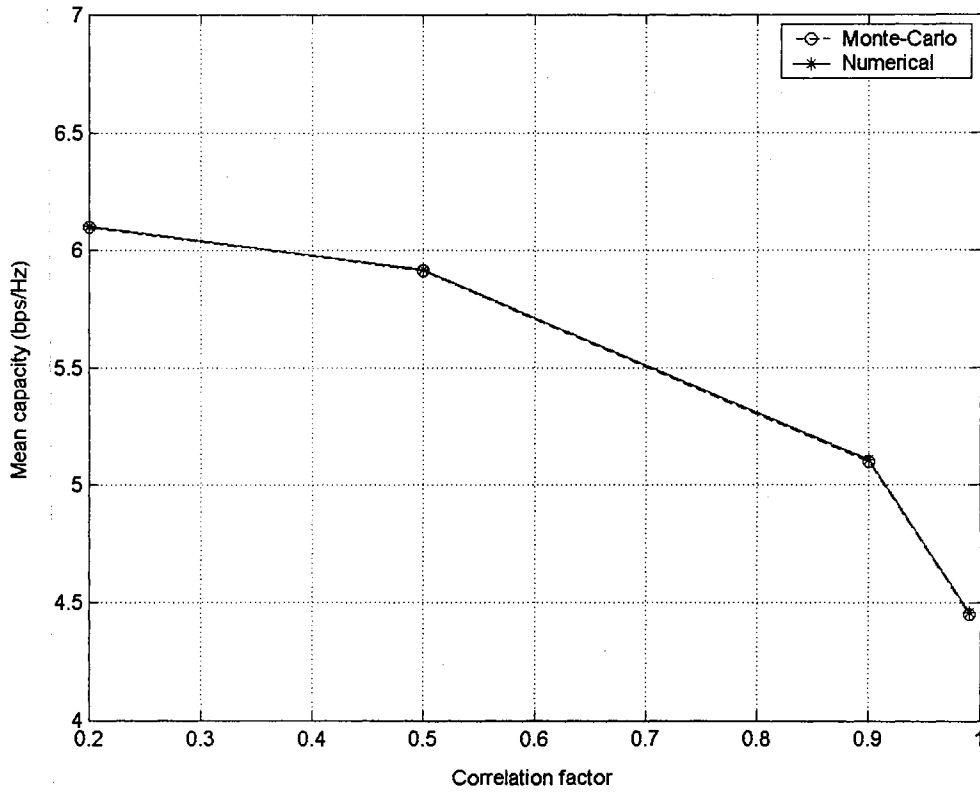


Figure 6.10 Mean capacity of 2×2 standard MIMO systems.

6.3.2 Mean Capacity of MSD-MIMO

For M -BS selection MIMO system, we apply equation (20) to the system mean capacity calculation,

$$E[C] = K_{\Sigma} \sum_{k=1}^{n_t} \int_0^{\infty} \frac{1}{\omega^{n_t}} \det \left\{ \int_0^{\infty} \left(\frac{\lambda'}{\omega} \right)^{j-1} \cdot e^{-\frac{\lambda'}{\omega \sigma_i}} \cdot U_{k,j} \left(\log_2 \left(1 + \frac{\rho \lambda'}{n_t} \right) \right) d\lambda' \right\}_{i,j=1,\dots,n_t} p_{\omega_{\max}}(\omega) d\omega. \quad (6.30)$$

Results are shown in Figure 6.11 for different number of BSs. In this evaluation, the MT and each BS has three antennas. The BS that provides the strongest large-scale component will be selected. It is shown that as the number of BSs increases, mean capacity increases dramatically for all correlation situations. However, the rate of the capacity increase is reduced as more BSs are added.

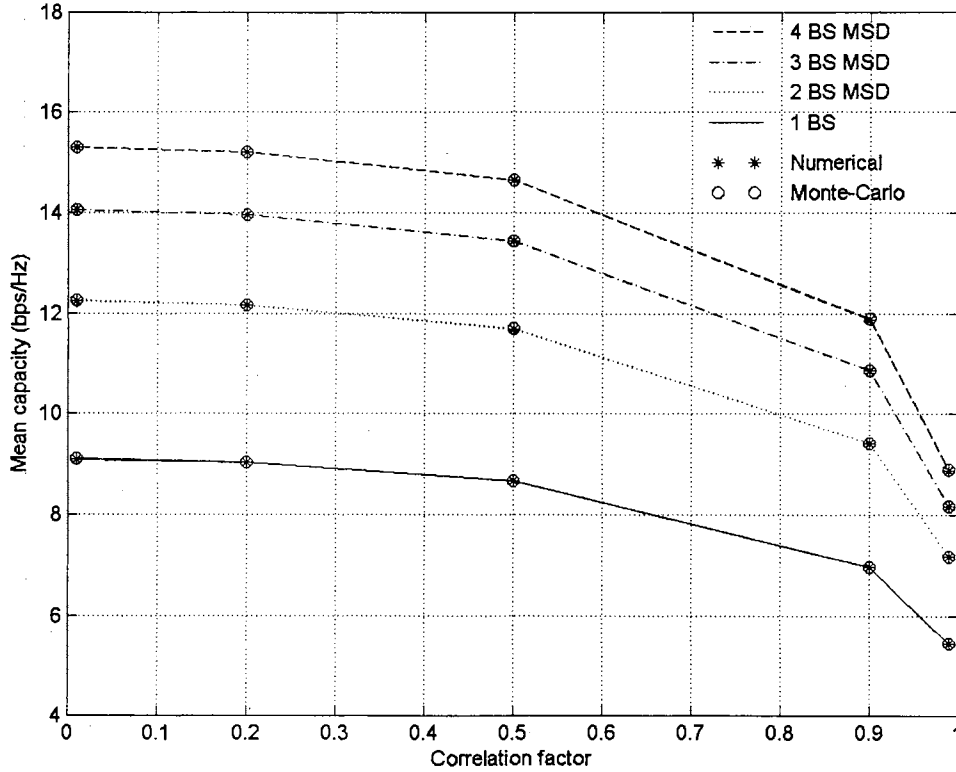


Figure 6.11 Mean capacity of 3×3 MSD-MIMO systems.

6.4 Summary

The exact capacity outage expression of MSD-MIMO systems using a c.f. approach has been developed. From the results, it can be concluded that the shadowing effect is a more dominant factor in decreasing the MIMO capacity compared to multipath correlation. In regards to the MSD BS selection schemes, it was shown that the more complex optimum selection scheme has a negligible advantage in outage capacity performance compared to the simpler suboptimal selection method. Based on the analysis of MSD systems in correlated composite fading environments, it can be concluded that the MSD-MIMO scheme can provide a capacity outage performance that is beyond the performance range of a MIMO system. The exact capacity outage equations and simulation results provide an accurate method to quantitatively analyze the performance gain of MSD technology in MIMO systems. The mean capacities of MSD-MIMO systems are also analyzed and the same conclusions are obtained.

CHAPTER VII

CONCLUSIONS AND FUTURE WORK

7.1 Conclusions

Futuristic mobile communication systems will be required to support broadband networking applications, where the reliability and robustness of the wireless link quality will be of prime concern. Having a communication link be disconnected in the middle of an application session, or not being able to connect to ones service provider due to poor signal reception are among the issues that are under rigorous research. Based on the evolution of the wireless industry and its current requirements, this dissertation focuses on the investigation of MIMO systems, which is a newly-proposed signal transmission scheme with great potential to dramatically increase the transmission data rate [1], [15].

In this dissertation, MIMO systems are investigated from several aspects, e.g. correlation effect, adaptive data rate, and capacity in multi-cell environments. It is shown that the inherent structure of MIMO technology makes it sensitive to the wireless channel environment. Namely, the signal correlation factor of the multipath signal profile is one aspect that needs to be taken care of very carefully. This study adds a dimension to the existing studies by investigating the effects of shadowing to the MIMO system capacity.

In a general MIMO system, the transmitted directional signals from a BS are under a common shadowing influence even though the multipath signal scattering profile may be uncorrelated. In such a system, there would be significant reductions in obtainable channel capacity despite of an ample scattering profile. It is shown in this dissertation that shadowing is a more dominating factor to the channel capacity compared to multipath correlation.

In this dissertation, macroscopic diversity is introduced into MIMO systems and its impacts are investigated by evaluating the capacity upper bounds. It is shown that without increasing any system resources, the outage capacity of interest is significantly increased by simply distributing antennas at different locations around a cell.

The c.f. method [37] is used to bypass the evaluation of eigenvalue distributions and directly give the capacity distribution curves of MIMO systems. Large-scale shadowing components are integrated into this approach to reflect the effects of macroscopic diversity. This method is used in analyzing the exact outage capacity of the proposed MSD-MIMO systems. Two methods are considered in selecting BSs in MSD-MIMO systems: an optimum selection method which selects the BS providing the largest capacity, and a suboptimum selection scheme which selects the BS suffering the least shadowing. It is shown that both methods give significant performance improvements compared to MIMO systems without macroscopic diversity. The outage capacity of interest is more than doubled just by incorporating one extra BS in the MSD-MIMO systems, and introducing more BSs gives continuous capacity increase. The capacity gain of the MSD-MIMO systems is quantified by the c.f. method.

This study gives the feasible system structures and their performance evaluation methods for designing the future broadband 4G cellular systems. This dissertation shows that macroscopic diversity in MIMO systems gives another dimension to optimize the system performance and it brings special benefits in the MIMO system design. Given a wireless environment, specific data rates and outage requirements, engineers can use the methods provided in this dissertation to quickly evaluate different BS deployment schemes. This evaluation method, together with link budget design and cell planning, will

help to realize the system design to meet the most critical requirements. It is expected that macroscopic diversity MIMO systems will play an important role in the future broadband 4G systems.

7.2 Future Work

Most of the former investigations on MIMO systems have focused on the flat fading case. As the data rate increases, time-domain adjacent symbols will eventually smear into each other and cause inter-symbol interference (ISI). Equalization methods are usually used for recovering data in channels with ISI. But these methods either need complex computations or do not give satisfactory solutions in certain circumstances [33]. In this area, orthogonal frequency division multiplexing (OFDM) is a good candidate to be implemented. OFDM divides the whole frequency band into multiple narrow bands and converts a frequency selective fading channel into multiple flat fading channels. Data is transmitted in parallel in the frequency domain. When implementing OFDM in MIMO systems, data will be transmitted along the frequency domain as well as the spatial domain. It becomes more flexible to adjust transmit parameters to maximize the system performance. However, this will also require more computation power and make systems more complicated. Feasible system structures and signal transmitting/receiving schemes need to be carefully investigated and selected.

In most former MIMO technology investigations, capacity has mainly been used as the performance measurement. However, only pursuing the highest possible data rate without considering the characteristics and requirements of other networking layers in the whole protocol stack does not give the optimal system performance. Especially, when

different classes of traffic are transmitted in the system, it is possible to optimize the physical layer scheduling and transmitting schemes according to the specific traffic requirements. In future research, this cross-layer optimization can be used to implement higher-layer information in the MSD-MIMO scheme to better satisfy the service requirements of different applications.

BIBLIOGRAPHY

- [1] G. J. Foschini and M. J. Gans, "On limits of wireless communications in a fading environment when using multiple antennas," *Wireless Personal Commun.*, vol. 6, pp. 311–335, Mar. 1998.
- [2] F. R. Farrokhi, A. Lozano, G. J. Foschini, and R. A. Valenzuela, "Spectral efficiency of FDMA/TDMA wireless systems with transmit and receive antenna arrays," *IEEE Trans. Wireless Commun.*, vol. 1, no. 4, pp. 591–599, Oct. 2002.
- [3] A. Lozano, F. R. Farrokhi, and R. A. Valenzuela, "Lifting the limits on high-speed wireless data access using antenna arrays," *IEEE Commun. Mag.*, vol. 39, no. 9, pp.156–162, Sept. 2001.
- [4] D.-S. Shiu, *Wireless Communication using Dual Antenna Arrays*. Boston, MA: Kluwer, 2000.
- [5] D. Gesbert, H. Bloskei, D.A. Gore, and A.J. Paulraj, "Outdoor MIMO wireless channels: models and performance prediction," *IEEE Trans. Commun.*, vol. 50, no. 12, pp. 1926–1934, Dec. 2002.
- [6] D. Chizhik, F. R. Farrokhi, J. Ling, and A. Lozano, "Effect of antenna separation on the capacity of BLAST in correlated channels," *IEEE Commun. Lett.*, vol. 4, no. 11, pp. 337–339, Mar. 2001.
- [7] F. R. Farrokhi, G. J. Foschini, A. Lozano, and R. A. Valenzuela, "Link-optimal space-time processing with multiple transmit and receive antennas," *IEEE Commun. Lett.*, vol. 5, no. 3, pp. 85–87, Mar. 2001.

- [8] T. M. Cover and J. A. Thomas, *Elements of Information Theory*, New York: Wiley, 1991.
- [9] G. L. Stuber, *Principles of mobile communication*, 2nd ed. Dordrecht, Netherlands: Kluwer, 2000.
- [10] D. Chizhik, G. J. Foschini, M. J. Gans, and R. A. Valenzuela, "Keyholes, correlations and capacities of multielement transmit and receive antennas," *IEEE Trans. Wireless Commu.*, vol.1, no. 2, pp. 361–368, Apr. 2002.
- [11] P. B. Wong, D. C. Cox, "Low-complexity cochannel interference cancellation and macroscopic diversity for high-capacity PCS," *IEEE Trans. Veh. Technol.*, vol.47, no. 1, pp. 124–132, Feb. 1998.
- [12] F. Graziosi, M. Pratesi, M. Ruggieri, and F. Santucci, "A multicell model of handover initiation in mobile cellular networks," *IEEE Trans. Veh. Technol.*, vol. 48, no. 3, pp. 802–814, May 1999.
- [13] F. Graziosi, and F. Santucci, "A general correlation model for shadow fading in mobile radio systems," *IEEE Commun. Lett.*, vol. 6, no. 3, pp. 102–104, Mar. 2002.
- [14] A. J. Viterbi, A. M. Viterbi, K. S. Gilhousen, and E. Zehavi, "Soft handoff extends CDMA cell coverage and increases reverse link capacity," *IEEE J. Select. Areas Commun.*, vol. 12, no. 8, pp. 1281–1288, Oct. 1994.
- [15] I. E. Telatar, "Capacity of multi-antenna Gaussian channels," *European Transactions on Telecommunications*, vol. 10, pp. 585–595, Nov/Dec. 1999.
- [16] A. J. Goldsmith, and S.-G. Chua, "Variable-rate variable-power MQAM for fading channels," *IEEE Trans. Commun.*, vol. 45, no. 10, pp. 1218–1230. Oct. 1997.

- [17] Z. J. Haas and C. Li, "The multiply-detected macrodiversity scheme for wireless cellular systems," *IEEE Trans. Veh. Technol.*, vol. 47, no. 2, pp. 506–530, May 1998.
- [18] Y.-S. Yeh, J. C. Wilson, and S. C. Schwartz, "Outage probability in mobile telephony with directive antennas and macrodiversity," *IEEE J. Select. Areas Commun.*, vol. 2, no. 4, pp. 507–511, July 1984.
- [19] A. M. D. Turkmani, "Probability of error for M-branch macroscopic selection diversity," *Proc. Inst. Elect. Eng.-I Commun., Speech and Visions*, vol. 139, no. 1, pp. 71–78, Feb. 1992.
- [20] C. A. Balanis, *Antenna Theory, Analysis and Design*, 2nd edition; New York: Wiley, 1997.
- [21] V. H. McDonald, "The cellular concept," *Bell Sys. Tech. J.*, vol. 58, pp. 15–41, Jan. 1979.
- [22] W. C. Y. Lee, "Smaller cells for greater performance," *IEEE Commun. Magazine*, vol. 29, no. 11, pp. 19–30, Nov. 1991.
- [23] H. Bolcskei, D. Gesbert, and A. J. Paulraj, "On the capacity of OFDM-based spatial multiplexing systems," *IEEE Trans. Commun.*, vol. 50, no. 2, pp. 225–234, Feb. 2002.
- [24] U. M. Diwekar, *Introduction to Applied Optimization*. Norwell, MA: Kluwer, 2003.
- [25] D. Gesbert, M. Shafi, D.-S. Shiu, P. J. Smith, and A. Naguib, "From theory to practice: an overview of MIMO space-time coded wireless systems," *IEEE J. Select. Areas Commun.*, vol. 21, no. 3, pp. 281–302, Apr. 2003.

- [26] G. J. Foschini, "Layered space-time architecture for wireless communication in a fading environment when using multielement antennas," *Bell Labs Tech. J.*, pp. 41–59, Autumn 1996.
- [27] J. H. Winters, "Optimum combining in digital mobile radio with cochannel interference," *IEEE J. Select. Areas Commun.*, vol. 2, no. 4, pp. 528–539, July 1984.
- [28] J. H. Winters, J. Salz, R. D. Gitlin, "The impact of antenna diversity on the capacity of wireless communication systems," *IEEE Trans. Commun.*, vol. 42, no. 2/3/4, pp. 1740–1751, Feb/Mar/Apr. 1994.
- [29] D.-S. Shiu, G. J. Foschini, M. J. Gans, and J. M. Kahn, "Fading correlation and its effect on the capacity of multielement antenna systems," *IEEE Trans. Commun.*, vol. 48, no. 3, pp. 502–513, Mar. 2000.
- [30] X. Mestre, J. R. Fonollosa, A. Pages-Zamora, "Capacity of MIMO channels: asymptotic evaluation under correlated fading," *IEEE J. Select. Areas Commun.*, vol. 21, no. 5, pp. 829–838, June 2003.
- [31] C.-N. Chuah, D. N. C. Tse, J. M. Kahn, R. A. Valenzuela, "Capacity scaling in MIMO wireless systems under correlated fading," *IEEE Trans. Inform.*, vol. 48, no. 3, pp. 637–650, Mar. 2002.
- [32] S. T. Chung and A. J. Goldsmith, "Degrees of freedom in adaptive modulation: a unified view," *IEEE Trans. Commun.*, vol. 49, no. 9, pp. 1561–1571, Sept. 2001.
- [33] J. G. Proakis, *Digital Communications*, 3rd ed. New York: McGraw-Hill, 1995.
- [34] L. W. Couch II, *Modern Communication Systems, Principles and Applications*, NJ: Prentice Hall, 1994.

- [35] A. T. James, "Distribution of matrix variates and latent roots derived from normal samples," *The Annals of Mathematical Statistics*, vol. 35, pp. 475–501, 1964.
- [36] R. J. Muirhead, *Aspects of Multivariate Statistical Theory*, New York: Wiley, 1982.
- [37] M. Chiani, M. Z. Win, A. Zanella, "On the capacity of spatially correlated MIMO Rayleigh-fading channels," *IEEE Trans. Inform. Theory*, vol. 49, no. 10, pp. 2363–2371, Oct. 2003.
- [38] S. T. Chung and A. Goldsmith, "Adaptive multicarrier modulation for wireless systems," *Signals, Systems and Computers, 2000, Conference Record of the Thirty-Fourth Asilomar Conference on*, vol. 2, pp. 1603–1607, Nov. 2000.
- [39] M. T. Ivrlac, W. Utschick, J. A. Nossek, "Fading correlations in wireless MIMO communication systems," *IEEE J. Select. Areas Commun.*, vol. 21, no. 5, pp. 819–828, June 2003.
- [40] S. Catreux, V. Erceg, D. Gesbert, and R. W. Heath, "Adaptive modulation and MIMO coding for broadband wireless data networks," *IEEE Commun. Mag.*, vol. 40, no. 6, pp. 108–115, June 2002.
- [41] S. Thoen, L. V. D. Perre, M. Engels, H. D. Man, "Adaptive loading for OFDM/SDMA-based wireless networks," *IEEE Trans. Commun.*, vol. 50, no. 11, pp. 1798–1810, Nov. 2002.
- [42] S. Catreux, P. F. Driessen, L. J. Greenstein, "Data throughputs using multiple-input multiple-output (MIMO) techniques in a noise-limited cellular environment," *IEEE Trans. Wireless Commun.*, vol. 1, no. 2, pp. 226–235, Apr. 2002.

- [43] S. Catreux, L. J. Greenstein, V. Erceg, "Some results and insights on the performance gains of MIMO systems," *IEEE J. Select. Areas Commun.*, vol. 21, no. 5, pp. 839–847, June 2003.
- [44] L. Zheng; D. N. C. Tse, "Diversity and multiplexing: a fundamental tradeoff in multiple-antenna channels," *IEEE Trans. Inform. Theory*, vol. 49, no. 5, pp. 1073–1096, May 2003.
- [45] A. Goldsmith, S. A. Jafar, N. Jindal, S. Vishwanath, "Capacity limits of MIMO channels," *IEEE J. Select. Areas Commun.*, vol. 21, no. 5, pp. 684–702, June 2003.
- [46] A. M. D. Turkmani, "Performance evaluation of a composite microscopic plus macroscopic diversity system," *Proc. Inst. Elect. Eng.-I Commun., Speech and Visions*, vol. 138, pp. 15–20, Feb. 1991.
- [47] R. C. Bernhardt, "Macroscopic diversity in frequency reuse radio systems," *IEEE J. Select. Areas Commun.*, vol.5, no. 5, pp. 862–870, June 1987.
- [48] C. E. Shannon, "A mathematical theory and communication," *Bell Sys. Tech. J.*, vol. 27, pp. 379–423, July 1948 and pp. 623–656, Oct. 1948.
- [49] C. E. Shannon, "Communication in the presence of noise," *Proceedings of the IRE*, vol. 37, pp. 10–21, Jan. 1949.
- [50] J. H. Winters, "Smart antennas for wireless systems," *IEEE Personal Commun.*, vol. 5, no. 1, pp. 23–27, Feb. 1998.
- [51] A. Paulraj and C. B. Papadias, "Space-time processing for wireless communications," *IEEE Signal Processing Mag.*, vol. 14, no. 6, pp. 49–83, Nov. 1997.

- [52] P. Vandenameele, L. V. D. Perre, M. G. E. Engels, B. Gyselinckx, H. J. D. Man, "A combined OFDM/SDMA approach," *IEEE J. Select. Areas Commun.*, vol. 18, no. 11, pp. 2312–2321, Nov. 2000.
- [53] R. B. Ertel, P. Cardieri, K. W. Sowerby, T. S. Rappaport, J. H. Reed, "Overview of spatial channel models for antenna array communication systems," *IEEE Personal Commun.*, vol. 5, no. 1, pp. 10–22, Feb. 1998.
- [54] T. S. Rappaport, A. Annamalai, R. M. Buehrer, and W. H. Tranter, "Wireless communications: past events and a future perspective," *IEEE Commun. Mag.*, vol. 40, no. 5, pp. 148–161, May 2002.
- [55] G. J. Foschini, G. D. Golden, R. A. Valenzuela, P. W. Wolniansky, "Simplified processing for high spectral efficiency wireless communication employing multi-element arrays," *IEEE J. Select. Areas Commun.*, vol. 17, no. 11, pp. 1841–1852, Nov. 1999.
- [56] P. W. Wolniansky, G. J. Foschini, G. D. Golden, R. A. Valenzuela, "V-BLAST: An Architecture for Realizing Very High Data Rates Over the Rich-Scattering Wireless Channel," *Proc. ISSSE-98*, Sept. 29 – Oct. 2, pp. 295–300, 1998.
- [57] Z. Hong, K. Liu, R. W. Heath, A. M. Sayeed, "Spatial multiplexing in correlated fading via the virtual channel representation," *IEEE J. Select. Areas Commun.*, vol. 21, no. 5, pp. 856–866, June 2003.
- [58] Q. H. Spencer, A. L. Swindlehurst, M. Haardt, "Zero-forcing methods for downlink spatial multiplexing in multiuser MIMO channels," *IEEE Trans. Signal Processing*, vol. 52, no. 2, pp. 461–471, Feb. 2004.

- [59] K. Liu, V. Raghavan, and A. M. Sayeed, "Capacity scaling and spectral efficiency in wide-band correlated MIMO channels," *IEEE Trans. Inform.*, vol. 49, no. 10, pp. 2504–2526, Oct. 2003.
- [60] G. D. Golden, G. J. Foschini, R. A. Valenzuela, and P. W. Wolniansky, "Detection algorithm and initial laboratory results using V-BLAST space-time communication architecture," *IEE Electron. Lett.*, vol. 35, no. 1, pp. 14–16, Jan. 1999.
- [61] G. J. Foschini, D. Chizhik, M. J. Gans, C. Papadias, and R. A. Valenzuela, "Analysis and performance of some basic space-time architectures," *IEEE J. Select. Areas Commun.*, vol. 21, no. 3, pp. 303–320, Apr. 2003.
- [62] K.-W. Ng, R. S. Cheng, and R. D. Murch, "Iterative bit & power allocation for V-BLAST based OFDM MIMO system in frequency selective fading channel," *IEEE Wireless Communications and Networking Conference, 2002.* vol. 1, pp. 17–21 Mar. 2002.
- [63] T. S. Rappaport, *Wireless Communications: Principles & Practice*, Upper Saddle River, NJ: Prentice Hall, 1996.
- [64] W. C. Lee, *Mobile Communications Engineering*, New York: McGraw Hill, 1982.
- [65] W. C. Lee, "Effects on correlation between two mobile radio base-station antennas," *IEEE Trans. Commun.*, vol. 21, no. 11, pp. 1214–1224, Nov. 1973.
- [66] S. B. Rhee and G. I. Zysman, "Results of suburban base-station spatial diversity measurements on the UHF band," *IEEE Trans. Commun.*, vol. 22, no. 10, pp. 1630–1634, Oct. 1974.
- [67] W. C. Jakes, *Microwave Mobile Communications*, New York: Wiley, 1974.

- [68] S. L. Loyka and J. R. Mosig, "Channel capacity of MIMO architecture using the exponential correlation matrix" *IEEE Commun. Lett.*, vol. 5, no. 9, pp. 369–371, Sept. 2001.
- [69] S. P. Stapleton, X. Carbo, and T. Mckeen, "Tracking and diversity for a mobile communications base station array antenna," *IEEE VTC Proc. 1996*, vol. 3, pp. 1695–1699, 1996.
- [70] S. C. Schwartz and Y. S. Yeh, "On the distribution function and moments of power sums with log-normal components," *Bell Sys. Tech. J.*, vol. 61, pp. 1441–1462. Sept. 1982.
- [71] A. T. James, "Calculation of zonal polynomial coefficients by use of the Laplace-Beltrami operator," *Ann. Math. Statist.*, vol. 39, pp. 1711–1718, 1968.
- [72] R. D. Gupta and D. Richards, "Calculation of zonal polynomial," *Ann. Inst. Statist.*, vol. 31, pp. 207–213, 1979.
- [73] A. Kowata and R. Wada, "Zonal polynomials on the space of 3×3 positive definite symmetric matrices," *Hiroshima Math. J.*, vol. 22, pp. 433–443, 1992.
- [74] R. Gutierrez, J. Rodriguez, and A. J. Saez, "Approximation of hypergeometric functions with matricial argument through their development in series of zonal polynomials," *Electronic Trans. Numerical Analysis*, vol. 11, pp. 121–130, 2000.
- [75] G. J. Foschini and J. Salz, "Digital communications over fading radio channels," *Bell Sys. Tech. J.*, vol. 62, pp. 429–456, Feb. 1983.
- [76] D. Chizhik, J. Ling, P. Wolniansky, R. Valenzuela, N. Costa, and K. Huber, "Multiple-input-multiple-output measurements and modeling in Manhattan," *IEEE J. Select. Areas Commun.*, vol. 21, no. 3, pp. 321–331, Apr. 2003.

- [77] J. Ling, D. Chizhik, P. Wolniansky, R. Valenzuela, N. Costa, and K. Huber, "Multiple transmit multiple receive (MTMR) capacity survey in Manhattan," *IEE Electron. Lett.*, vol. 37, pp. 1041–1042, Aug. 2001.
- [78] P. Lancaster and M. Tismenetsky, *The Theory of Matrices*, 2nd edition with applications, Orlando, FL: Academic, 1985.
- [79] S. Verdu, *Multiuser Detection*, Cambridge, UK: Cambridge University Press, 1998.
- [80] D. Liu and J.-M. Chung, "Enhanced OFDM time and frequency synchronization through optimal code correlation," *Proc. MWSCAS'02*, vol. 1, pp.176–179, Aug. 2002.
- [81] R. W. Chang, "High-speed multichannel data transmission with bandlimited orthogonal signals," *Bell Sys. Tech. J.*, vol. 45, pp. 1775–1796, Dec. 1966.
- [82] B. R. Salberg, "Performance of an efficient parallel data transmission system," *IEEE Trans. Commun. Technol.*, vol. 15, no. 6, pp. 805–811, Dec. 1967.
- [83] S. B. Weinstein and P.M. Ebert, "Data transmission by frequency-division multiplexing using the discrete Fourier transform," *IEEE Trans. Commun. Tech.*, vol. 19, no. 5, pp.628–634, Oct. 1971.
- [84] A. Peled and A. Ruiz, "Frequency domain data transmission using reduced computational complexity algorithms," *Proc. IEEE Int. Conf. Acoust., Speech, Signal Processing*, pp. 964–967, Apr. 1980.
- [85] W. Y. Zou and Y. Wu, "COFMD: an overview," *IEEE Trans. Broadcasting*, vol. 41, pp. 1–8, Mar. 1995.
- [86] R. V. Nee and R. Prasad, *OFDM for Wireless Multimedia Communication*, Boston: Artech, 2000.

- [87] W.-C. Jeong and J.-M. Chung, "Analysis of macroscopic diversity combining of MIMO signals in mobile communications," *International J. Elect. and Commun., AEÜ*, accepted for publication.
- [88] J.-M. Chung, D. Liu, K. Ramasamy and S. Varadarajan, "OFDM frame synchronization in slotted ALOHA mobile communication systems," *IEEE Proc. VTC '01*, vol.3, pp. 1373–1377, Oct. 2001.
- [89] W. Roh and A. Paulraj, "MIMO channel capacity for the distributed antenna," *Proc. IEEE VTC Fall 2002*, vol. 2, pp. 706–709, Sept. 2002.
- [90] A. Abdi and M. Kaveh, "A space-time correlation model for multielement antenna systems in mobile fading channels," *IEEE J. Select. Areas Commun.*, vol. 20, no. 3, pp. 550–560, Apr. 2002.
- [91] V. A. Aalo, "Performance of maximal-ratio diversity systems in a correlated Nakagami-fading environment," *IEEE Trans. Commun.*, vol. 43, no. 8, pp. 2360–2369, Aug. 1995.
- [92] C. C. Martin, J. H. Winters, and N. S. Sollenberger, "Multiple-input multiple-output (MIMO) radio channel measurements," *IEEE VTC'2000 Fall*, vol. 2, pp. 774–779 Sept. 24–28, 2000.
- [93] W.-C. Jeong, J.-M. Chung, and D. Liu, "Exact capacity outage analysis of MIMO systems applying macroscopic selection diversity in mobile communications," submitted to *IEE Proc. on Commun.*

- [94] W.-C. Jeong, D. Liu, and J.-M. Chung, "MIMO Systems Capacity Analysis Applying Macroscopic Selection Diversity Schemes," submitted to *IEE Electron. Lett.*
- [95] W.-C. Jeong, J.-M. Chung, and D. Liu, "Performance analysis of macroscopic diversity combining of MIMO signals in mobile communications," *Proc. VTC'03*, vol.3, pp. 1838–1842, Oct. 2003.
- [96] J. F. Hayes, "Adaptive feedback communications," *IEEE Trans. Commun. Technol.*, vol. 16, no. 1, pp. 29–34, Feb. 1968.
- [97] I. Gradshteyn and I. Ryzhik, *Tables of Integrals, Series, and Products*. San Diego, CA: Academic, 1980.
- [98] J. J. Steinbugl. (1999) Evolution toward third generation wireless networks [Online]. Available:
http://www.cse.ohio-state.edu/~jain/cis788-99/ftp/3g_wireless/index.html
- [99] Brough Turner & Marc Orange. (2002) 3G tutorial [Online]. Available:
http://www.nmscommunications.com/file/3G_Tutorial.pdf
- [100] J. Uddenfeldt, "Digital cellular – its roots and its future," *IEEE Proc.*, vol. 86, no. 7, pp. 1319–1324, July 1998.
- [101] C. Smith, *3G Wireless Networks*, New York: McGraw-Hill, 2002.
- [102] J. Korhonen, *Introduction to 3G Mobile Communications, 2nd ed.* Norwood, MA: Artech, 2003.
- [103] R. Steele, C.-C. Lee, and P. Gould, *GSM, cdmaOne and 3G Systems*. West Sussex, England: Wiley, 2001.

- [104]J. S. Lee and L. E. Miller, *CDMA Systems Engineering Handbook*. Norwood, MA: Artech, 1998.
- [105]G. M. Calhoun, *Third Generation Wireless Systems*. Norwood, MA: Artech, 2003.
- [106]P. Chaudhury, W. Mohr, and S. Onoe, "The 3GPP proposal for IMT-2000," *IEEE Commun. Mag.*, vol. 37, is. 12, pp. 72–81, Dec. 1999.
- [107]ETSI Mobile Competence Centre, *Overview of 3GPP Release 99 Summary of all Release 99 Features*, July 2004.
- [108]ETSI Mobile Competence Centre, *Overview of 3GPP Release 4 Summary of all Release 4 Features*, Sept. 2003.
- [109]ETSI Mobile Competence Centre, *Overview of 3GPP Release 5 Summary of all Release 5 Features*, 2004.
- [110]<http://www.umtsworld.com>.
- [111]3GPP2 C.S0001-D v1.0, *Introduction to cdma2000 Spread Spectrum Systems*, Feb. 2004.
- [112]3GPP2 C.S0002-D v1.0, *Physical Layer Standard for cdma2000 Spread Spectrum Systems*, Feb. 13, 2004.
- [113]3GPP2 C.0024-A v1.0, *cdma2000 High Rate Packet Data Air Interface Specification*, Mar. 2004.
- [114]N. T. Sindhushayana, P. J. Black, "Forward link coding and modulation for CDMA2000 1xEV-DO (IS-856)," *PIMRC 2002*, vol. 4, pp. 1839–1846, 2002.
- [115]L. Ma; Z. Rong, and R. T. Derryberry, "Performance of cdma2000 1xEV-DV system," *VTC 2003-Spring*, vol. 2, pp. 1163–1167, 2003.

- [116]M. Juntti, M. Vehkaperä, J. Leinonen, Z. Li, D. Tujkovic, S. Tsumura, and S. Hara, “MIMO MC-CDMA communications for future cellular systems,” *IEEE Commun. Mag.*, vol. 43, no. 2, pp. 118–124, Feb. 2005.
- [117]H. W. Arnold, D. C. Cox, and R. R. Murray, “Macroscopic diversity performance measured in the 800-MHz portable radio communications environment,” *IEEE Trans. Antennas Propagat.*, vol. 36, pp. 277–281, Feb. 1988.
- [118]J. Zhang and V. Aalo, “Effect of macrodiversity on average-error probabilities in a Rician fading channel with correlated lognormal shadowing,” *IEEE Trans. Commun.*, vol. 49, no. 1, pp. 14–18, Jan. 2001.
- [119]J. Weitzen and T. J. Lowe, “Measurement of angular and distance correlation properties of log-normal shadowing at 1900 MHz and its application to design of PCS systems,” *IEEE Trans. Veh. Technol.*, vol. 51, no. 2, pp. 265–273, Mar. 2002.
- [120]L. Fenton, “The sum of log-normal probability distributions in scatter transmission systems,” *IEEE Trans. Commun.*, vol. 8, no. 1, pp. 57–67, Mar. 1960.

VITA

2

Dongfang Liu

Candidate for the Degree of

Doctor of Philosophy

Thesis: MACROSCOPIC DIVERSITY APPLICATIONS OF MULTI-INPUT MULTI-OUTPUT (MIMO) SYSTEMS FOR BROADBAND MOBILE COMMUNICATION

Major Field: Electrical Engineering

Biographical:

Personal Data: Born in Xingtai, China, on December 18, 1971, the son of Ruifeng Liu and Yuehua Yin.

Education: Received Bachelor of Science degree and Master of Science degree in Electrical Engineering from University of Science and Technology Beijing, Beijing, China in July 1993 and April 1996, respectively. Completed the requirements for the Doctor of Philosophy with a major in Electrical Engineering at Oklahoma State University in May 2005.

Experience: Hardware/System Engineer, Automation Institute, Beijing, China (1996–2000). Research Assistant, ACSEL and OCLNB labs, School of Electrical and Computer Engineering, Oklahoma State University, Stillwater, Oklahoma (2000–2005). Teaching Assistant, School of Electrical and Computer Engineering, Oklahoma State University, Stillwater, Oklahoma (2002–2003). Senior Engineer, Qualcomm, Inc. (2005–).

Professional Memberships: The Institute of Electrical and Electronic Engineers, Phi Kappa Phi honor society.